Long-term Changes of the Tropical Atmospheric Circulations

A Dissertation Presented

by

Hua Song

To

The Graduate School

in Partial Fulfillment of the

Requirements

for the Degree of

Doctor of Philosophy

in

Marine and Atmospheric Science

Stony Brook University

August 2009

Stony Brook University

The Graduate School

Hua Song

We, the dissertation committee for the above candidate for the

Doctor of Philosophy degree, hereby recommend

acceptance of this dissertation.

Dr. Minghua Zhang - Dissertation Advisor
Professor, School of Marine and Atmospheric Sciences

Dr. Edmund K.M. Chang - Chairperson of Defense
Professor, School of Marine and Atmospheric Sciences

Dr. Marvin A. Geller - Member
Professor, School of Marine and Atmospheric Sciences

Dr. Dong-Ping Wang - Member
Professor, School of Marine and Atmospheric Sciences

Dr. Amy C. Clement - Outside Member
Professor, Division of Meteorology and Physical Oceanography
University of Miami, Miami, Florida

This dissertation is accepted by the Graduate School

Lawrence Martin
Dean of the Graduate School

Abstract of the Dissertation

Long-term Changes of the Tropical Atmospheric Circulations

by

Hua Song

Doctor of Philosophy

in

Marine and Atmospheric Science

Stony Brook University

2009

Large-scale tropical circulations, such as Walker, Hadley and monsoon circulations, play a significant role in regulating weather and climate on global and regional scales, and their year-to-year variations can greatly impact the earth's climate. In this dissertation, I have used observation and reanalysis datasets as well as atmospheric general circulation models to investigate the changes of the tropical atmospheric circulations in a warmer climate. My study shows that the Walker circulation has weakened in the latter half of the 20th century when the global sea surface temperature has increased, and this can be explained by using the thermodynamic constraint of the atmospheric heat budget in the tropics. The boreal winter Hadley circulation has significantly strengthened in the ECMWF reanalyses and moderately strengthened in the NCEP/NCAR reanalysis from 1958 to 2002. However, by using independent data and an argument of atmospheric moist static energy budget, I have found that the large trend in the ECMWF reanalysis is unrealistic, and the strengthening trends in the two reanalyses are likely an artifact. I have also found the rising motion in the northern portion of the boreal summer Hadley circulation has weakened, which is largely attributed to changes of the summer monsoons during this period.

By using surface rain gauge and satellite measurements, I report that Asian summer monsoon precipitation decreased over India but increased over southeast China from 1980 to 2002 while the patterns become opposite after 2002, and these are realistically captured in the NCEP/NCAR reanalysis. I have found how rainfall variations are associated with wind patterns in the lower troposphere. Lastly, I conducted model simulations to study the causes for the observed Asian monsoon precipitation changes by using the NCAR CAM3 forced with the observed SST variations. The SST forcing, primary from the tropics, especially from the tropical Indian ocean, is able to induce most of the observed Asian summer monsoon changes from 1980 to 2007.

Table of Contents

List of Figures

List of Tables

List of Acronyms

AM: Atmospheric Model

AMIP: Atmospheric Model Intercomparison Project

CAM: Community Atmosphere Model

CAMS: Climate Anomaly Monitoring System

CAS: Chinese Academy of Sciences

CCSM: Community Climate System Model

CLM: Community Land Surface Model

CMAP: CPC Merged Analysis of Precipitation

COADS: Comprehensive Ocean-Atmosphere Data Set

CPC: Climate Prediction Center

DJF: December-January-February

DOM: Data Ocean Model

ECMWF: European Centre for Medium-Range Weather Forecasts

EECRA: Extended Edited Cloud Report Archive

ENSO: El Niño Southern Oscillation

ERSLP: Extended Reconstructed Sea Level Pressure

GCM: General Circulation Model

GFDL: Geophysical Fluid Dynamic Laboratory

GFDL-CM2: GFDL Coupled Model, version 2

GHCN: Global Historical Climatology Network

HadISST: Hadley Centre Global Sea Ice and Sea Surface Temperature

IAP: Institute of Atmospheric Physics

IITM: Indian Institute of Tropical Meteorology

IPCC: Intergovernmental Panel on Climate Change

ISCCP: International Satellite Cloud Climatology Project

JJA: June-July-August

MPI-OM: Max Plank Institute-Ocean Model

NCAR: National Center for Atmospheric Research

NCEP: National Center for Environmental Prediction

NOAA: National Oceanic and Atmospheric Administration

PREC/L: Precipitation Reconstruction Data over Land

SLP: Sea Level Pressure

SOM: Slab Ocean Model

SST: Sea Surface Temperature

UKMO: United Kingdom Meteorological Office

UKMO-HadGEM1: UKMO-Hadley Centre Global Environmental Model, version 1

Acknowledgements

First and foremost, I would like to thank my advisor, Dr. Minghua Zhang, for his incessant support, encouragement, and patience during my doctoral studies. The completion of this dissertation would not be possible without his insightful advice and continuous encouragement.

I am also very grateful to my committee, Dr. Edmund K.M. Chang, Dr. Marvin Geller, Dr. Dong-Ping Wang and Dr. Amy Clement. Their invaluable comments and advices have benefited me considerably in the research.

I am privileged to be educated by the faculty of SoMAS. Special thanks go to Dr. Edmund K.M. Chang. I have learned a lot from his well-organized and excellent dynamic classes.

My thanks also go to Dr. Wuyin Lin for helping me a lot with the model setup. I also thank my colleagues, Moguo Sun, Yanluan Lin, Xiaosong Yang, Jae Lee, Yanjuan Guo, Jie Gong, Howard Teich and Gang Zeng for their countless help and useful advice. My life in Stony Brook has been enriched by many friends. They are Qian Jiang, Aiying Chen, Fanghua Xu, Xiaona Li, Yuan Liu and Tiantian.

Finally, I dedicate this work to my mother, who alone raised my sister and me up and afforded us a good education. I also thank my parents-in-law for taking care of my baby daughter. Last but not least, I thank my husband Tiehan, who is always there, sharing my joy and pain.

Chapter 1

Introduction

1.1 Tropical Atmospheric Circulations

Large-scale tropical atmospheric circulations, such as Walker, Hadley and monsoon circulations are the strongest driving forces of weather and climate in low latitudes. As fundamental regulators of the earth's energy budget, the year-to-year variations of these circulations also have a great impact upon the global climate variability.

The Walker circulation is an east-west atmospheric circulation pattern characterized by rising air over Indonesia and the western Pacific and sinking air over the eastern Pacific, and closely related to the zonal surface pressure gradient between a high pressure system over the eastern Pacific ocean and a low pressure system over Indonesia (Julian and Chervin, 1978). The Hadley circulation is defined as the zonally averaged meridional circulation with ascending motion over the intertropical convergence zone (ITCZ) and descending motion over the subtropical high-pressure belt. Energy associated with the equatorial maximum in solar radiation released through vigorous atmospheric convection is the ultimate driver of the mean position of the Hadley circulation (Lindzen and Hou, 1988; Hou, 1998; Rind, 1998).

The monsoon circulation, driven essentially by the thermal contrast between the continent and adjacent oceanic regions, is characterized by seasonal reversals of wind and precipitation regimes (e.g., Webster, 1987). The Walker, Hadley and monsoon circulations are all related with each other. For example, the upward motions of the atmosphere associated with the Asian summer monsoon also contribute significantly to the rising branch of the Hadley circulation.

Changes of the tropical atmospheric circulations can be driven by internal variabilities and external forcings such as sea surface temperature patterns, aerosols and greenhouse gases. The interannual changes of the Walker, Hadley and monsoon circulations associated with the El Niño/Southern Oscillation (ENSO) have been extensively studied in the past (e.g., Arkin, 1982; Webster et al., 1998; Oort and Yienger, 1996; Wang et al., 2000; Lim and Kim, 2007), but the long-term changes of the tropical circulations on the time scale beyond the time scales of ENSO have not been thoroughly studied yet.

The global mean surface temperature has increased by about 0.3°C–0.6°C since the late nineteenth century with rapid warming occurring over the last few decades of the 20th century (Intergovernmental Panel on Climate Change (IPCC), 1995). How the atmospheric circulation on a global scale has changed with such temperature increase is still an open question.

Recently, several studies have attempted to evaluate the long-term changes in the intensity of tropical circulations in the last several decades. These can be categorized into three groups based on the source of data: satellite measurements, reanalysis, and model simulations. Chen et al. (2002) used satellite observations of the earth's radiation budget to infer an intensification of the Hadley and Walker circulations since 1985. The accuracy of the satellite record and their method however are strongly contested by Trenberth et al. (2002). Using the NCEP/NCAR reanalysis data, Quan et al. (2004) and Tanaka et al. (2004) reported the intensification of the Hadley circulation after the 1950s. Mitas and Clement (2005) showed that the Hadley circulation in the boreal winter has intensified in both the NCEP/NCAR and the ECMWF reanalyses, and the magnitude of the strengthening is much larger in the ECMWF reanalysis. However, Mitas and Clement (2006) showed that the intensification of the Hadley can not be reproduced in most models. Previous studies have shown weakening of the atmospheric Walker circulation in a warmer climate (Betts and Ridgeway, 1989; Knutston and Manabe, 1995), but the results are only restricted to models. Several studies on the other hand cautioned against the large uncertainties in the reanalyis data to infer the long-term changes of the Hadley and Walker circulations (Trenberth, 2002). Therefore, it is still not clear whether the Hadley and Walker circulations have changed over the period when global temperature has increased, and how to reconcile results from reanalyses and models.

Many studies have also investigated changes of the summer monsoon rainfall over Asia, most of them describing intraseasonal and interannual variability, and relationships with El Niño (e.g., Lau and Nath, 2006; Hoyos and Webster, 2007; Lim and Kim, 2007). Some previous studies have also examined the rainfall variation of Asian monsoon on decadal time scales and shown the decrease of Asian summer monsoon rainfall in the last fifty years of the 20th century (e.g., Stephenson et al., 2001; Quan et al., 2003; Tanaka et al., 2004). Nevertheless, how the rainfall variation is associated with the change in monsoon circulation and the physical mechanisms of the changes are not clear.

1.2 Objectives

The main purpose of my thesis is to investigate the changes of the Walker, Hadley and Asian monsoon circulations in a warmer climate, and to understand the corresponding physical mechanisms. I will address the following questions:

(1) What changes of the tropical atmospheric circulations have occurred in the last several decades? Specifically, have there been robust changes in the Hadley circulations, the Walker circulations, and the Asian monsoon?

(2) Are evidences afforded by reanalysis products, numerical models, and more direct measurements consistent with each other in describing the changes of the large-scale atmospheric circulation? If they are not, which dataset is more reliable?

(3) What is the underlying physical mechanism or cause of the inferred changes of the tropical atmospheric circulations?

In carrying out my study, I recognize that the NCEP/NCAR and ECMWF reanalysis products, even though they provide a comprehensive description of the atmospheric states, suffer from the impact of sparse radiosonde input data with known biases in trends and model deficiencies (Trenberth and Guillemot, 1998; Trenberth et al., 2001, Bengtsson et al., 2004; Kinter et al., 2004). I have therefore attempted to find other independent datasets whenever possible. I have further used atmospheric general circulation models (AGCM) to provide additional support to my conclusions.

The dissertation is organized as follows: Chapter 2 provides a brief description of the data used in the study. Chapter 3 presents the long-term change of the Walker circulation, both observation and model outputs are analyzed. The long-term change of the Hadley circulation is presented in Chapter 4. The Hadley circulations in the boreal winter and boreal summer are separately discussed. Special attention is paid to the trend difference of the boreal winter Hadley circulation in the two reanalysis products. Changes of the Asian summer monsoon precipitation and winds are discussed in Chapter 5. In Chapter 6, I conduct GCM experiments by using the NCAR CAM3 to investigate the role of SST in the change of the Asian summer monsoon. The conclusions and description of future work are given in Chapter 7.

Chapter 2

Data Descriptions

In the study, I have used the monthly mean data from the NCEP/NCAR and ECMWF reanalysis products. I have also used the observational data, which are: sea level pressure data from the NOAA ERSLP, cloud data from the EECRA, station precipitation data from the IITM and the CAS, and the interpolated precipitation data from the GHCN PREC/L based on rain-gauge measurements and the CMAP based on both rain gauges and satellite measurements.

2.1 NCEP/NCAR Reanalysis

The National Center of Environmental Prediction/National Center for Atmospheric Research (NCEP/NCAR) reanalysis has two unique characteristics: the length of the period covered and the assembly of a very comprehensive observational database (Kalnay et al., 1996). The NCEP/NCAR reanalysis system has three major modules: data decoder and quality control preprocessor, data assimilation module with an automatic monitoring system, and archive module. The collected observational datasets are the global rawinsonde data, COADS surface marine data (SLP, surface temperature and wind, etc.), aircraft data (temperature, wind, etc.), surface land synoptic data, satellite sounder data of retried temperature and water vapor, SSM/I surface wind speeds and satellite cloud drift winds. The data assimilation model is spectral T62 resolution with 28 vertical hybrid levels. The reanalysis gridded output variables are classified into four classes, depending on the relative influence of the observational data and the model on the gridded variable. An A-class indicates that the analysis variable is strongly influenced by observational data, and hence is the most reliable (e.g., upper-air temperature and wind). B-class indicates that, although there are observational data that directly affect the value of the variable, the model also has a very strong influence on the analysis value (e.g., humidity, surface temperature, surface pressure and vertical velocity). C-class variables such as precipitation, clouds and surface fluxes are completely determined by the model during the data assimilation and should be used with caution. D-class represents a field that is obtained from climatological values and does not depend on the model. The output reanalysis files of atmospheric variables are calculated every 6 hours on a 2.5ºLat × 2.5ºLon global grid at 17 vertical pressure levels from January 1948 to present. The monthly mean NCEP/NCAR reanalysis data can be downloaded from the NOAA website (http://www.cdc.noaa.gov/data/gridded/data.ncep.reanalysis.html). The data caveats can be found at http://www.cdc.noaa.gov/data/reanalysis/problems.shtml.

One of the well known problems of the NCEP/NCAR reanalysis is the violation of mass and energy conservations due to the data assimilation process. Therefore, whenever it is used, I will employ other independent datasets to indirectly verify the particular features in the reanalysis.

2.2 ECMWF Reanalysis

The European Center for Medium Range Weather Forecasting (ECMWF) 40-year reanalysis (ERA-40) is a re-analysis of meteorological observations from September 1957 to August 2002 (Uppala et al., 2005). ERA-40 is a new, 45-year second-generation reanalysis carried out by ECMWF with the goal of producing the best possible set of analyses. It nearly accommodated all available ground, ship, space observations into a 3D-variational data assimilation system. The assimilation model is spectral T159 resolution with 60 vertical hybrid levels. The ERA-40 data assimilation system was designed to produce analyses of atmospheric temperature, horizontal winds, humidity, and ozone, and a number of surface variables. The system did not impose any overall hydrological balance, and the dynamical balance on the analyses was not designed to ensure correct long-term balance of atmospheric circulations driven by diabatic heating and small-scale wave-breaking. One of the most serious problems diagnosed in ERA-40 is the excessive tropical oceanic precipitation in short-range forecasts run from the analyses (Uppala et al., 2005). This problem will have an impact on the trend reanalysis as I will reveal. All the ERA-40 data are available from the NCAR Mass Storage System (MSS) (http://www.cgd.ucar.edu/cas/catalog/ecmwf/era40/). Publications related to the data quality of the ERA-40 can be found on the ECMWF web site (http://www.ecmwf.int/publications/library/do/references/list/192).

Like in the case of the NCEP/NCAR reanalysis, whenever the ECMWF reanalysis is used, I also employ other independent datasets to indirectly verify the particular features in the reanalysis.

2.3 ERSLP

The extended reconstructed sea level pressure (ERSLP) analysis data was constructed using the most recently available Comprehensive Ocean-Atmosphere Data Set (COADS) and additional coastal and island station observations (Smith and Reynolds, 2004a). Improved statistical methods were employed in the construction similar to those used for the widely used Smith and Reynolds SST data (Smith and Reynolds, 2004b). The monthly 2^o lat by 2^o lon ERSLP data span 1854 to 1997. In the nineteenth century, the reconstruction appears to underestimate the SLP-anomaly amplitude, and error estimates for the reconstruction are largest. Spatial variations between the reconstruction and several comparison analyses are highest in the second half of the twentieth century, suggesting greater reconstruction reliability after 1950. The ERSLP data can be downloaded at http://www.ncdc.noaa.gov/oa/climate/research/slp/. In my research, I only used data after 1950.

2.4 EECRA

The surface synoptic cloud observations obtained from the Extended Edited Cloud Report Archive (EECRA) are used. Detailed information of the EECRA cloud data can be found in Hahn and Warren (1999). The EECRA contains surface synoptic weather reports for the entire globe, gathered from various available data sets. The cloud reports included in the EECRA have passed through extensive quality control tests. The EECRA contains 81 million cloud observations from ships and 311 million from land stations. It includes the amounts, either inferred or directly reported, of low, middle, and high clouds, both overlapped and non-overlapped amounts. The data I used (Courtesy of

Dr. Joel Norris) span from December 1951 to December 1997. Information of the EECRA data can be found at http://cdiac.ornl.gov/epubs/ndp/ndp026c/ndp026c.html.

2.5 Observational Precipitation

Two station precipitation datasets are used. One is the Indian Institute of Tropical Meteorology Indian regional/subdivisional monthly rainfall dataset (IITM-IRM), which was derived from 306 almost uniformly distributed stations. The data span from 1871 to 2006. Detailed description of the station data can be found on the website: http://www.tropmet.res.in/static_page.php?page_id=53. The other station data is the monthly accumulated precipitation dataset from 160 land stations in China from 1951 to 2004, which is from the Institute of Atmospheric Physics (IAP), Chinese Academy of Sciences (CAS). The station data can be downloaded from the website: http://dss.ucar.edu/datasets/ds578.1/.

Two other interpolated rain-gauge-based grid precipitation datasets are also used. One is the monthly precipitation reconstruction data over land (PREC/L), compiled and objectively analyzed from rain gauge measurements in the Global Historical Climatology Network (GHCN) and the Climate Anomaly Monitoring System (CAMS) datasets at the National Center for Environmental Prediction (NCEP) (Chen et al., 2002). The other is the CPC (Climate Prediction Center) Merged Analysis of Precipitation (CMAP), which was objectively analyzed from both rain gauges and satellite infrared and microwave measurements (Xie and Arkin, 1997). The PREC/L dataset is from January 1948 to April 2008, and the CMAP dataset is from January 1979 to July 2008.

Because each of these dataset is processed through several steps, none of them has an explicit specification of the error uncertainties. Investigation of uncertainties for each dataset is itself a separate study that is beyond the scope of my research. In my thesis, I therefore will not consider possible systematic biases of the datasets in the statistical significance tests.

Chapter 3

Long-term Change of the Walker Circulation

Large-scale vertical circulation in the tropics is an integral part of the atmospheric system that consists of centers of low and high pressures. Any trend in the vertical circulation should therefore accompany trends in other components of the system. In this chapter, I first use a sea level pressure (SLP) dataset that was constructed from relatively abundant ship-based measurements to investigate the variation of Walker circulation over the tropical Pacific. I will then present corroborative evidences by using the operational reanalysis products. At the end, I will show model results and discuss the physical mechanism of the variation of the Walker circulation.

3.1 Data and Models

The ERSLP data from the NOAA National Climate Data Center are used. Here, I use the data after 1950 since the ship-based COADS data have better coverage during this period (Woodruff et al., 1987).

Monthly mean SLP, 1000-hPa zonal wind and 500-hPa vertical pressure velocity data from the NCEP/NCAR and ECMWF reanalyses are also used (Kalnay et al., 1996;

Uppala et al., 2005). The NCEP/NCAR reanalysis is from January 1948 to March 2009, and the ECMWF ERA-40 reanalysis is from September 1957 to August 2002.

The two general circulation models (GCMs) I use are the Geophysical Fluid Dynamics Laboratory (GFDL) Atmospheric Model (AM) 2.12b (GFDL Global Atmospheric Model Development Team, 2005) and the National Center for Atmospheric Research (NCAR) Community Atmospheric Model, version 3 (CAM3) (Collins et al., 2006). The NCAR CAM3 used is a standard version of CAM 3.5, which is integrated for 20 years for every run with the last 15-year data being used. The physical parameterizations of these two GCMs are listed in Table 1 of Wyant et al. (2006).

3.2 Long-term Change of the Walker Circulation

In the tropical Pacific, the most conspicuous features of the SLP distribution are the subtropical highs north and south of the equator and the low pressure center in the tropical western Pacific (TWP) (Figure 3.1a). Together with the Coriolis force due to the rotation of the Earth, the pressure gradient forces directing from the highs to the low drive the northeast and southeast surface trade winds on the two sides of the equator. Surface air converges in the western Pacific to form the rising branch of atmospheric circulation, and diverges from the two centers of the subtropical highs to form its subsidence branch. The upward motions in the rising branch are mostly manifested in tropical convection with horizontal scales of several kilometers to hundreds of kilometers, while the downward branch is characterized by subsidence of clear air on scales of thousands of kilometers. Figure 3.1b shows the linear trend of annual mean SLP in the NOAA ERSLP from 1950 to 1997. The shading represents regions of changes above the

95% confidence level. The statistical significance tests are carried out by using the Student's t-distribution of the trends with the number of degrees of freedom calculated based on autocorrelation of the time series. It is seen that the SLP over the tropical western Pacific is significantly increased while that over the eastern Pacific is significantly decreased, leading to weaker surface low in the tropical western Pacific and weaker subtropical highs, and reduced surface pressure gradient forces cross the tropical Pacific.

The difference of area-averaged sea-level pressure between the subtropical high in the northeastern subtropical Pacific (160^{o}W-110^{o}W, 15^{o}N-35^{o}N) and the TWP (110^{o}E-160^{o}W, 10^{o}S-10^{o}N) in the NOAA data is shown as a time series in Figure 3.2a by the green solid line. There are large interannual and interdecadal variations, including the climate shift in the middle of 1970s that coincided with the time of introduction of satellite measurements (e.g., Trenberth and Hurrell, 1994; Deser et al., 2004; Kinter et al., 2004). There is, however, a clear trend of the decrease of sea level pressure gradient in the five decades.

The corresponding pressure differences in the NCEP/NCAR and the ECMWF reanalyses are also shown in Figure 3.2a. There are good agreements among the two reanalysis products and the NOAA data during the period when ERSLP are available before 1997, all of them indicating decreasing gradient of sea level pressure. The gradient of sea level pressure in the NOAA data decreased by $18 \pm 7\%$ from 1950 to 1997, while it is $22 \pm 8\%$ in the NCEP/NCAR reanalysis from 1950 to 1997, and $11 \pm 8\%$ in the ECMWF reanalysis from 1958 to 1997. The error uncertainties represent the 95% confidence ranges.

After 1997, however, the SLP gradient in the two reanalyses shows a reversed change relative to the earlier trend. Examination of the global mean sea surface temperature (Figure 3.3a) indicates that the warming trend of SST in the last century also leveled off after 1998. Furthermore, there is a reverse of the linear trend of the east-west SST gradient in the tropical Pacific before and after 1997 (Figure 3.3b). Because of the short time duration after 1998, I will therefore primarily focus on the period before 1997 when there is a statistical warming trend in the SST and when the ERSLP data are available in this chapter.

Figure 3.2b shows the variations of the pressure gradient between TWP and the tropical eastern Pacific (150^{o}W-80^{o}W, 10^{o}S-10^{o}N). The decreases of the pressure gradient is $26 \pm 18\%$ in the NOAA data, $20 \pm 19\%$ in the NCEP/NCAR reanalysis from 1950 to 1997, and $21 \pm 24\%$ in the ECMWF reanalysis from 1958 to 1997, respectively. Both of the NOAA ERSLP and NCEP/NCAR reanalysis show significantly decreased zonal pressure gradient.

Figure 3.2c shows the variations of the pressure gradient between TWP and the southeastern subtropical Pacific (120^{o}W-70^{o}W, 35^{o}S-15^{o}S). The decreases of the pressure gradient are $6 \pm 9\%$ in the NOAA data, $15 \pm 9\%$ in the NCEP/NCAR reanalysis from 1950 to 1997, and $17 \pm 9\%$ in the ECMWF reanalysis from 1958 to 1997, respectively. While the trend in the NOAA data does not pass the ninety-five percent confidence test, both of the two reanalyses show significantly decreased trends. We note that the COADS SLP data in the Southeast Pacific is relatively sparse comparing to other regions (Woodruff et al., 1987).

Since there is a seasonal variation of the pressure pattern in Figure 3.1a, I carried out separate analyses for the boreal winter and summer by using average domains appropriate for each season. The trend results are very similar. I also examined the possible changes in the locations of the subtropical highs, and found no systematic variation in the locations that can explain the pressure gradient trends.

Because of the overall consistencies in the SLP variation among the NOAA ERSLP and the two reanalyzes, I next use the two reanalysis datasets to examine the changes in the surface winds. Figures 3.4a and 3.4b show the climatology and linear trends of 1000-hPa zonal wind in the NCEP/NCAR and ECMWF reanalyses, respectively. In the NCEP/NCAR reanalysis, the trade winds show strong weakening trends over the tropical central to eastern Pacific. While in the ECMWF reanalysis, the trade winds are weakened in the eastern Pacific but strengthened in the tropical western Pacific. The area mean trade winds in the tropical central to eastern Pacific are significantly weakened in the NCEP/NCAR and ECMWF reanalyses with different magnitudes (Figures 3.4c and 3.4d).

Vertical velocity would provide a more direct measure of the strength of the overturning atmospheric circulation. However, this variable in the reanalyses is much less reliable (Kalnay et al., 1996; Gibson et al., 1999) because in the tropics it is more strongly coupled with convective processes whose parameterizations in the models contain large uncertainties (e.g., Zhang, 1996). Furthermore, it is more directly subject to the recently reported biases in the trends of the input radiosonde temperature (Sherwood et al., 2005; Santer et al., 2005; Mitas and Clement, 2006). Nevertheless, it should be still constrained to some degree by the surface winds and surface pressure gradient force.

Climatology and linear trends of 500-hPa vertical pressure velocity in the NCEP/NCAR reanalysis are shown in Figure 3.5a. Both rising motions in the warm pool and sinking motions in the cold tongue are weakening in the NCEP/NCAR reanalysis (Figures 3.5b and 3.5c), consistent with the weakening trade winds shown in Figure 3.4a, revealing a weakened Walker circulation. This is most clearly seen in the frequency distribution and the occurrence of strong vertical motions in Figure 3.6. In the ECMWF reanalysis, the pattern is somewhat different (Figure 3.5d). The rising motions in the warm pool are significantly strengthened (Figure 3.5e) while the sinking motions in the cold tongue is mildly weakened (Figure 3.5f). In the next chapter, I will present evidence that this trend over the tropical western Pacific in the ECMWF reanalysis is likely spurious.

3.3 Model Results

During the period from 1950 to 1997, SST averaged in the whole tropics has risen by about 0.4K according to Smith and Reynolds (2004b). I have postulated that the decrease of the sea level pressure gradient is an intrinsic characteristic of a warmer climate. Next I will use the GFDL AM2 and the NCAR CAM3 to examine this more closely. Control simulations were carried out by using prescribed seasonally varying monthly SSTs. The SSTs are then uniformly perturbed by -2K and +2K (Cess et al., 1996). Hereafter, the three runs are referred as -2K, control and +2K runs. There is therefore no ENSO forcing in the models. The experiments were conducted as part of the Climate Process Team on low latitude climate feedbacks (Bretherton et al., 2004).

Figure 3.7 shows the simulated annual mean SLP from the -2K, control and +2K runs in the GFDL and NCAR models. In the GFDL AM2, the SLP over the tropical western Pacific becomes higher (lower) while the SLP over the tropical eastern Pacific becomes lower (higher) with homogeneously increased (decreased) SST. In the NCAR CAM3, the SLP over the tropical Pacific (20ºS-20ºN) becomes higher (lower) but with larger magnitude over the western Pacific, while the SLP over the northeastern subtropical Pacific and southeastern subtropical Pacific become lower (higher) with homogeneously increased (decreased) SST. Such SLP changes in the two models lead to the reduced (enhanced) SLP gradients over the tropical Pacific when forced by the warmer (colder) SST. The quantitative values differ among the models, but the sign of the pressure gradient variation across the Pacific is consistent in all the simulations and with the observations. We note that the reductions in the models are smaller than in the observational analyses when normalized to a unit global temperature increase. Part of this could be related to the spatial distribution of the observed SST increase that is larger in the tropical eastern Pacific than in the tropical western Pacific (Wittenberg, 2004). This is also seen in Figure 3.3b, which indicated a decreasing trend of SST zonal gradient in the tropical Pacific before 1997.

Figures 3.8a and 3.8b show annual mean zonal wind averaged from 15ºS to 15ºN in the GFDL and NCAR models. Its variations when the SST is perturbed are shown in Figures 3.8c to 3.8f. It is seen that the trade winds over the tropical Pacific and the Walker circulation are weaker (stronger) when SST is uniformly increased (decreased), which is consistent with the reduced (enhanced) pressure gradient across the Pacific shown in Figure 3.7. Associated with the reduction (increase) of sea level pressure gradient and trade winds, the models exhibited weakening (strengthening) of the overall intensity of the vertical circulation in a warmer (colder) climate, as shown in the subsidence rate at 500-hPa level in the eastern Pacific (Figure 3.9). When averaged from 30^{o}S to 30^{o}N and normalized to 1K SST increase, the monthly subsidence rate decreased by about 3% percent in the models. The probability distributions of 500-hPa vertical pressure velocity in the whole tropics (Figure 3.10) show that in a warmer climate, the distribution becomes narrower, with the strong vertical motions shifting to mild motions, indicating the weakened high and low systems in the tropical Pacific. This weakening of the vertical circulation and narrowing of the frequency distribution of the vertical pressure velocity in the tropics have been also reported in Knutson and Manabe (1995) and in Bony et al. (2005). What I emphasize here is that the weakening of the vertical circulation is consistent with the reduction of sea level pressure gradient across the tropical Pacific in the models, which is consistent with the ERSLP data.

Since the reduction of vertical circulation in a warmer climate can be physically explained through the requirement of enthalpy conservation of the tropical troposphere (Held and Soden, 2006), the decrease of surface pressure gradient is therefore an intrinsic characteristic of the tropical atmosphere. When the tropical SST warms up, vertical stability of the atmosphere is increased. In the subsidence region, the increased stability accommodates weaker subsidence to maintain the thermodynamic balance in the subsidence regions. An alternative explanation is to consider the heat budget of the tropical atmosphere as a whole, where the dominant balance is between latent heating and radiative cooling. As surface temperature increases, the radiative cooling of the atmosphere does not change as much as the vertical gradient of moisture. Thus, the vertical circulation must decrease so that the latent heating does not over-compensate the radiative cooling. This leads to less wind divergences and convergences in the upper troposphere, and smaller surface pressure gradient. The reported reduction of sea level pressure gradient can be therefore considered as an indirect evidence of the weakening of the atmospheric vertical circulation in the tropical Pacific.

3.4 Discussion

The reduction of sea level pressure gradient collaborates well with model predictions of the weakening vertical circulation and temperature lapse rate change in a warmer climate. This reduction in pressure gradient may have important implications to the interpretation of future climate changes. As the surface pressure gradient weakens, the trade winds should also weaken. Under such a circumstance, the SST contrast between the warm pool and the cold tongue across the Pacific should also decrease since the equatorial cold tongue is driven by upwelling of cold water in the eastern Pacific due to surface trade winds. The observed spatial pattern of SST change in the tropical Pacific from 1950 to 1997 indeed contains evidence of this feature (Figure 3.11).

Figure 3.11a shows the climatology 30ºS-30ºN latitudinal mean SST from the HadISST observational dataset. SST is much warmer in the tropical western Pacific (100ºE-180ºE) and colder in the tropical eastern Pacific (120ºW-70ºW), leading to an east-west SST gradient over the tropical Pacific. Time evolution of the latitudinal mean SST anomalies is shown in Figure 3.11b, indicating that overall the tropical SST are warmer in the late 20th century than in the early 20th century. SST in the tropical western Pacific has been increased by about 0.29K from 1950 to 1997, while SST in the tropical eastern Pacific has been increased by about 0.45K, which leads to a weakening of the east-west SST gradient from 1950 to 1997 (Figure 3.3b).

Exactly whether change in the SST gradient is the consequence or the cause of the variation of the trade winds should be an important topic of future research. Our analysis suggests that the weakening of the trade winds can occur under conditions of uniform change of SST. Previous modeling results from coupled GCMs are also somewhat consistent with the decrease of SST gradient in a warmer climate (e.g., Knutson and Manabe, 1995; Meehl et al., 2000). Along this line of deduction, SST anomaly in a global warming scenario would be somewhat similar to an El Niño signature in which the anomaly should be larger in the eastern Pacific than in the western Pacific. Further observational and modeling studies are needed to confirm these speculations.

I have also calculated the trends of Walker circulation change extended through 1997 to 2008. The SLP difference between the northeastern subtropical Pacific high and TWP low decreased by 11 ± 8% from 1950 to 2008 and 11 ± 7% from 1958 to 2001 in the NCEP/NCAR reanalysis, and 4 ± 9% from 1958 to 2001 in the ECMWF reanalysis. The SLP difference between the equatorial eastern Pacific and TWP decreased by 0 ± 17% from 1950 to 2008 and 5 ± 18% from 1958 to 2001 in the NCEP/NCAR reanalysis, and 15 ± 24% from 1958 to 2001 in the ECMWF reanalysis. The SLP difference between the southeastern subtropical Pacific and TWP decreased by 5 ± 8% from 1950 to 2008 and 7 ± 9% from 1958 to 2001 in the NCEP/NCAR reanalysis, and 11 ± 9% from 1958 to 2001 in the ECMWF reanalysis. Results show that the east-west SLP gradients cross the tropical Pacific still show downward trends from 1950 through 1997 to 2008, but most of the trends do not pass the 95% confidence level. On the other side, the 1000-hPa zonal wind over the equatorial Pacific is weakened by 2.26 ± 0.45 m/s/100years from 1950 to 2008 and 2.49 ± 0.66 m/s/100years from 1958 to 2001 in the NCEP/NCAR reanalysis, and 0.39 ± 0.56 m/s/100years from 1958 to 2001 in the ECMWF reanalysis. The rising motions over the tropical western Pacific are weakened by 13.92 ± 2.71 hPa/day/100years from 1950 to 2008 and 16.48 ± 3.39 hPa/day/100years from 1958 to 2001 in the NCEP/NCAR reanalysis, but strengthened by 11.13 ± 3.32 hPa/day/100years from 1958 to 2001 in the ECMWF reanalysis. Meanwhile, the sinking motions over the tropical western Pacific are weakened by 9.31 ± 3.48 hPa/day/100years from 1950 to 2008 and 13.90 ± 5.12 hPa/day/100years from 1958 to 2001 in the NCEP/NCAR reanalysis, slightly weakened by 1.79 ± 3.21 hPa/day/100years from 1958 to 2001 in the ECMWF reanalysis. Overall, the zonal wind and vertical motions over the tropical Pacific are still significantly weakened from 1950 to 2008, especially in the NCEP/NCAR reanalysis.

The global mean SST increases from 1950 to 1997, but it decreases after the late 1990s. Since my purpose is to study the effect of the global warming on the Walker circulation change, I only focus on the linear regression with the calendar years before 1997.

Finally, it should be noted that the weakening of the atmospheric vertical circulation does not necessarily lead to the weakening of the atmospheric hydrological cycle. One can think of the latter as a convolution of the dynamic circulation with water vapor content. Since moisture in the air increases with temperature, the hydrological cycle, defined as precipitation, should in fact intensify as long as the overall radiative cooling of the atmosphere increases in a global warming scenario. This may reconcile some seemingly conflicting results in previous studies that reported intensification of atmospheric circulations which refer primarily to the hydrological cycle (e.g., Kinter et al., 2004). As discussed earlier, however, trends in the dynamic circulation have their own significance in the climate system.

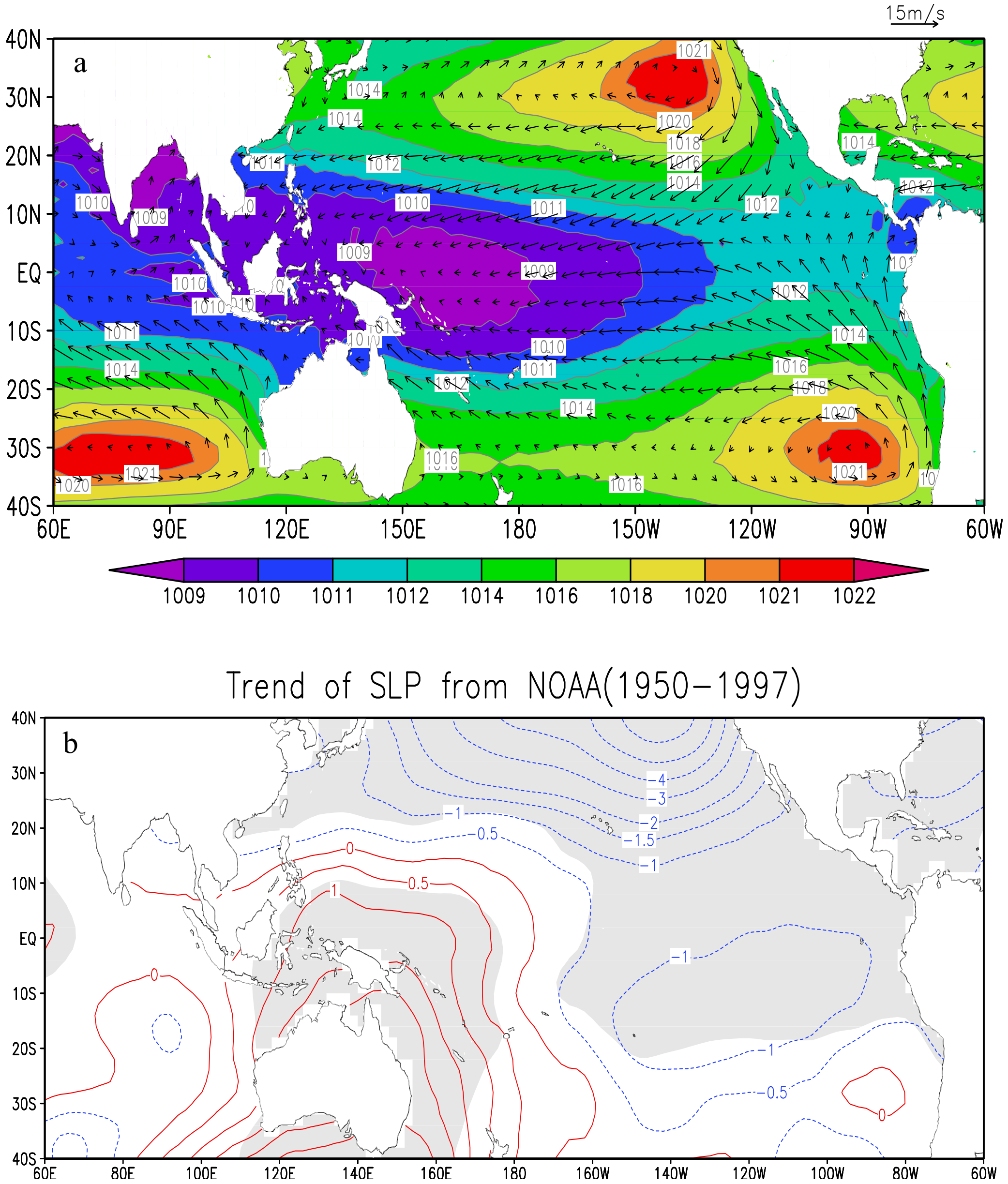

Figure 3.1: (a) is the climatology of annual mean SLP (image and contour). Arrows represent wind climatology at 1000-hPa level. Data are from the NCEP/NCAR reanalysis (b) is the linear trend of annual mean SLP from 1950 to 1997 from the NOAA ship-based observation (ERSLP). Units of SLP, wind and linear trend are hPa, m/s and hPa/100years, respectively. Areas where trends are statistically significant at a 95% confidence level are shaded in grey.

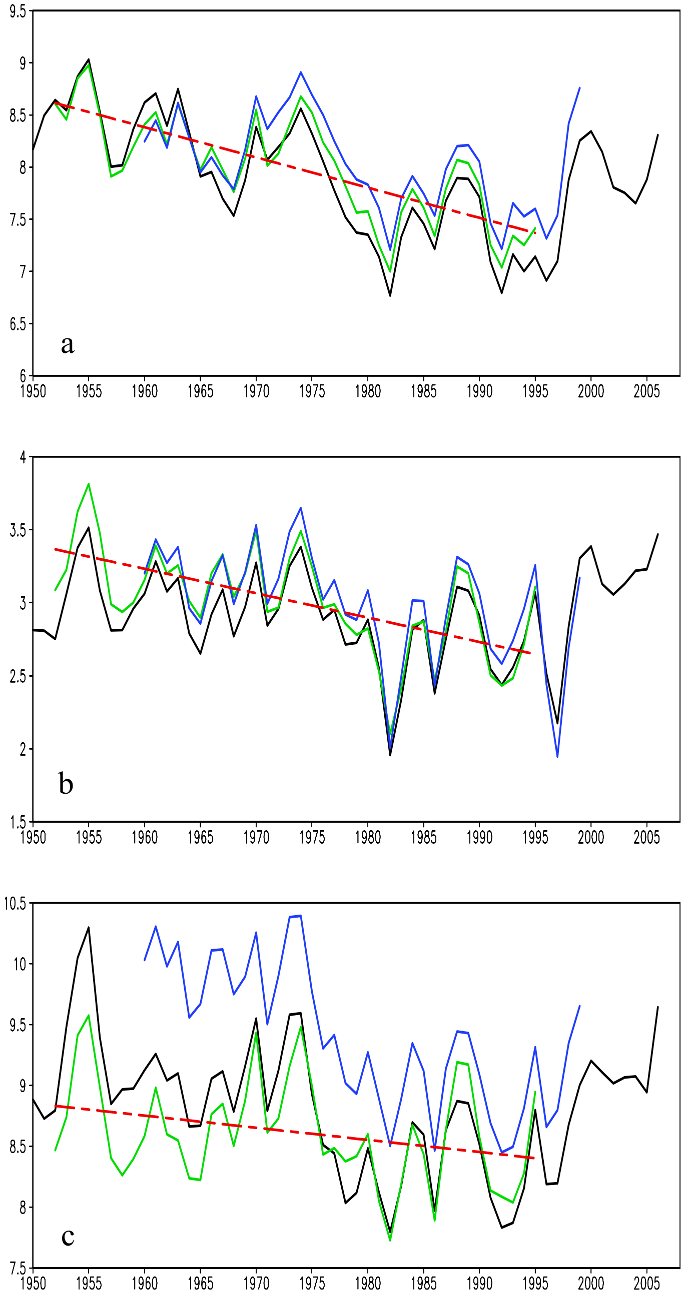

Figure 3.2: (a) Time series of the annual mean SLP difference between northeastern Pacific (160ºW-110ºW, 15ºN-35ºN) and TWP (110ºE-160ºW, 10ºS-10ºN). (b) Time series of the annual mean SLP difference between tropical eastern Pacific (120ºW-80ºW, 10ºS-10ºN) and TWP. (c) Time series of the annual mean SLP difference between southeastern Pacific (120ºW-70ºW, 35ºS-15ºS) and TWP. Plotted are 5-year running means. Green, black and blue lines are from the NOAA ERSLP, NCEP/NCAR reanalysis, and ECMWF reanalysis, respectively. The straight red lines are the linear regressions from using ERSLP. Unit of SLP difference is hPa.

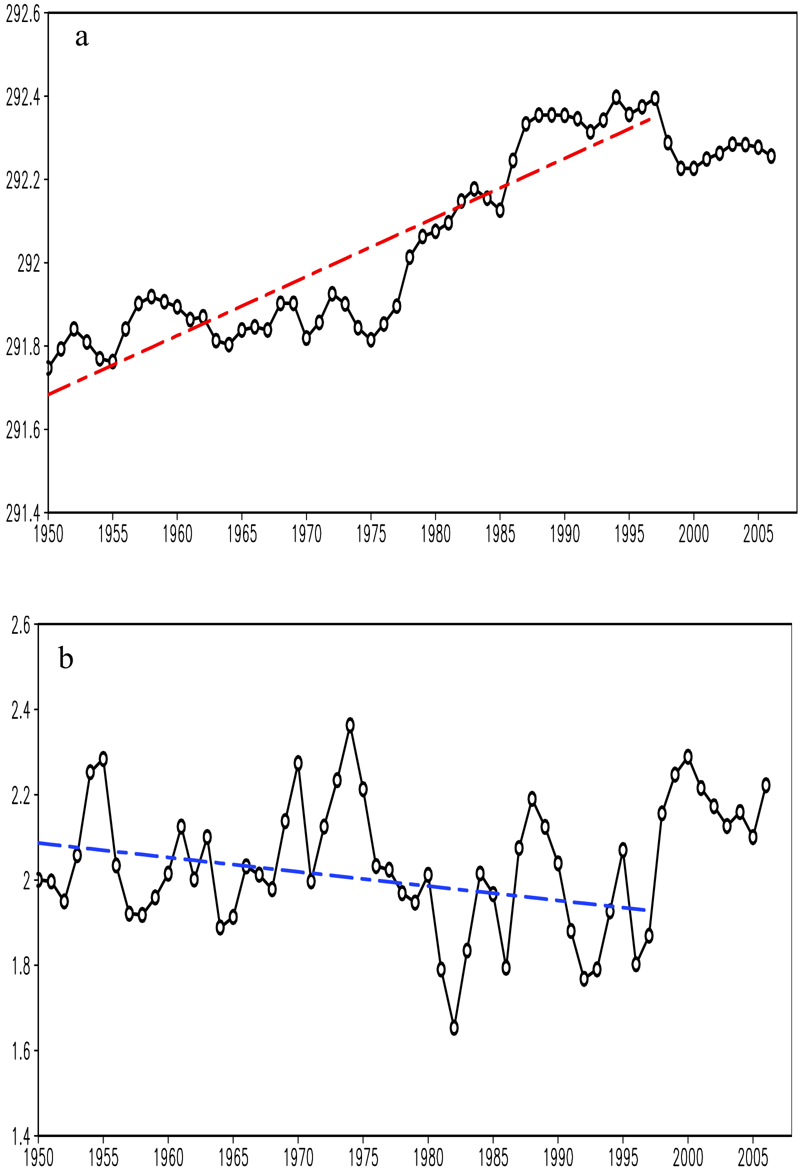

Figure 3.3: (a) Time series of global mean SST. (b) Time series of annual mean SST difference between TWP (100ºE-160ºW, 30ºS-30ºN) and TEP (160ºW-80ºW, 30ºS-30ºN). Plotted are 5-years running means. The straight dash lines are the linear regressions from 1950 to 1997. Trends are 1.42 ± 0.15 K/100years in (a), and -0.34 ± 0.28 K/100years in (b). The ± values define the 95% confidence intervals for the trends. Estimates are from HadISST dataset. Unit of SST is K.

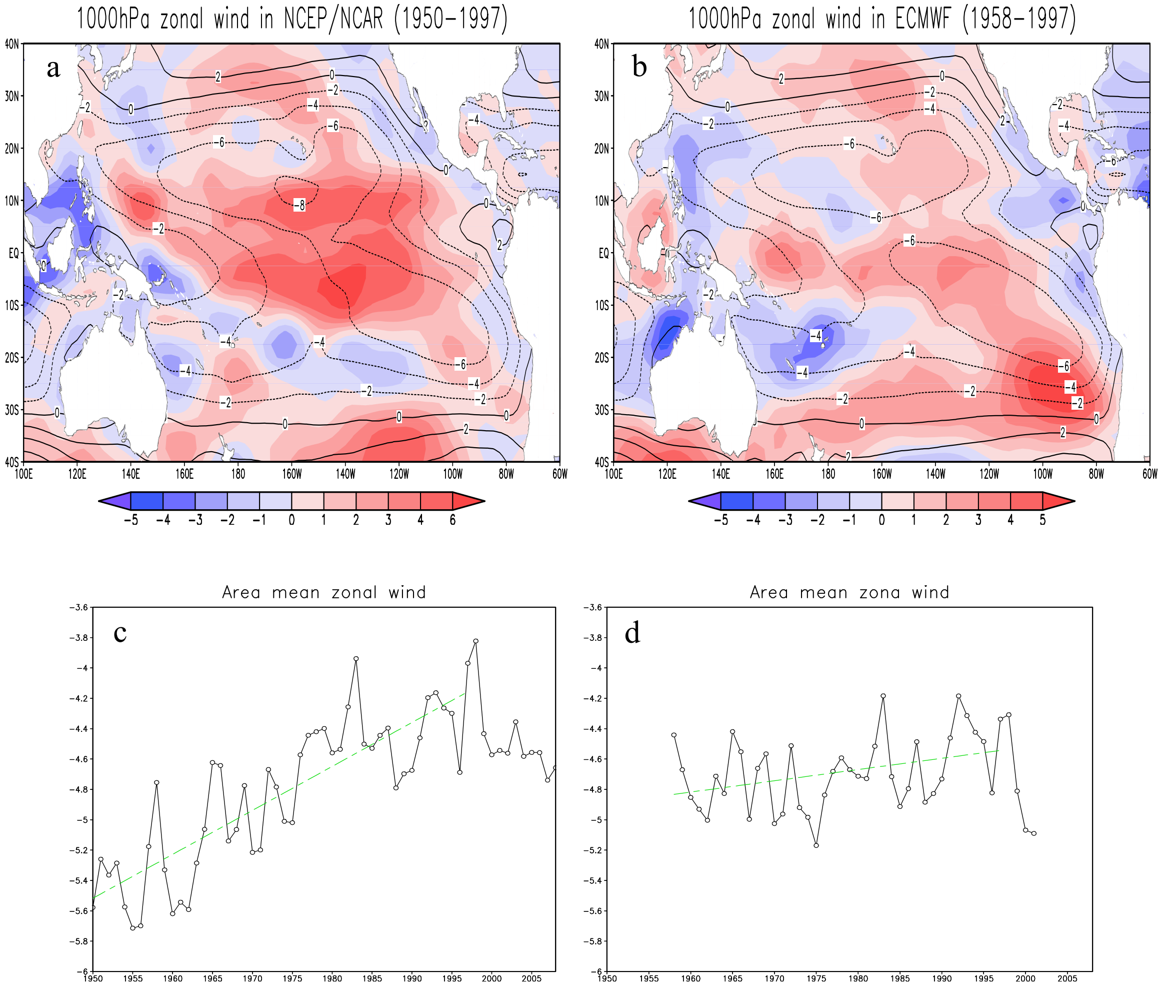

Figure 3.4: Climatology (contour) and linear trends (image) of annual mean 1000-hPa zonal wind in the NCEP/NCAR (a) and ECMWF (b) reanalyses. Area mean (160ºE-80ºW, 15ºS-15ºN) zonal wind in the NCEP/NCAR (c) and in ECMWF (d) reanalyses. Units of wind and trend are m/s and m/s/100years, respectively. Green lines are linear trend regressions. Trends of area mean zonal wind are 2.90±0.54 m/s/100years in the NCEP/NCAR reanalysis from 1950 to 1997 and 0.74±0.59 m/s/100years in the ECMWF reanalysis from 1958 to 1997. The ± values define the 95% confidence intervals for the trends.

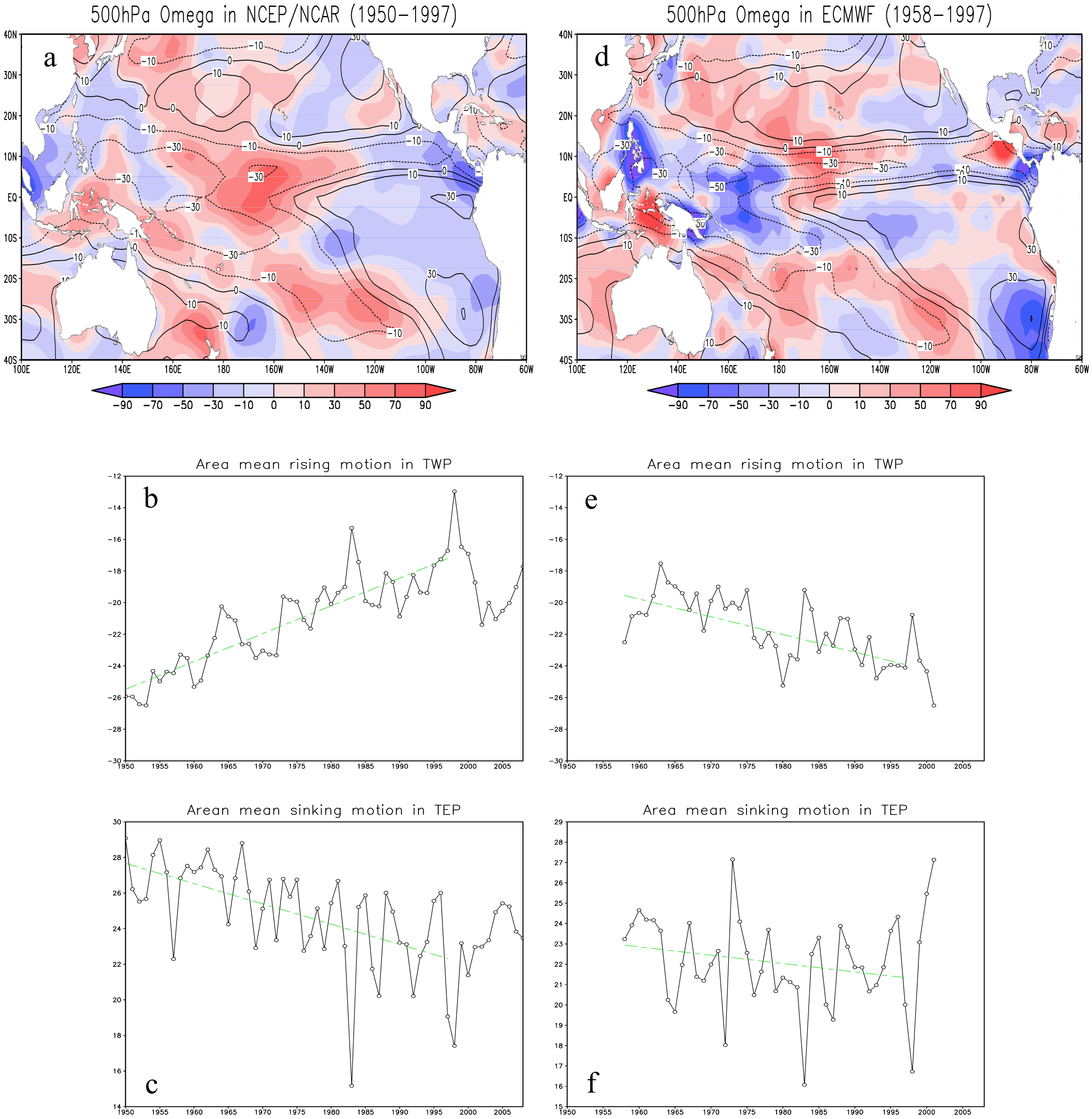

Figure 3.5: Climatology (contour) and linear trends (image) of annual mean 500-hPa vertical pressure velocity in the NCEP/NCAR reanalysis (a). Area mean rising motion in TWP (120ºE-140ºW, 15ºS-20ºN) (b) and area mean sinking motion in TEP (120ºW-80ºW, 30ºS-5ºN) (c) in the NCEP/NCAR reanalysis. (d) is same as (a) but in ECMWF reanalysis. (e) is same as (b) but in ECMWF reanalysis. (f) is same as (c) but in ECMWF reanalysis. Units of omega and trend are hPa/day and hPa/day/100years, respectively. Green lines are linear regressions. Trends of area mean rising motion are 17.56±2.71 hPa/day/100years in NCEP/NCAR from 1950 to 1997 and -11.20±3.85 hPa/day/100years in ECMWF from 1958 to 1997, trends of area mean sinking motion are -11.38±4.58 hPa/day/100years in NCEP/NCAR from 1950 to 1997 and -4.10±5.27 hPa/day/100years in ECMWF from 1958 to 1997. The ± values define the 95% confidence intervals for the trends.

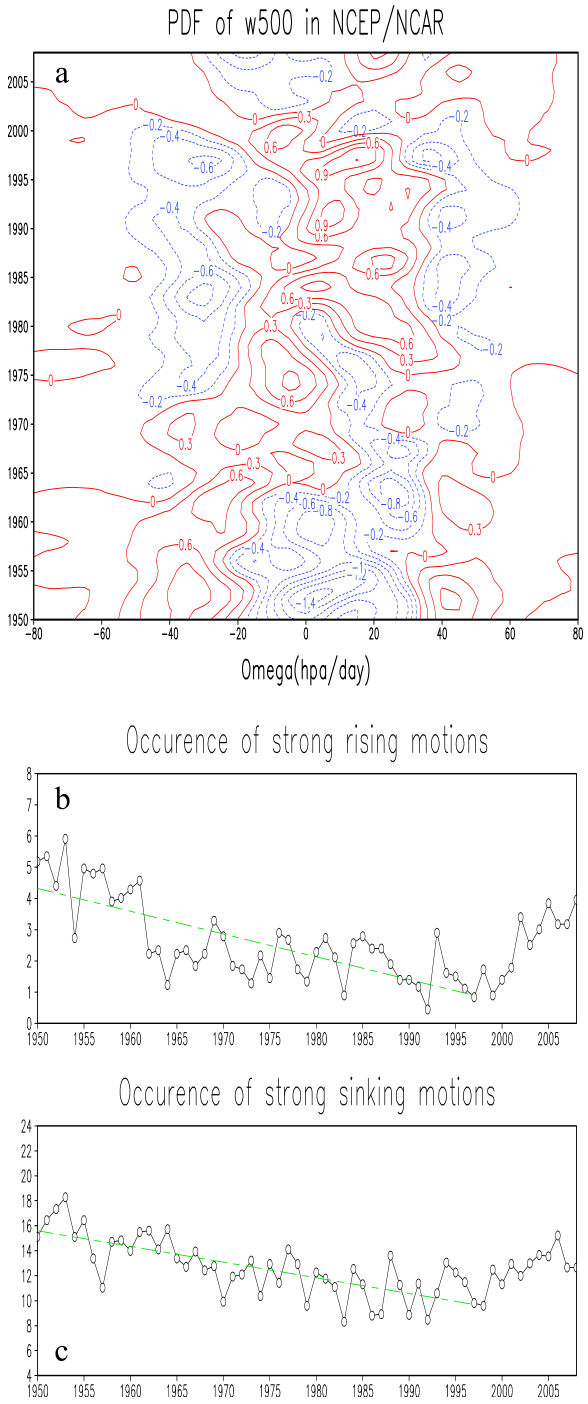

Figure 3.6: (a) PDF anomalies of annual mean 500-hPa vertical pressure velocity over the tropical Pacific (110ºE-80ºW, 30ºS-30ºN). (b) Occurrence of strong rising motions (omega<-40hPa/day) over tropical pacific. (c) Occurrence of strong sinking motions (omega>35hPa/day) over tropical pacific. Unit of PDF and occurrence are %. Data are from the NCEP/NCAR reanalysis. Green lines are linear regressions from 1950 to 1997. Trends are -7.30±1.75 %/100years in (b), and 12.57±3.18 %/100years in (c). The ± values define the 95% confidence intervals for the trends.

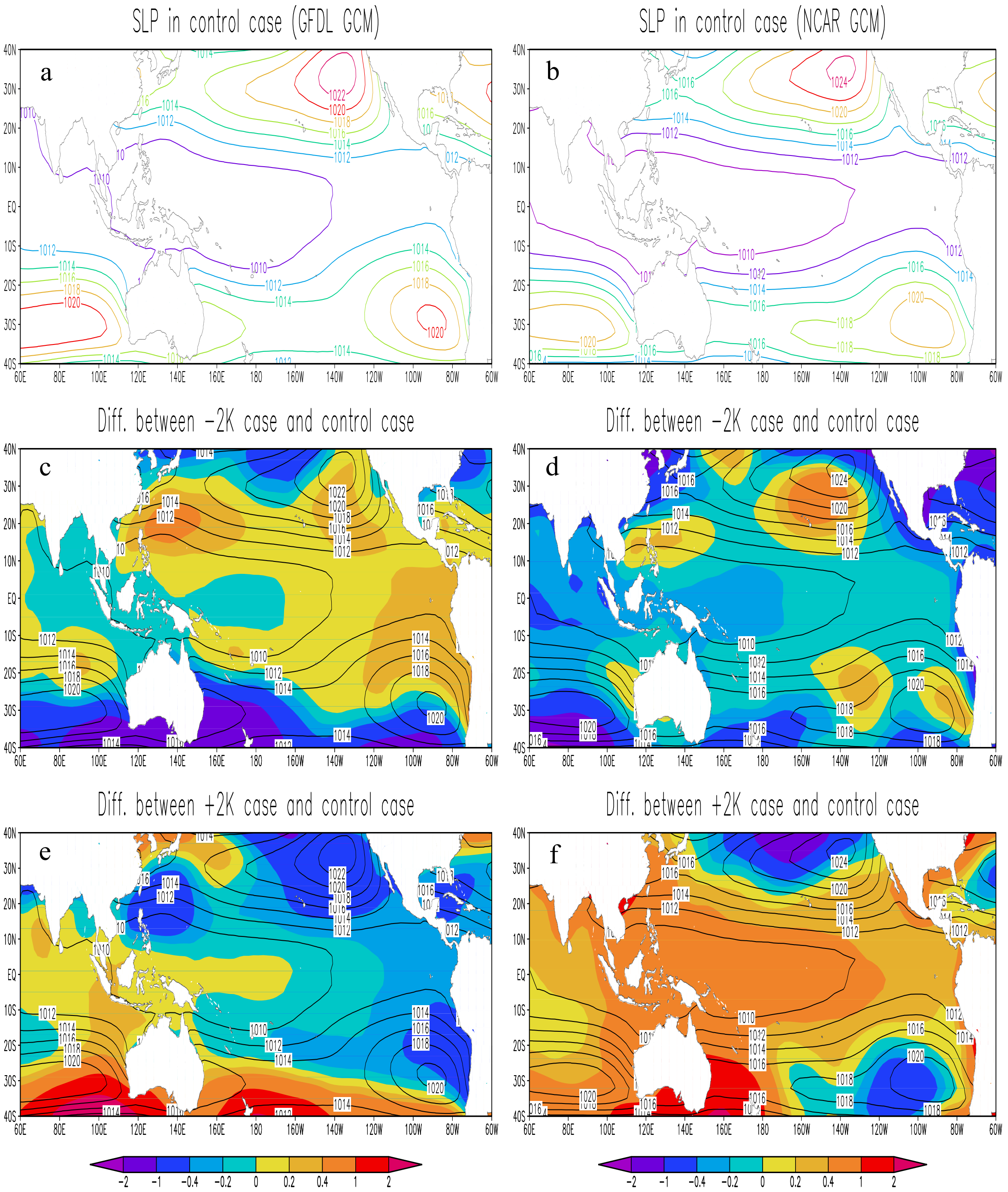

Figure 3.7: (a) and (b) are annual mean SLP in the control case, (c) and (d) are the difference in annual mean SLP between -2K case and control case, (e) and (f) are the difference in annual mean SLP between +2K case and control case. Left panel is from GFDL AM2 runs, right panel is from NCAR CAM3 runs. Unit of SLP is hPa.

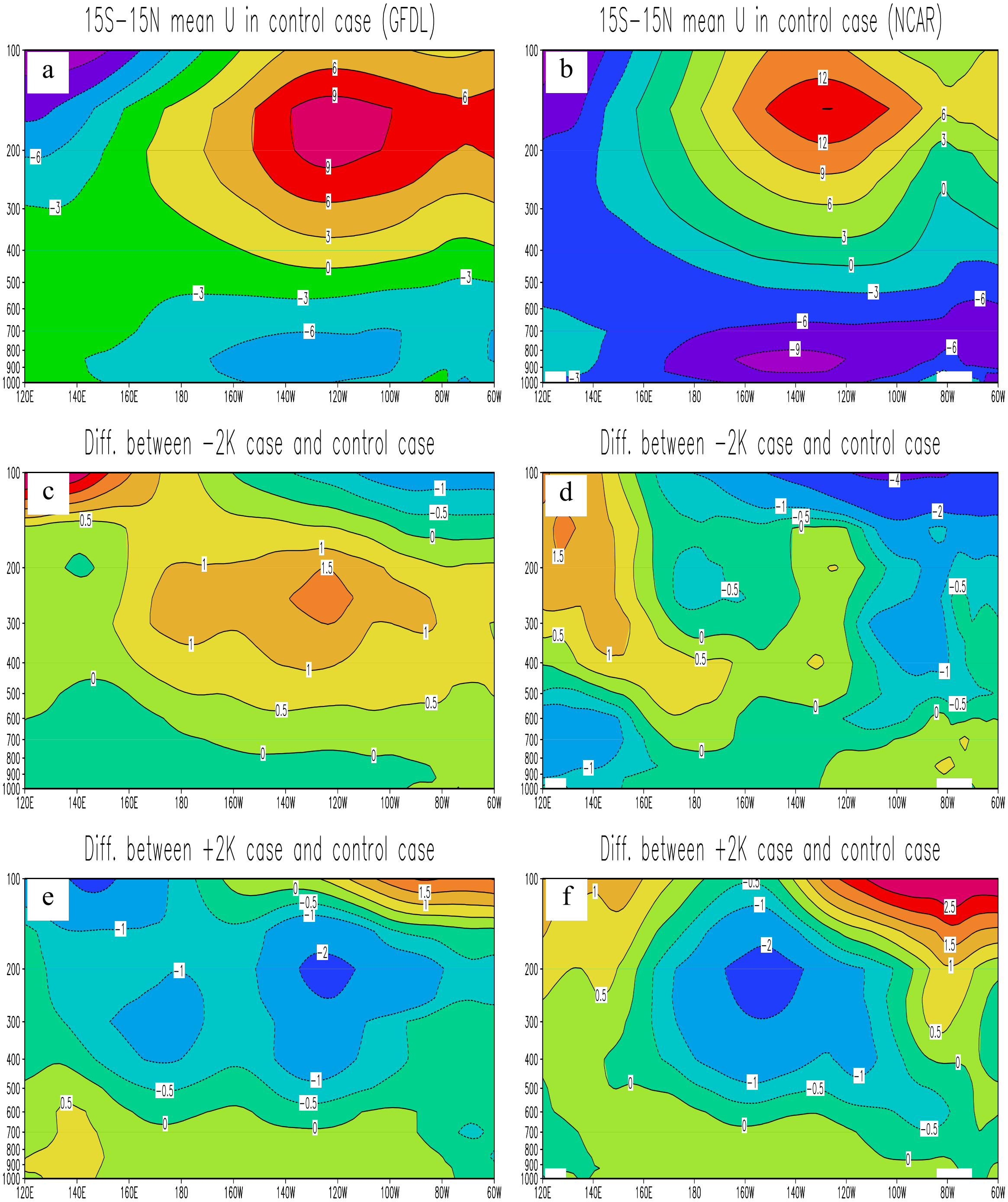

Figure 3.8: (a) and (b) are annual mean latitudinal mean zonal wind (15ºS-15ºN) in the control case, (c) and (d) are the difference in annual mean latitudinal mean zonal wind between -2K case and control case, (e) and (f) are the difference in annual mean latitudinal mean zonal wind between +2K case and control case. Left panel is from GFDL AM2 runs, right panel is from NCAR CAM3 runs. Unit of wind is m/s.

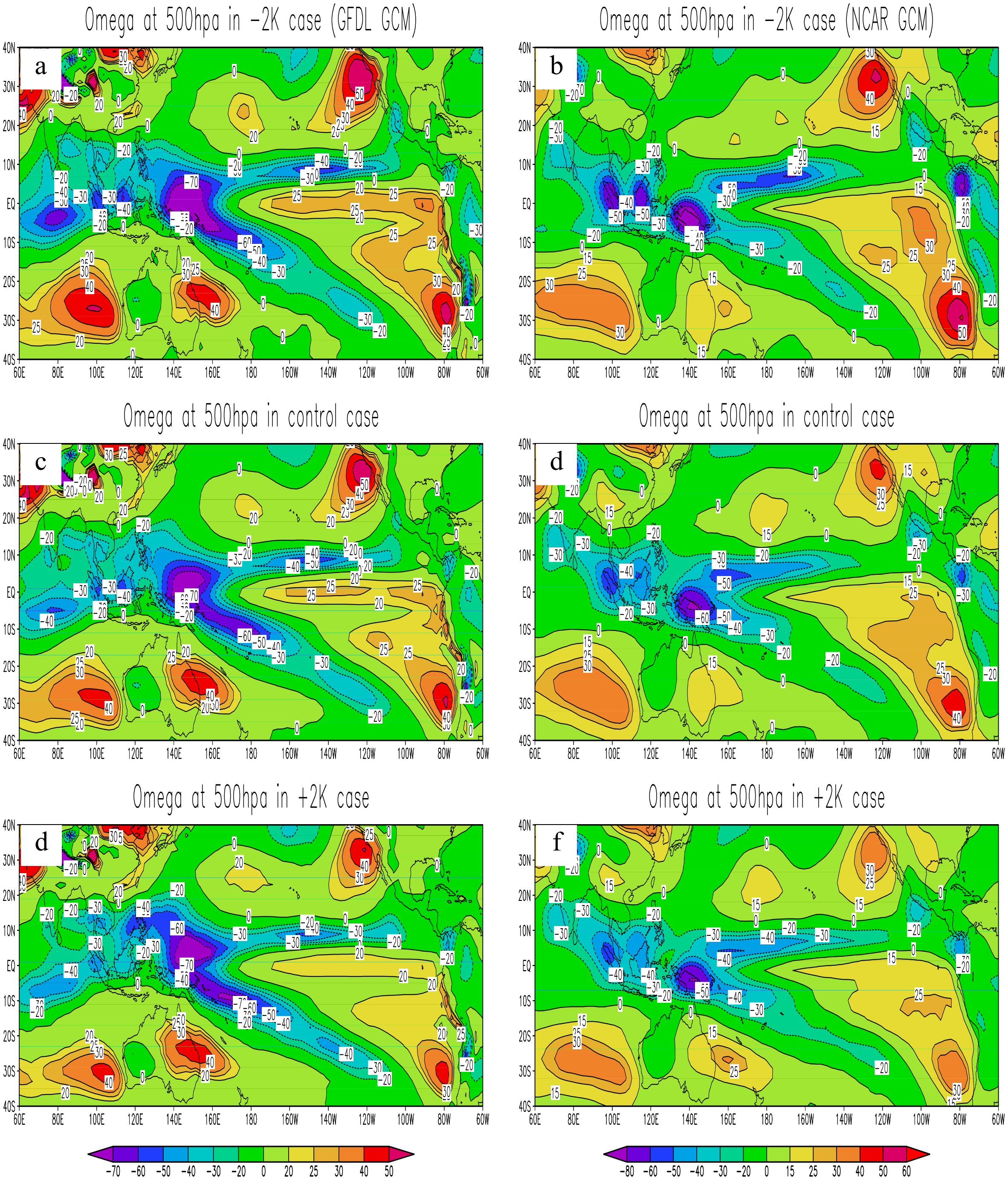
Omega at 500hpa in −2K case (GFDL GCM)

Omega at 500hpa in −2K case (NCAR GCM)

Omega at 500hpa in control case

Omega at 500hpa in control case

Omega at 500hpa in +2K case

Omega at 500hpa in +2K case

Figure 3.9: (a) and (b) are annual mean 500-hPa vertical pressure velocity (omega) in the control case, (c) and (d) are the difference in annual mean 500hPa omega between -2K case and control case, (e) and (f) are the difference in annual mean 500hPa omega between +2K case and control case. Left panel is from GFDL AM2 runs, right panel is from NCAR CAM3 runs. Unit of omega is hPa/day.

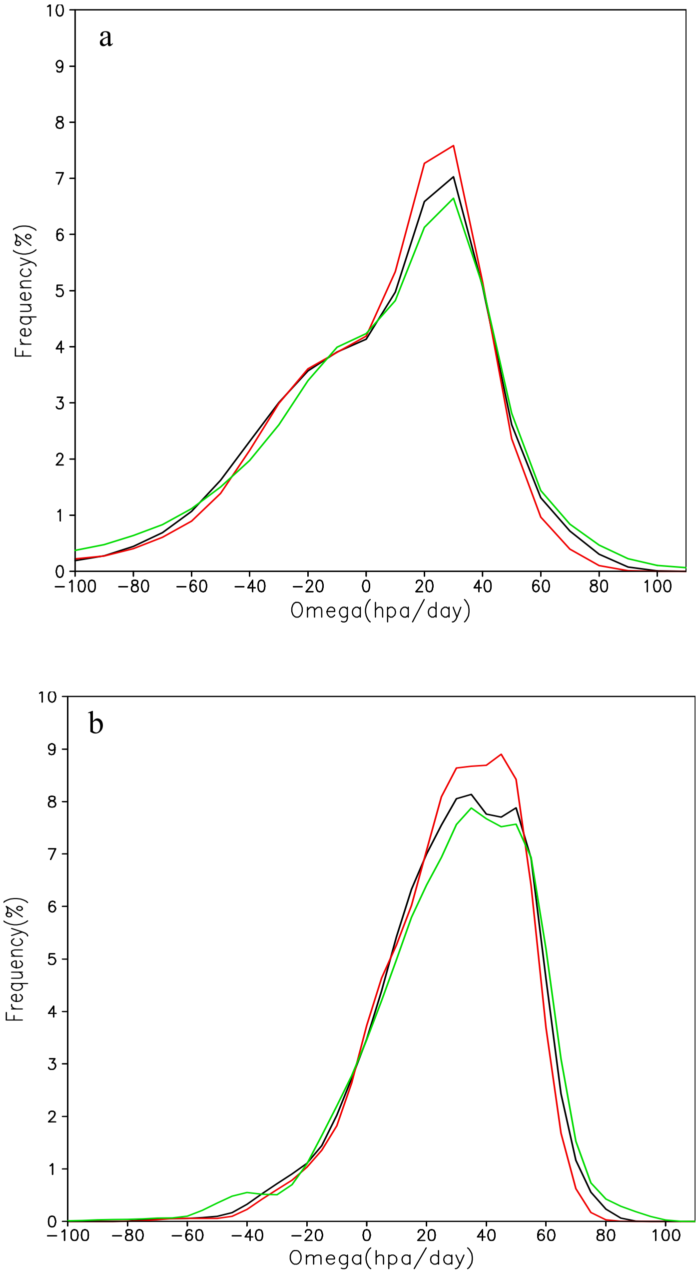

Figure 3.10: Probability distribution function (PDF) of annual mean 500-hPa vertical pressure velocity over the tropics from GFDL AM2 (a) and NCAR CAM3 (b) runs, Black line is from the control case, green line is from -2K case, and red line is from +2K case. Units of vertical pressure velocity and PDF are hPa/day and %, respectively.

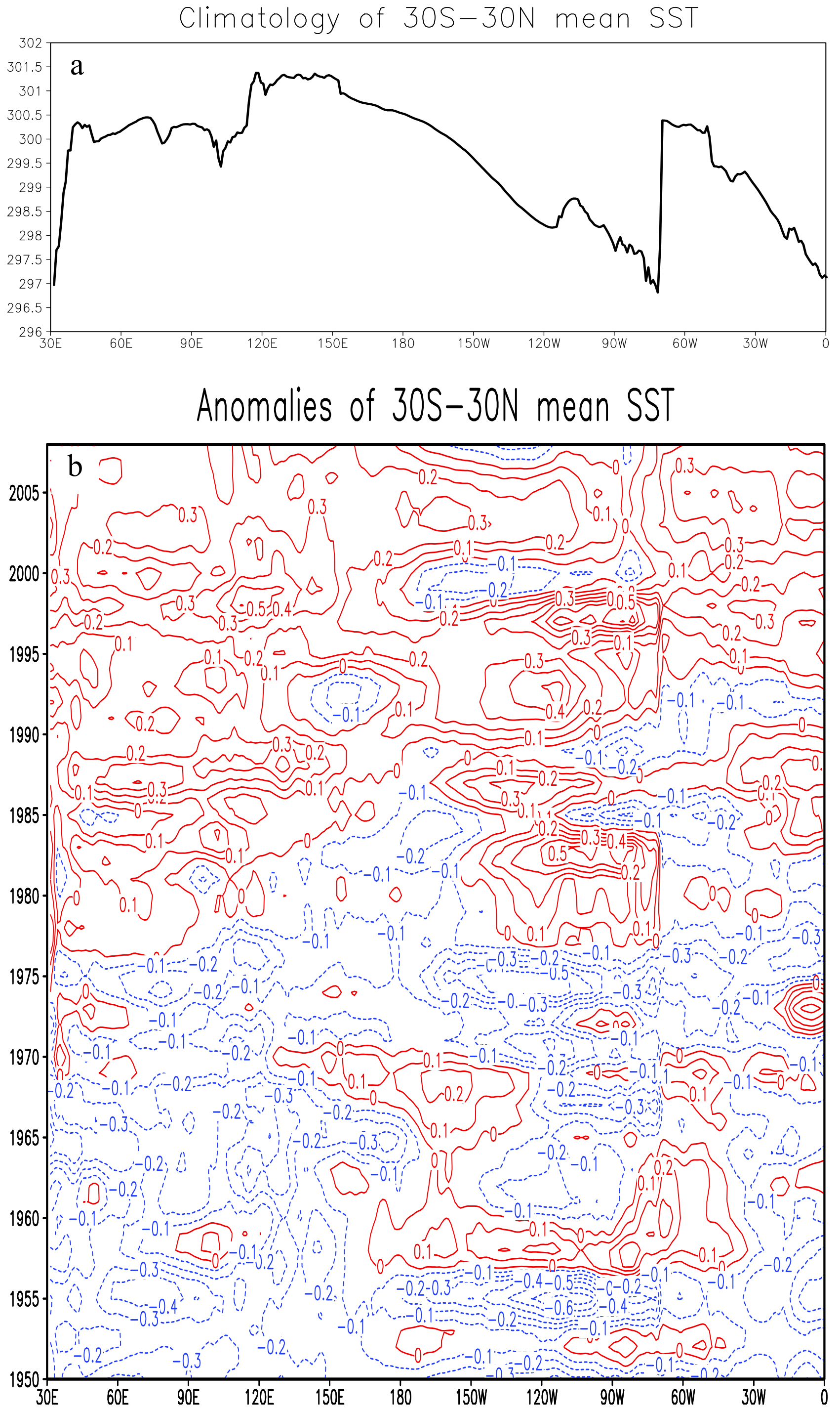

Figure 3.11: (a) is 59-year averaged 30ºS-30ºN latitudinal mean SST. (b) is the anomalies of 30ºS-30ºN latitudinal mean SST from 1950 to 2008. The data are from HadISST. Unit of SST is K.

Chapter 4

Long-term Change of the Hadley Circulation

In this chapter, long-term change of the Hadley circulation will be investigated. Special attention is paid to the trend difference of the Hadley circulation in the two reanalysis products, since both the NCAR/NCEP and ECMWF reanalyses used similar input data of operational radiosondes and satellite measurements but they showed significant differences in the intensity trend in the last fifty years. The first purpose of the study is to reveal consistent as well as inconsistent features of the Hadley circulation in the two reanalyses. The second purpose is to evaluate which product is more realistic. Model outputs of the AMIP runs are also analyzed and compared with the reanalysis results.

4.1 Data and Methods

Wind and precipitation fields from the NCEP/NCAR and ECMWF (ERA-40) reanalyses are used to investigate the long-term change of the Hadley circulation. Cloud fields and their radiative impacts in the reanalyses are also used. They are compared with the ship-based cloud observations from the EECRA (Courtesy of Dr. Joel Norris).

Upper-level cloud cover data from the EECRA have been used (Norris, 2005). The EECRA cloud data are independent of the two reanalyses.

Sea level pressures (SLP) in the two reanalyses are also used. They are compared with the observed SLP data in the ERSLP analysis of the NOAA National Climate Data Center from January 1950 to December 1997.

Outputs of the AMIP runs from the four widely used models: NCAR CCSM3, GFDL-CM2.1, MPI-OM and UKMO-HadGEM1 are also used. The AMIP runs include only the atmospheric component of the GCMs forced by the prescribed SSTs. More information can be found on the IPCC web site (http://www-pcmdi.llnl.gov/ipcc/about_ipcc.php). Model results are presented from 1979 to 2000.

The strength and geometry of the Hadley circulation can be quantified by using a stream function. The stream function expresses the fact that, for a two-dimensional flow, the conservation of mass equation couples motion in one direction with motion in the other direction, so one variable (stream function) can fully describe the flow (Cook, 2004). The stream function here is calculated by the vertical integration of the zonal mean meridional wind (Oort and Yienger, 1996).

The Helmholtz theorem (e.g., Arken, 1985) states that the horizontal wind vector $\vec{V}$ may be divided into a rotational component $\vec{V}_\psi$ and a divergent component $\vec{V}_d$. The rotational part does not contribute to atmospheric divergences associated with vertical motion. Here, the meridional component of the divergent wind V_d at 200-hPa and 850-hPa is used as an index to study the intensity changes of the Hadley circulation. The zonal average of meridional divergent wind V_d is the same as that of the total meridional wind.

4.2 Long-term Change of the Boreal Winter Hadley Circulation

Figure 4.1a shows the climatology of stream function during boreal winter (DJF) in the ECMWF reanalysis. As represented by the contours of stream function, the tropical Hadley cell is a major component of the global mass circulation, which also consists of the Ferrel cell in the mid-latitudes and the polar cell in the high latitudes. In boreal winter, the Northern Hemisphere Hadley cell dominates, with the maximum of 20.6×10^{10}kg/s located around 10ºN. Similar features are disclosed in the NCEP/NCAR reanalysis (figure not shown). Figures 4.1b and 4.1c are the linear trends of the DJF stream function in the NCEP/NCAR and ECMWF reanalyses from 1958 to 2002, which both clearly show a significantly strengthened Hadley cell. In this chapter, the entire data record of the ECMWF reanalysis is used, since there is no large difference in the variation of the Hadley circulation whether the end year is 1997 or 2002. Figures 4.1b and 4.1c show that the intensification of the Hadley circulation is much stronger in the ECMWF reanalysis than in the NCEP/NCAR reanalysis. In the following section 4.3, I will focus on this difference between the two reanalysis datasets in the boreal winter and reveal whether the trends are realistic.

4.3 Evaluation of the Difference between NCEP/NCAR and ECMWF Reanalyses

Figures 4.2a and 4.2b show the DJF climatology of the zonally averaged meridional wind V_d at 200-hPa and 850-hPa in the NCEP/NCAR and ECMWF reanalyses. The red line represents the zonal mean V_d at 200-hPa and the green line represents the zonal mean V_d at 850-hPa. A closed Hadley cell, as highlighted by the arrows, is seen clearly with northward wind at the upper level and southward wind at the lower level between 15^{o}S and 25^{o}N, consistent in the two reanalyses. The maximum rising motion, which can be judged roughly from the slopes of the curves, is around 15ºS-5ºS; and the maximum sinking motion is around 20ºN-30ºN. Figures 4.2c and 4.2d show the time evolution of the zonal mean 200-hPa V_d anomalies relative to the respective climatology in the two reanalyses since the 1950s. The data length in ECMWF reanalysis is slightly shorter than in the NCEP/NCAR reanalysis. It is seen that both reanalyses show consistent intensification of the 200-hPa northward meridional wind from 10^{o}S to 20^{o}N.

The intensification of the Hadley circulation is contributed by the climate shift in the 1970s that coincided with the introduction of satellite data around 1979 (Hurrell and Trenberth, 1999). Figures 4.2c and 4.2d however suggest that this increasing trend is present even before and after the 1970s transition period. This is most clearly seen in Figures 4.2e and 4.2f which show the time series of the difference between the maximum zonal mean V_d at 200-hPa and the minimum zonal mean V_d at 850-hPa in the two reanalyses. Figures 4.2e and 4.2f also show that the increasing trend of the Hadley circulation is much larger in the ECMWF than that in the NCEP/NCAR product, consistent with what Mitas and Clement (2005) found. The linear trends are about 1.94 m/s/100years and 4.15 m/s/100years in the NCEP/NCAR and ECMWF reanalyses, respectively.

To understand the trend differences, Figure 4.3 shows the spatial patterns of the meridional divergent winds at 200-hPa and their trends in the two reanalyses. While V_d

is not the actual meridional flow, it can be used to examine the regional contribution of the divergent wind to the zonal averaged circulation. The 10°N latitude is highlighted around which the zonal averaged V_d peaks. The climatology of V_d in Figures 4.3a and 4.3b shows that the 200-hPa V_d around 10°N is northward across the whole tropics except over the eastern oceans. The maxima are over regions of the Australian monsoon. These are similar in the two datasets.

The trends of V_d in the two products however exhibit large inconsistencies. In Figure 4.3c over the tropical western and central Pacific from 120°E to 140°W south of 10°N, the trend pattern in the NCEP/NCAR reanalysis is out of phase with the climatology of V_d, which suggests weakening of the overturning cell. In contrast, Figure 4.3d shows that in the ECMWF reanalysis south of 10°N the trend pattern is in phase with the climatology of V_d over the tropical western Pacific (TWP), indicating strengthening of the overturning cell. The trends of V_d over North America, Africa and the Eurasian continents in the two reanalysis products all have the same signs as the basic climatology that represent intensification of the circulation. As a result, the two reanalyses both exhibit increasing zonally averaged meridional wind at 200-hPa, but a much weaker trend in the NCEP/NCAR product, owing to the different trend pattern over the tropical western and central Pacific.

Since the two reanalysis products are both constrained by the radiosonde data in the assimilation processes, it is not surprising that the two data sets show somewhat consistent trends over the continents. Over the oceans, however, few in-situ measurements exist. The divergent winds are essentially a model product.

The trend features in Figures 4.3c and 4.3d can be characterized by the decreasing of the 200-hPa meridional divergences in the NCEP/NCAR reanalysis and the increasing of divergence in the ECMWF reanalysis in the TWP region from 110ºE to 160ºW and 20ºS to 10ºN, a region of the upward branch of the Hadley circulation. Rising motions are associated with outward transport of atmospheric energy in the troposphere because the moist static energy in the upper troposphere is much larger than that in the lower troposphere (it decreases with altitude below 600-hPa and increases rapidly with altitude above 600-hPa). I will therefore use the variation of the moist static energy budget to infer the reliability of the trends.

The total vertically integrated horizontal transport of the atmospheric moist static energy (which is denoted as TET) directed outward of an air column can be written as:

$$\begin{aligned} TET &= \frac{1}{g}\int_{p_T}^{p_s} \nabla\cdot(\vec{V}h)dp = \frac{1}{g}\int_{p_T}^{p_m} \nabla\cdot(\vec{V}h)dp + \frac{1}{g}\int_{p_m}^{p_s} \nabla\cdot(\vec{V}h)dp \\ &= \frac{1}{g}\overline{h}_{up}\int_{p_T}^{p_m}(\nabla\cdot\vec{V})dp + \frac{1}{g}\overline{h}_{low}\int_{p_m}^{p_s}(\nabla\cdot\vec{V})dp \end{aligned} \tag{4.1}$$

where $h = c_p T + gz + L_v q$ is the moist static energy of the atmosphere, p_T, p_m and p_s represent the pressures at the top of the divergence layer, at the divergence transition interface in the middle of the troposphere, and the bottom of the surface convergence layer, respectively. $\overline{h}_{up}$ and $\overline{h}_{low}$ are the wind-weighted moist static energy in the upper troposphere and in the lower troposphere. Here I have assumed a single baroclinic mode of winds in the troposphere which should be a good approximation in the tropics on annual time scales.

By using the vertical velocity ω in the middle of the troposphere:

$$\omega_{\max} = -\int_{p_T}^{p_m} (\nabla \cdot \vec{V})dp = \int_{p_m}^{p_s} (\nabla \cdot \vec{V})dp \tag{4.2}$$

Equation (4.1) can be rewritten as:

$$TET = -\frac{1}{g}\omega_{\max}\,(\bar{h}_{up} - \bar{h}_{low}) \tag{4.3}$$

Hence, the total energy transport can be considered as a proxy of the vertical velocity when the atmospheric thermodynamic structure is known. On the other hand, the total energy transport can be further related to other components of the atmospheric energy budget through:

$$TET = SWC + SWCF + LWC + LWCF + SH + LH \tag{4.4}$$

On the right-hand side of the above equation, the terms are the clear sky shortwave radiative heating in the atmosphere (SWC), shortwave cloud forcing (SWCF), clear sky longwave radiative heating (LWC), longwave cloud forcing (LWCF), sensible and latent heating (SH and LH). We note that the reanalyses generally do not conserve mass and energy (e.g., Trenberth, 1997). However, because few radiosonde data were available in the TWP region and the two reanalyses are mostly model products, the internal imbalance should be of less a concern. Furthermore, the energy components are only used here to demonstrate the differences between the two products.

The two left panels in Figure 4.4 show the climatology of all energy components in equation (4.4) averaged from 110ºE to 160ºW and 20ºS to 10ºN. The sources of the energy, in magnitude of decreasing order, are latent heating, clear-sky solar radiative heating, longwave cloud forcing, and turbulent heating from sensible heat fluxes. Major sinks of energy are the clear-sky longwave cooling (LWC) and atmospheric heat transport. It is noted here that the atmospheric shortwave cloud forcing is slightly negative in the NCEP/NCAR reanalysis, while it is positive in the ECMWF reanalysis, suggesting possible different amount of absorption of solar radiation in clouds in the two reanalyses. Overall, however, the climatologies are consistent among the two reanalyses.

Figures 4.4c and 4.4d show the differences of these components between the epochs of 1980 to 2000 and 1958 to 1975 in the NCEP/NCAR reanalysis and in the ECMWF reanalysis, respectively. The error bars represent the 95% statistical confidence intervals. Consistent with the deductions from the trends of the upward motion in the two reanalysis products, the total outward energy transport (TET) has decreased in the NCEP/NCAR reanalysis, but increased in the ECMWF reanalysis. The largest inconsistency in the two reanalyses is in the LWCF, with the NCEP/NCAR reanalysis showing decreased LWCF but the ECMWF reanalysis showing increased LWCF. Other components of the trends in Figure 4.4c and Figure 4.4d are mostly similar in the two reanalyses: (1) enhanced clear-sky longwave cooling (LWC), owing to the dominance of the Stafan-Boltzman temperature feedback and its lapse-rate effect over the water vapor greenhouse effect (e.g., Zhang et al. 1994), (2) statistically insignificant change of the surface sensible and latent heat fluxes, and (3) increased amount of the sum of clear-sky SWC and SWCF (with the small magnitudes of the change in SWC and SWCF here, the two are better viewed together rather than separately due to the definition of the SWCF (Soden et al., 2005)). Therefore, the difference in the LWCF largely contributed to the opposite signs in the atmospheric net outward energy transport between the NCEP/NCAR and ECMWF reanalyses.

Figure 4.5 shows the time series of area mean LWCF over the TWP (110ºE-160ºW, 20ºS-10ºN) in the two reanalyses. LWCF over the TWP are significantly decreased in the NCEP/NCAR reanalysis but significantly increased in the ECMWF reanalysis from 1958 to 2002.

The trend difference of LWCF in the two reanalyses is also found to correspond well to that in the high cloud amount in the two reanalyses. In the NCEP/NCAR reanalysis, consistent with the reduced LWCF, upper-level clouds decreased in 1980-1997 relative to that in 1958-1975 in the tropical western Pacific. In the ECMWF reanalysis, however, upper-level clouds increased in the later epoch, consistent with the increased LWCF. Changes of the upper-level clouds between epochs 1980-2000 and 1958-1975 for the two reanalyses also show the similar patterns to that in Figures 4.6a and 4.6b, respectively. Hence, over the TWP, the trends of the atmospheric outward energy transport, the longwave cloud forcing, upper level clouds, and the intensity of rising motion are all consistent among themselves in each individual reanalysis, but they have opposite signs in the NCEP/NCAR and ECMWF reanalyses.

The change of upper-level cloud from the independent EECRA data is now shown in Figure 4.6c. It is seen that over the TWP, the amount of upper-level clouds has decreased. This is more consistent with the NCEP/NCAR reanalysis in this region than with the ECMWF reanalysis. While many uncertainties can be attached to the observed cloud data, the trends of EECRA upper-level clouds do show a statistically significant decrease. Further calculation of changes in the total and low cloud amount gives similar pattern (not shown here).

Figure 4.7 shows the time series of area mean upper-level cloud over the TWP (110ºE-160ºW, 20ºS-10ºN) in the three datasets. High clouds over the TWP are significantly decreased in both the NCEP/NCAR reanalysis and EECRA data during the last fifty years, while they are significantly increased in the ECMWF reanalysis. Furthermore, the linear trend in the EECRA is -8.09 ± 6.45 %/100years relative to that of -4.67 ± 2.89 %/100years in the NCEP/NCAR reanalysis, implying possible larger weakening of the vertical circulation in the EECRA data.

It is beyond the scope of this study to explain the cause of the cloud changes in the two reanalyses. It is plausible that the enhanced upward motion increases the amount of high clouds in the reanalysis, due to more vigorous convection and detrainment of cirrus clouds, and vice versa. Here, the association of the trends between rising motions and the upper-level cloud amount over the TWP is made through the energy budget consideration of equation (4.4). Namely, strengthening vertical circulation corresponds to more outward energy transport, which is balanced by increasing LWCF due to the increasing amount of clouds; and vice versa.

A second verification can be gained on the atmospheric vertical circulation trends in the TWP from the sea level pressure (SLP), as used in Zhang and Song (2006) to report the weakening of the Walker circulation. Figure 4.8a shows the climatology (contour) and linear trend (image) of the SLP in the NOAA ERSLP data in DJF from 1951 to 1997 in the tropical Pacific. The ERSLP data exhibit increasing trends of SLP in the TWP and decreasing trends of SLP in the subtropics. The regional meridional gradient of SLP in the tropical western Pacific, a proxy of the intensity of meridional circulation, is therefore decreasing. The time variations of this gradient, when expressed as the difference of the SLP in the two boxes in Figure 4.8a (110ºE-180ºE & 20ºS-0ºS versus 110ºE-180ºE & 15ºN-30ºN) in the NOAA ERSLP data as well as in the two reanalyses, are shown in Figure 4.8b. It is seen that this measure of the trend is also more consistent with the NCEP/NCAR reanalysis than with the ECMWF reanalysis, reinforcing our conclusion from the analysis of upper-level clouds. Furthermore, the decreasing trend is larger in the ship-based data than in the NCEP/NCAR reanalysis.

The above analysis leads me to the following conclusions: (1) the different magnitudes of the strengthening of the Hadley circulation in the ECMWF and NCEP/NCAR reanalyses for the boreal winter are largely contributed by the differences over the tropical western Pacific where input data to the operational analyses are sparse; (2) the differences in the trends between the two reanalyses are consistent with those in the moist static energy transport and the longwave cloud radiative forcing; (3) the NCEP/NCAR reanalysis, which shows a less strengthening of the Hadley circulation than the ECMWF reanalysis, is more consistent with independent observations from EECRA and ERSLP; and (4) even the NCEP/NCAR reanalysis may have overestimated the strengthening of the Hadley circulation based on the comparison with the EECRA and ERSLP data.

4.4 Long-term Change of the Boreal Summer Hadley Circulation

Figure 4.9a shows the climatology of stream function during boreal summer (JJA) seasons in the ECMWF reanalysis. In boreal summer, the Southern Hemisphere Hadley cell dominates, with the minimum of -25.7×10^{10} kg/s located around 5ºS. Figures 4.9b and 4.9c are the linear trends of the JJA stream function in the NCEP/NCAR and ECMWF reanalyses from 1958 to 2002. The trend patterns in the two reanalyses show large spatial differences. Overall, it is seen in the two reanalyses that, in the north part of the Hadley circulation, the stream functions show weakening trends, while in the south part, the stream functions show strengthening trends, corresponding to reduced upward vertical circulation centered around 15^{o}N, but increased upward motion near the equator and downward motion around 30^{o}S. As will be shown later, this spatial pattern is related with the zonal asymmetry of the upward motion that is displaced south to the summer monsoon systems in the Northern Hemisphere.

Figures 4.10a and 4.10b show the JJA climatology of the zonal mean meridional vertical shear (v_{200}-v_{850}) in the NCEP/NCAR and ECMWF reanalyses. Figures 4.10c and 4.10d show the time evolutions of the zonal mean meridional vertical shear anomalies relative to the respective climatology in the two reanalyses since 1958. It is seen that both reanalyses show a southward shift of the minimum vertical shear from 1958 to 2002.

Figures 4.11a and 4.11b show the JJA climatology of the zonal mean precipitation in the two reanalyses. Time evolutions of the zonal mean precipitation anomalies in the two reanalyses are shown in Figures 4.11c and 4.11d. The maximum zonal mean precipitation is around 8ºN. In the NCEP/NCAR reanalysis, precipitation around 7ºN to 25ºN changed from the positive anomalies to negative anomalies since 1958 while precipitation around 15ºS to 7ºN changes from the negative anomalies to positive anomalies, revealing a southward shift of zonal mean precipitation belt, which is also seen in the ECMWF reanalysis despite no significant changes around 10ºN-25ºN.

Figure 4.12a shows the climatology of JJA 500-hPa vertical pressure velocity in the NCEP/NCAR reanalysis. It is seen that there is a broad rising motion over the Asian monsoon region around 50ºE-140ºW, 15ºS-30ºN and over the regions of the North American monsoon and African monsoon, which are all located mostly to the north of the equator. The zonal maximum is around 10^{o}N as highlighted in the figure.

Linear trends of 500-hPa vertical pressure velocity in the two reanalyses are shown in Figures 4.12b and 4.12c. The strongly enhanced upward motions dominate in the equatorial regions, leading to an overall increase of zonal mean upward motion near the equator in both reanalyses (Figure 4.12d). From 10ºN-20ºN, however, both reanalyses indicate overall decrease of upward motion, which are contributed by the changes of monsoon systems and the changes over the central Pacific.

There are also some differences between the two reanalyses over the tropical Pacific: the vertical motions are weakened in the NCEP/NCAR reanalysis but not clear in the ECMWF reanalysis. Another difference is that rising motions over east Asia are intensified in the NCEP/NCAR reanalysis but weakened in the ECMWF reanalysis. This difference is further seen in Figure 4.12d which shows the climatology and trends of zonally averaged omega. In the climatology, the region with strongest ascending motions is around 10ºN. The trends in both the NCEP/NCAR and ECMWF reanalyses (red and blue lines) indicate that rising motions to the north of 10ºN are weakened with the former showing larger magnitude while those to the south of 10ºN are strengthened. Those trends lead to a southward shift of the strongest ascending belt.

Since the boreal summer Hadley circulation is closely associated with monsoon variations, in the next chapter I will focus on one monsoon system, namely the Asian monsoon, to investigate whether the trends in the two reanalysis products are real and what are the possible physical causes. Before that, I will compare in the next section the changes of the Hadley circulation in the reanalyses during both the boreal winter and summer seasons with those in general circulation models, following closely the methods used by Mitas and Clement (2006), so as to draw further conclusions on which features of the Hadley circulation changes are real.

4.5 Extent of the Hadley Circulation

In this section, I will investigate the changes of the mean intensity, the north-edge, the south-edge and the extent of the Hadley circulation from 1958 to 2002 in the two reanalyses. The mean intensity of the Hadley cell is defined by the maximum of the absolute stream function value, the north-edge latitude is defined by the northern latitude where the stream function is zero at 500-hPa, the south-edge latitude is defined by the southern latitude where the stream function is zero at 500-hPa. The extent of the Hadley cell is defined by the difference between the north-edge latitude and south-edge latitude. My focus is on the Northern Hemisphere (NH) Hadley cell in boreal winter and the Southern Hemisphere (SH) Hadley cell in boreal summer.

4.5.1 Boreal Winter Hadley Circulation

Figures 4.13a and 4.13b show that NH Hadley cell is significantly strengthened from 1958 to 2002 in both reanalyses. The north-edge of the Hadley cell shows poleward expansion from 1958 to 2002 in the two reanalyses, but both trends do not pass the 95% confidence levels (Figures 4.13c and 4.13d). The south-edge shows significantly poleward expansion in the NCEP/NCAR reanalysis, but equatorward shrink in the ECMWF reanalysis (Figures 4.13e and 4.13f). As a result, the extent of the NH Hadley cell is expanded from 1958 to 2002 in the NCEP/NCAR reanalysis, but changes little in the ECMWF reanalysis (Figures 4.13g and 4.13h). The consistent feature is therefore the intensification of the boreal winter Hadley circulation.

4.5.2 Boreal Summer Hadley Circulation

Figures 4.14a and 4.14b show that SH Hadley cell is slightly weakened from 1958 to 2002 in the NCEP/NCAR reanalysis, but significantly strengthened in the ECMWF reanalysis. The north-edge of the Hadley cell shows equatorward movement from 1958 to 2002 in the two reanalyses (Figures 4.14c and 4.14d). The south-edge shows significantly poleward expansion in the NCEP/NCAR reanalysis, but equatorward shrink in the ECMWF reanalysis (Figures 4.14e and 4.14f). As a result, the extent of the SH Hadley cell slightly shrank from 1958 to 2002 in the NCEP/NCAR reanalysis, but largely shrank in the ECMWF reanalysis (Figures 4.14g and 4.14h).

In my study, I consider it more fruitful to focus separately on the northern and southern portions of the zonally averaged Hadley cell since they represent vertical motions of different atmospheric systems in different longitudes. This had led to the finding of the consistent features of the two reanalyses: the weakening of the vertical upward motion in the northern portion that corresponds to the weakening of summer monsoon.

4.6 Change of the Hadley Circulation in the AMIP Simulations

4.6.1 Boreal Winter Hadley Circulation

The pattern of the global mass circulation (Figure 4.1a) is simulated well in the NCAR CCSM3 (Figure 4.15a), GFDL-CM2.1, MPI-OM and UKMO-HadGEM1 (figures not shown), though the magnitude of the simulated Hadley cell is somewhat weaker. Figures 4.15b to 4.15e are the time series of the maximum stream function in low latitudes for the boreal winter season in the four models. In the four AMIP runs, the Hadley circulation does not show statistically significant trends as shown in the two reanalyses (Figures 4.15f and 4.15g). Trends from 1979 to 2000 are 2.89 ± 10.9, 1.02 ± 8.73, 4.85 ± 13.87, 1.60 ± 9.80, in NCAR GCM, GFDL GCM, MPI GCM, UKMO GCM respectively in unit of 10^{10}kg/s/100yrs, versus 5.78 ± 6.00 and 25.89 ± 10.76 in the NCEP/NCAR and ECMWF reanalyses. Mitas and Clement (2006) argue that it is due to the significant discrepancies in the thermodynamic structure between models and reanalyses; the former show a warming trend throughout the troposphere with stronger warming aloft, while the latter show a cooling trend in the tropical mid-troposphere (Figure 4.16). As a result, the static stability averaged over the rising branch of the Hadley cell is increased in the four AMIP models but decreased in the two reanalysis (Figure 4.17). This difference is consistent with the different trends of the Hadley circulation in the models and in the reanalysis, since an increased static stability would correspond to weaker vertical motion (Mitas and Clement, 2006). Which change is more realistic of the vertical stability in the reanalysis and in the models is still an open question. Several previous studies cautioned on the quality of the reanalysis data in describing the humidity and water cycle (Trenberth and Guillemot, 1998; Trenberth et al., 2001) and on the possible impact on the trend of the introduction of satellite measurements around 1979 (Bengtsson et al., 2004; Kinter et al., 2004). The more serious challenges are however from the following two aspects. First, direct analysis of winds from the historical rawinsonde archive does not support a statistically significant trend of the Hadley circulation (Mitas and Clement, 2005). Second, temperature in the historical radiosondes may contain a systematic trend bias, owing to the daytime warm bias of radiosondes that has been gradually phased out in the last several decades (Sherwood et al., 2005). This temperature bias could have a direct impact on the Hadley circulation trend in the reanalyses through the data assimilation system (Mitas and Clement, 2006). Nevertheless, these two arguments do not automatically rule out the strengthening of the zonally averaged Hadley circulation in the real atmosphere, because the rawinsonde stations are sparse in the tropics and the quantitative impact of the temperature trend biases on the reanalyses has yet been assessed.

Our analysis using cloud and sea level pressure data has given additional hint that the strengthening of the overall vertical circulation in the reanalysis may be overestimated. Rind (1998) pointed out that the latitudinal temperature gradient governs the Hadley cell intensity, while global mean temperature governs the Hadley cell extent. Figures 4.18a and 4.18b show the zonal mean surface air temperatures are increased from 1979 to 2000 in the northern hemisphere in both winter and summer seasons. Figure 4.18c shows that the zonally averaged meridional temperature gradient ($T_{[30^{\circ}S-10^{\circ}N]}-T_{[15^{\circ}N-40^{\circ}N]}$) over the Hadley cell has decreased in the boreal winter from 1979 to 2000. This is also evidence against the increased strength of the Hadley circulation in the boreal winter in the two reanalyses.

4.6.2 Boreal Summer Hadley Circulation

During the boreal summer, Figure 4.19 shows the variation of the minimum values of the zonally averaged stream functions in the four models and in the two reanalyses. Just like in the boreal winter, the models exhibited some weakening of the Hadley circulation, but with marginal or little statistical significance, at 4.73 ± 4.59, -0.67 ± 7.65, 7.35 ± 8.12, 1.27 ± 8.81 in unit of 10^{10}kg/s/100years for the NCAR GCM, GFDL GCM, MPI GCM, and UKMO GCM respectively at the 90% confidence interval. The two reanalyses exhibited some strengthening, with -3.46 ± 4.49 and -12.62 ± 7.43 in the NCEP/NCAR and ECMWF reanalyses.

This discrepancy of the Hadley circulation change in the boreal summer is again consistent with the difference of the variation in the atmospheric static stability between the models and the reanalyses, which is shown in Figures 4.19 and 4.20. In the models, the troposphere becomes more statically stable in a warmer climate; in the reanalyses however, they have become less stable, especially in the tropics and subtropics. reanalyses, respectively. As discussed earlier, there are known uncertainties in the tropospheric temperature trends that could have impacted the reanalyses.

In the previous discussion on the DJF difference of the Hadley circulation between models and reanalyses, I have used the meridional gradient of surface air temperature to show that its change, which has decreased from 1979 to 2000, is inconsistent with the strengthening of the Hadley circulation in the reanalyses. The change of the meridional gradient of surface air temperature in the JJA season during this period is shown in Figure 4.18d. In contrast to the DJF season, the zonal mean meridional surface temperature gradient ($T_{[5^oS\text{-}35^oN]}$-$T_{[40^oS\text{-}10^oS]}$) has increased with time in

JJA. This by itself would support a strengthening of the Hadley circulation. There is therefore less evidence to rule out that the strengthened Hadley circulation in the reanalysis is real.

As shown in Figures 4.9b and 4.9c, however, the trend of the JJA Hadley circulation in the northern portion is opposite to that in the southern portion in the reanalyses, i.e., the rising motion has weakened from 10°N to 20°N, but strengthened at the equator. I therefore examined the change of the simulated Hadley circulation separately for the two portions by using the vertical pressure velocity. Since there is no output of vertical pressure velocity in the MPI AMIP run, I calculated the zonal mean 850-hPa divergence ($\nabla\vec{V}$) to qualitatively represent the 500-hPa vertical pressure velocity. Variations of the zonal mean vertical pressure velocity at 500-hPa averaged from 11°N to 22°N in the models and the two reanalyses are shown in Figure 4.22. It is seen that in the latitudes from 11°N to 22°N, the AMIP models except GFDL model and the two reanalyses all show weakening of the rising motions. Figure 4.23 shows the corresponding figure in the latitudes of 5°S to 8°N. The two reanalyses showed strengthening of the rising motion, but only the MPI GCM and UKMO GCM showed strengthening with much smaller statistical significance than that in the reanalyses.

The above discussion leads to the following conclusions: (1) The models and the reanalyses are consistent in showing weakening of the rising motion in the northern portion of the JJA Hadley circulation from 11°N to 22°N; (2) The models simulated an overall weakening of the whole Hadley circulation, but the reanalyses showed an overall strengthening. This may be related with the difference of the change in the vertical stability of the atmosphere. The difference of the rising motion change between the models and reanalyses is mainly near the equator.

4.7 Summary and Discussion

I have found that while both the NCEP/NCAR and ECMWF reanalyses show intensification of the zonal mean Hadley circulation in the boreal winter from 1958 to 2002, the difference in the strengthening of the boreal winter Hadley circulation between the two reanalyses is primarily over the tropical western Pacific where few atmospheric radiosonde measurements exist. In the NCEP/NCAR reanalysis, the meridional divergent flow of the Hadley circulation over the TWP is weakening, while that in the ECMWF reanalysis is strengthening. Over the continents where more sounding data are available, the two reanalyses all exhibit intensification of the boreal winter Hadley circulation. This explains the intensification of the zonal mean Hadley circulation in the two reanalyses, with the trend in the ECMWF reanalysis being about two to three times stronger than that in the NCEP/NCAR reanalysis.

I have also shown corroborative trends of the atmospheric transport of moist static energy out of the TWP, the longwave cloud forcing, and upper-level cloud cover with those of the vertical circulation in either the NCEP/NCAR reanalysis or the ECMWF reanalysis. I have reported decreasing trend in all these variables over the TWP in the NCEP/NCAR reanalysis, but increasing trends of all these variables in the ECMWF reanalysis. I have also shown that cloud trend from ship-based measurements is more consistent with the NCEP/NCAR reanalysis than with the ECMWF reanalysis. Evaluation of the trend of the meridional gradient of sea level pressure over the TWP from independent data reached the same conclusion, all indicating weakening of the meridional flow of the Hadley circulation over the TWP. Furthermore, I have presented evidence that even the NCEP/NCAR reanalysis may have overestimated the strengthening of the Hadley circulation in the boreal winter. The strengthening of the DJF Hadley circulation in the reanalyses is therefore likely an artifact.

In the boreal summer, the Hadley circulation is contributed by rising motions over the monsoon systems that are displaced to the south and over the oceans near the equator. The rising motions have become overall weaker in the monsoon region but stronger over the equator in both reanalyses. Therefore, both of the two datasets show a southward shift of zonally averaged meridional wind shear and precipitation belt.

In contrast to the NCEP/NCAR and ECMWF reanalyses that show intensification of the zonally averaged Hadley circulation in the boreal winter, models do not show any statistically significant trends in this season. Previous studies of Mitas and Clement (2005) by using radiosonde data and of Sherwood et al. (2005) on the temperature bias in the historial radiosonde record, are consistent with the inference from my study by using ship-based cloud data, sea level pressure data, and the meridional gradient of surface air temperature, that the strengthening of the boreal winter Hadley circulation in the two reanalyses is overestimated and is likely an artifact. It is therefore necessary to investigate the Hadley circulation trend from different perspectives. The present study examines this problem by isolating a special feature in the two reanalyses in trying to understand the puzzle.

In the boreal summer, the models and reanalyses agree in their weakening of the rising vertical motion in the northern portion of the Hadley cell from about 10^{o}N to 20^{o}N.

They disagree in the variation of the total Hadley circulation in terms of the minimum value of the zonally averaged stream function. The difference is largely near the equator. In the following chapter, I will further investigate change of the rising motion in the northern portion of the Hadley circulation by focusing on the monsoon system.

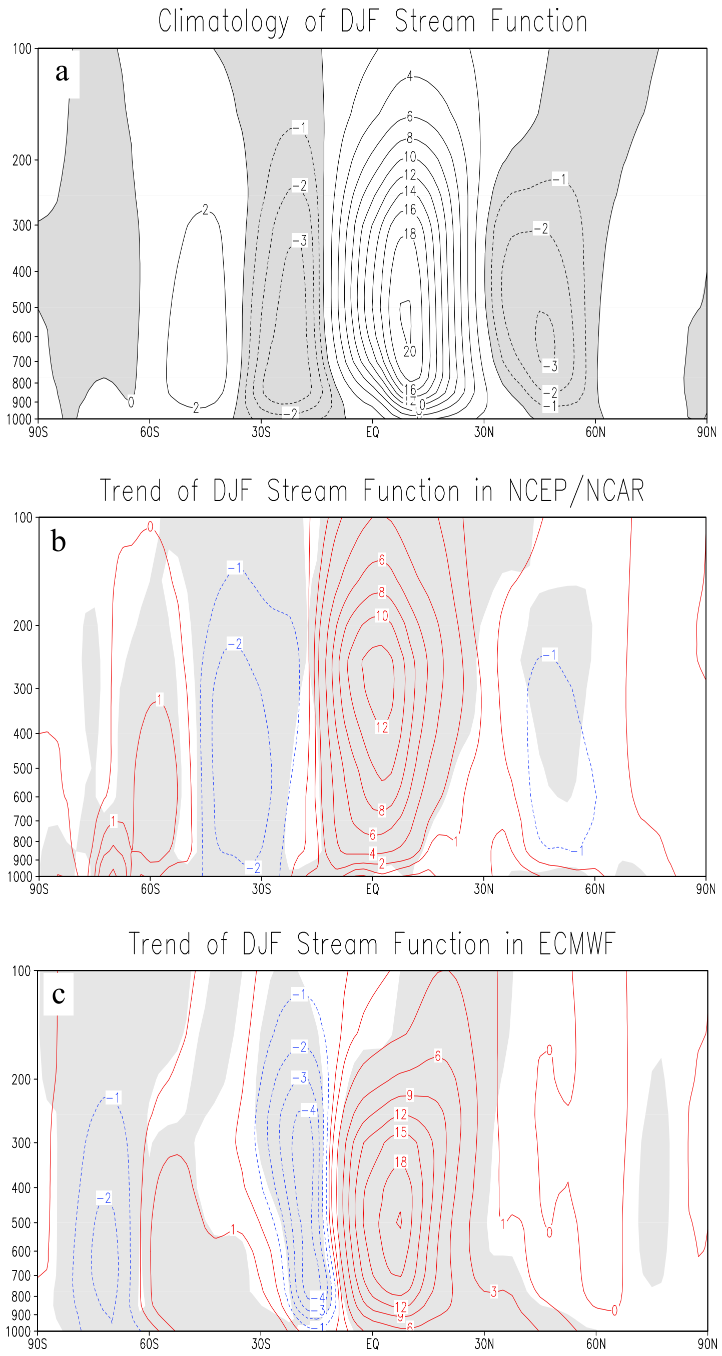
Climatology of DJF Stream Function

Trend of DJF Stream Function in NCEP/NCAR

Trend of DJF Stream Function in ECMWF

Figure 4.1: (a) is climatology of DJF stream function in the ECMWF reanalysis, (b) and (c) are linear trends of DJF stream function in NCEP/NCAR and ECMWF reanalyses respectively. Linear trends are calculated from 1958 to 2002. Units of stream function and trend are 10^{10}kg/s and 10^{10}kg/s/100years, respectively. Areas where trends are statistically significant at a 95% confidence level are shaded in light grey in (b) and (c).

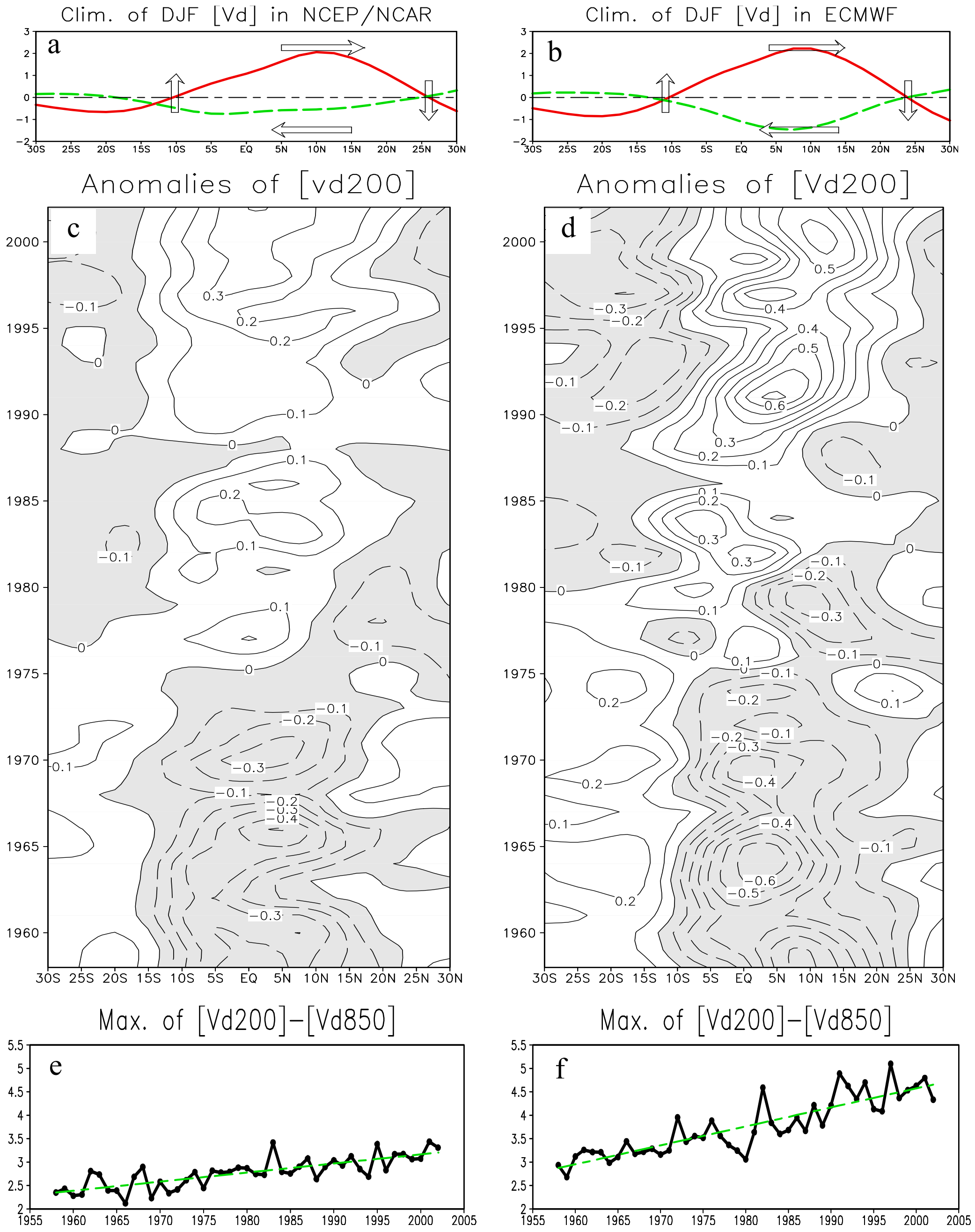

Figure 4.2: (a) and (b) are the climatologies of the DJF zonal mean meridional divergent winds at 200-hPa (red solid line) and 850-hPa (green dash line) in NCEP/NCAR and ECMWF reanalyses respectively. (c) and (d) are the time-latitude cross section of the anomalous zonal mean meridional divergent wind at 200-hPa in NCEP/NCAR and ECMWF reanalyses. Negative values are shaded in grey. (e) and (f) are the time series of the maximum differences between the zonal mean meridional divergent wind at 200-hPa and 850-hPa in NCEP/NCAR and ECMWF reanalyses. Unit of wind is m/s. Trends are 1.94 ± 0.47 m/s/100years in NCEP/NCAR and 4.15 ± 0.71 m/s/100years in ECMWF from 1958 to 2002. The ± values define the 95% confidence intervals for the trends.

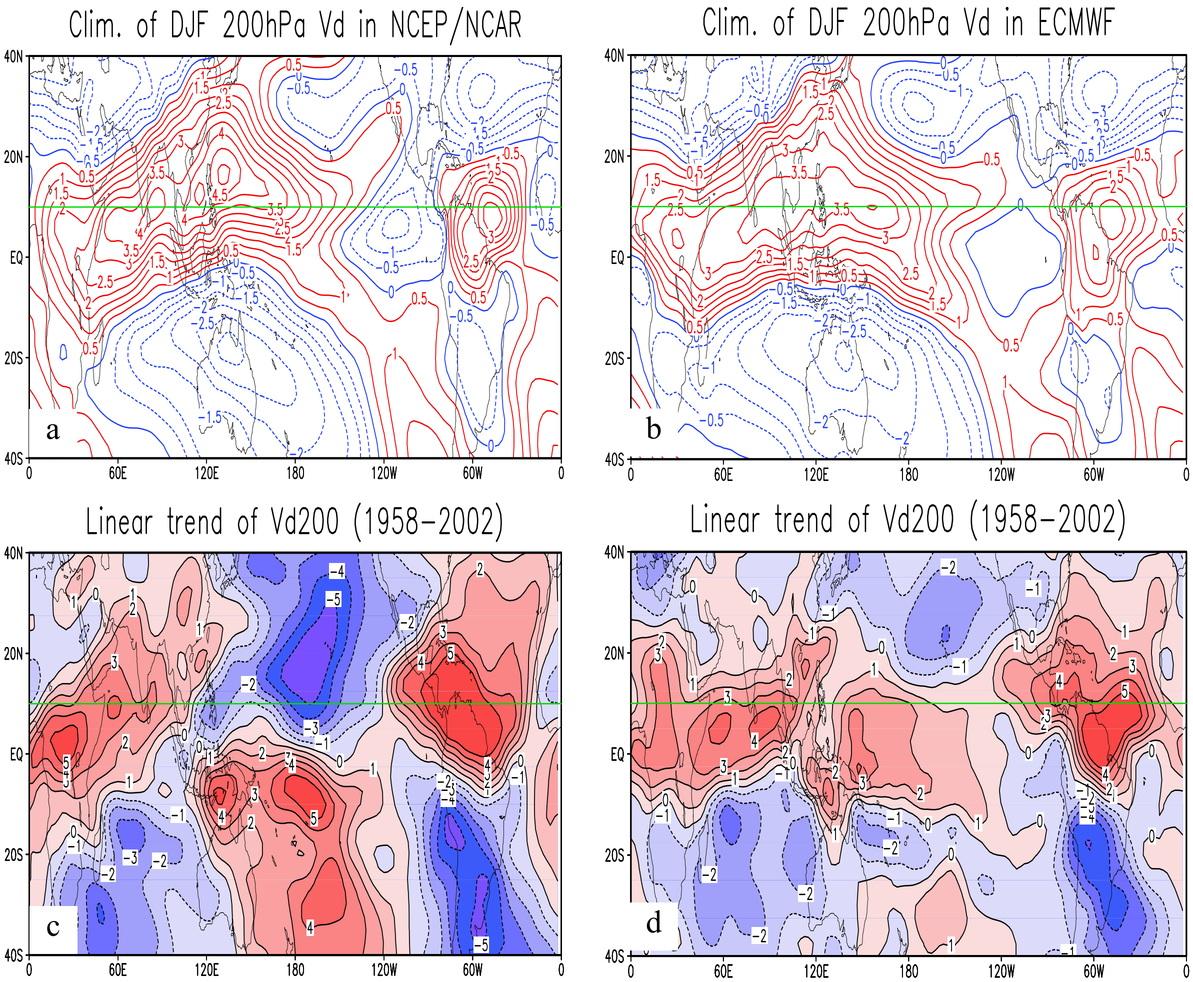

Figure 4.3: (a) and (b) are the climatologies of the DJF 200-hPa meridional divergent wind distribution in the NCEP/NCAR and ECMWF reanalyses, respectively. Unit of wind is m/s. The 10°N latitude line is highlighted. (c) and (d) are the linear trends of the 200-hPa meridional divergent wind in the NCEP/NCAR and ECMWF reanalyses, respectively. Unit of trend is m/s/100years.

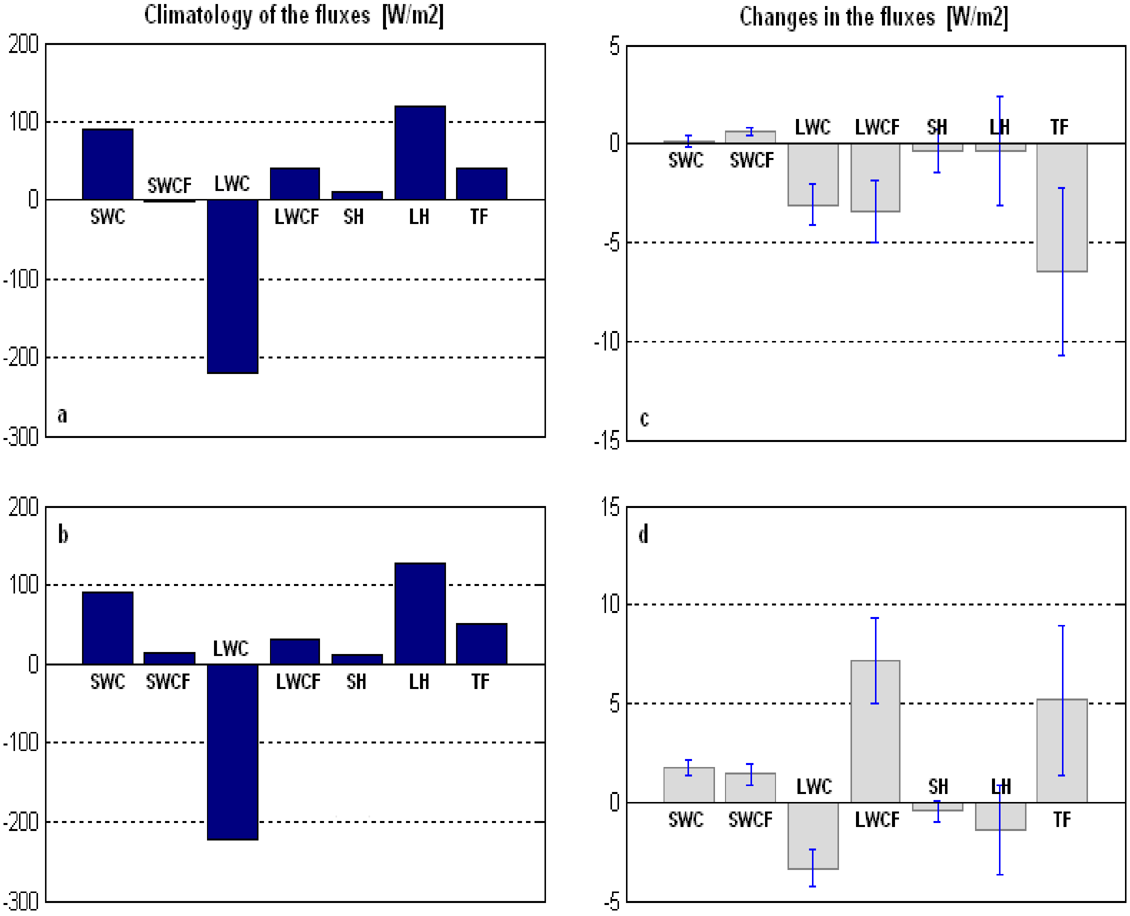

Figure 4.4: (a) and (b) are the climatologies of the DJF SWC, SWCF, LWC, LWCF, SH, LH and TF over the TWP in the NCEP/NCAR and ECMWF reanalyses. Unit is W/m^2. (c) and (d) are the changes of the SWC, SWCF, LWC, LWCF, SH, LH and TF over the TWP in the NCEP/NCAR and ECMWF reanalyses between 1980 to 2000 and 1958-1975. Unit is W/m^2. The error bars represent the 95% confidence intervals for the changes.

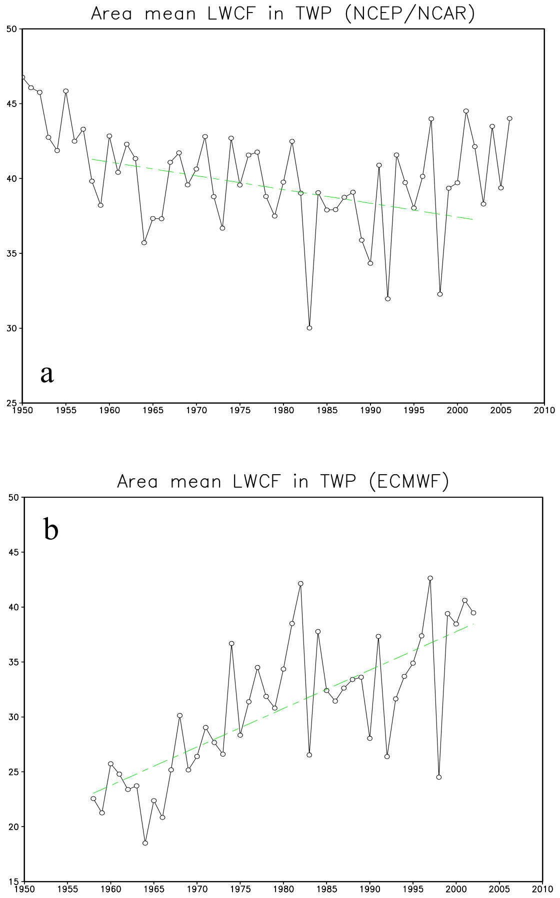

Figure 4.5: Area mean DJF LW cloud forcing over tropical western Pacific (110ºE-160ºW, 20ºS-10ºN) in the NCEP/NCAR (a), and ECMWF (b) reanalyses. Unit is W/m^2. Green dash lines are linear regressions from 1958 to 2002. Trends are -9.18 ± 6.83 W/m^2/100years in NCEP/NCAR reanalysis and 35.03 ± 9.17 W/m^2/100years in ECMWF reanalysis. The ± values define the 95% confidence intervals for the trends.

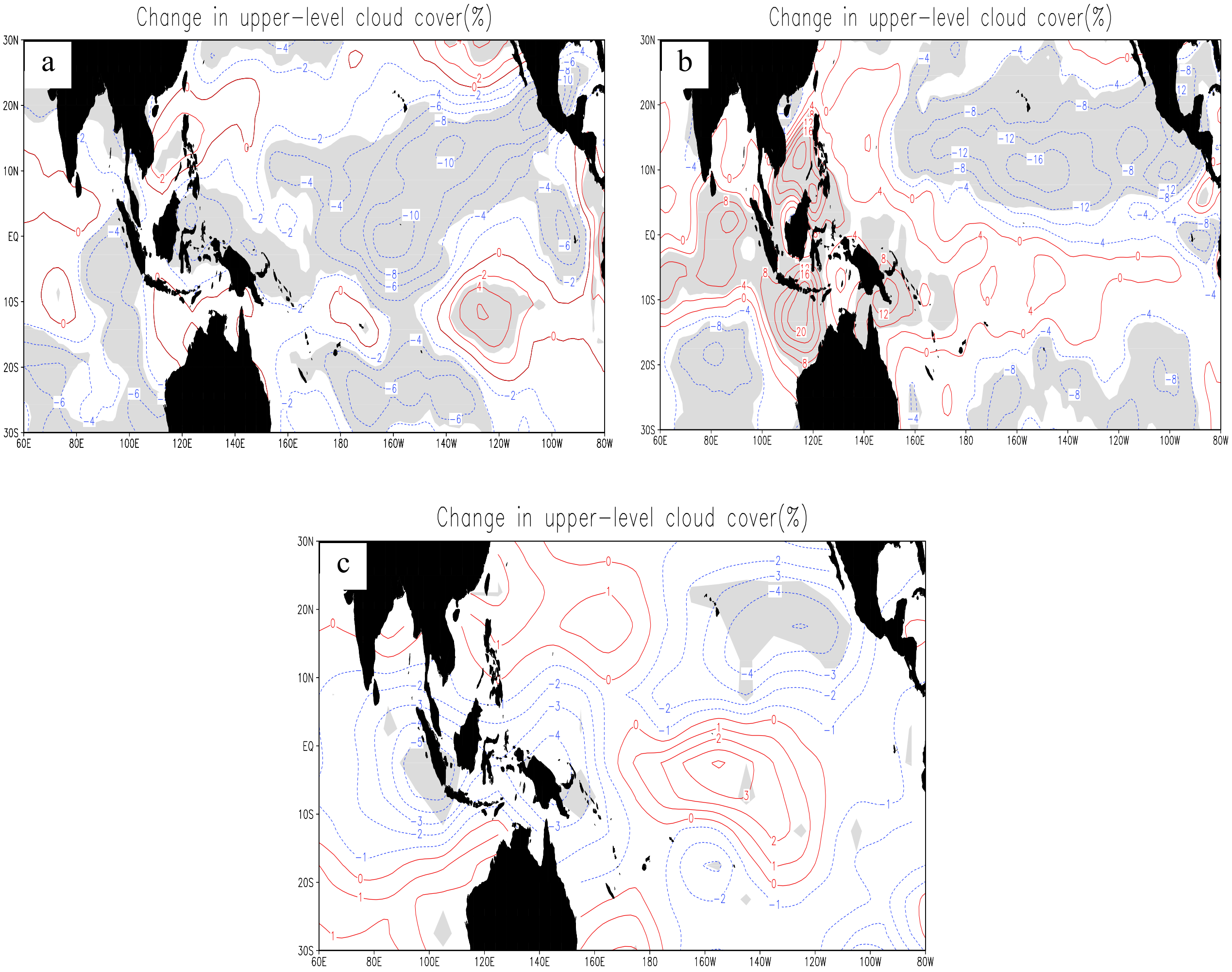

Figure 4.6: (a), (b) and (c) are changes of the DJF upper-level cloud cover in the NCEP/NCAR, ECMWF and EECRA. Unit is %. Areas where differences are statistically significant at a 95% confidence level are shaded in grey.

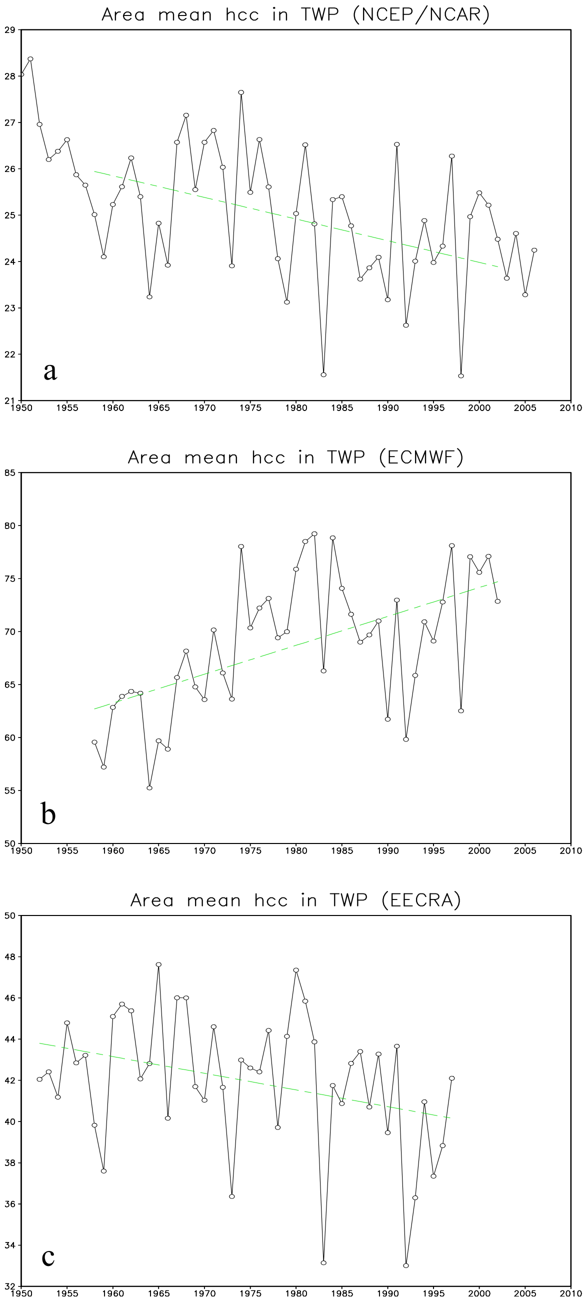

Figure 4.7: Area mean DJF upper-level cloud cover over the tropical western Pacific (110ºE-160ºW, 20ºS-10ºN) in the NCEP/NCAR (a), ECMWF (b) and EECRA (c). Unit is %. Green dash lines are linear regressions from 1958 to 2002 in the two reanalyses and from 1952 to 1997 in EECRA. Trends are -4.67 ± 2.89 %/100years in NCEP/NCAR reanalysis, 27.29 ± 11.42 %/100years in ECMWF reanalysis, and -8.09 ± 6.45 %/100years in EECRA. The ± values define the 95% confidence intervals for the trends.

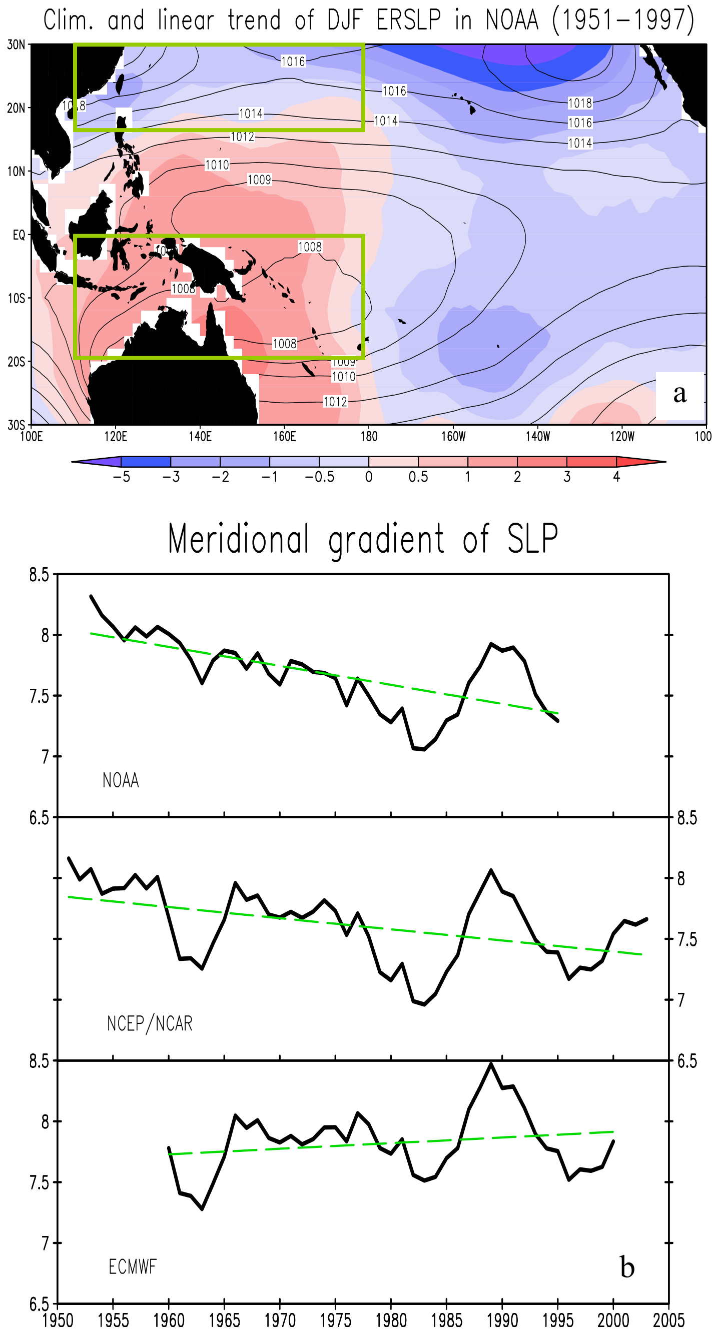

Figure 4.8: (a) is the climatology (contour) and linear trend (image) of the DJF ERSLP from the NOAA; (b) is the time series and linear trends of the SLP differences between the two boxes in the subtropical and tropical western Pacific regions in (a) from NOAA ship-based observations, NCEP/NCAR reanalysis, and ECMWF reanalysis. Plotted are five-year running averages. Units of SLP and linear trend are hPa and hPa/100years respectively. Trends are -1.71 ± 0.87 hPa/100years from 1951 to 1997 in NOAA, -1.12 ± 0.98 hPa/100years from 1951 to 1997 and -0.43 ± 0.99 hPa/100years from 1958 to 2002 in NCEP/NCAR reanalysis, and 0.36 ± 0.96 hPa/100years from 1958 to 2002 in ECMWF reanalysis. The ± values define the 90% confidence intervals for the trends.

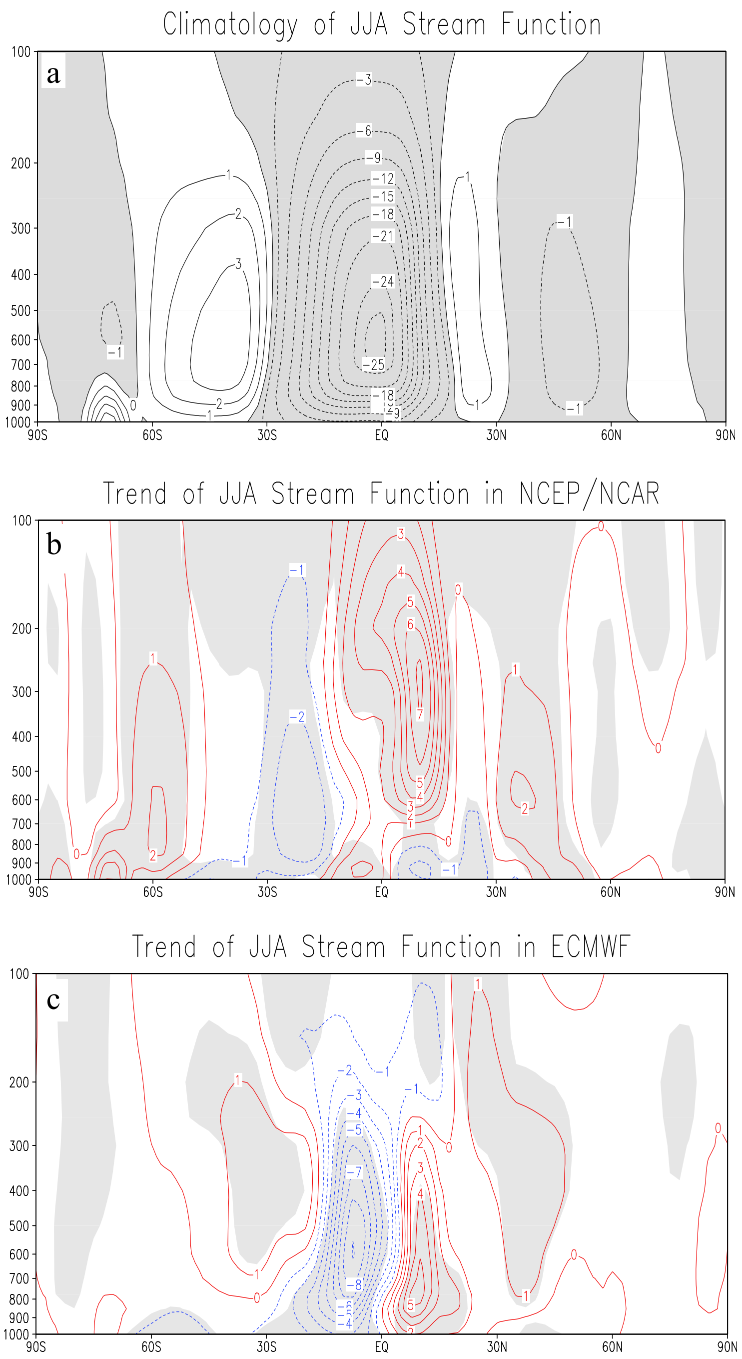

Figure 4.9: (a) is climatology of JJA stream function in the ECMWF reanalysis, (b) and (c) are linear trends of JJA stream function in NCEP/NCAR and ECMWF reanalyses, respectively. Linear trends are calculated from 1958 to 2002. Units of stream function and trend are 10^{10}kg/s and 10^{10}kg/s/100years, respectively. Areas where trends are statistically significant at a 95% confidence level are shaded in light grey in (b) and (c).

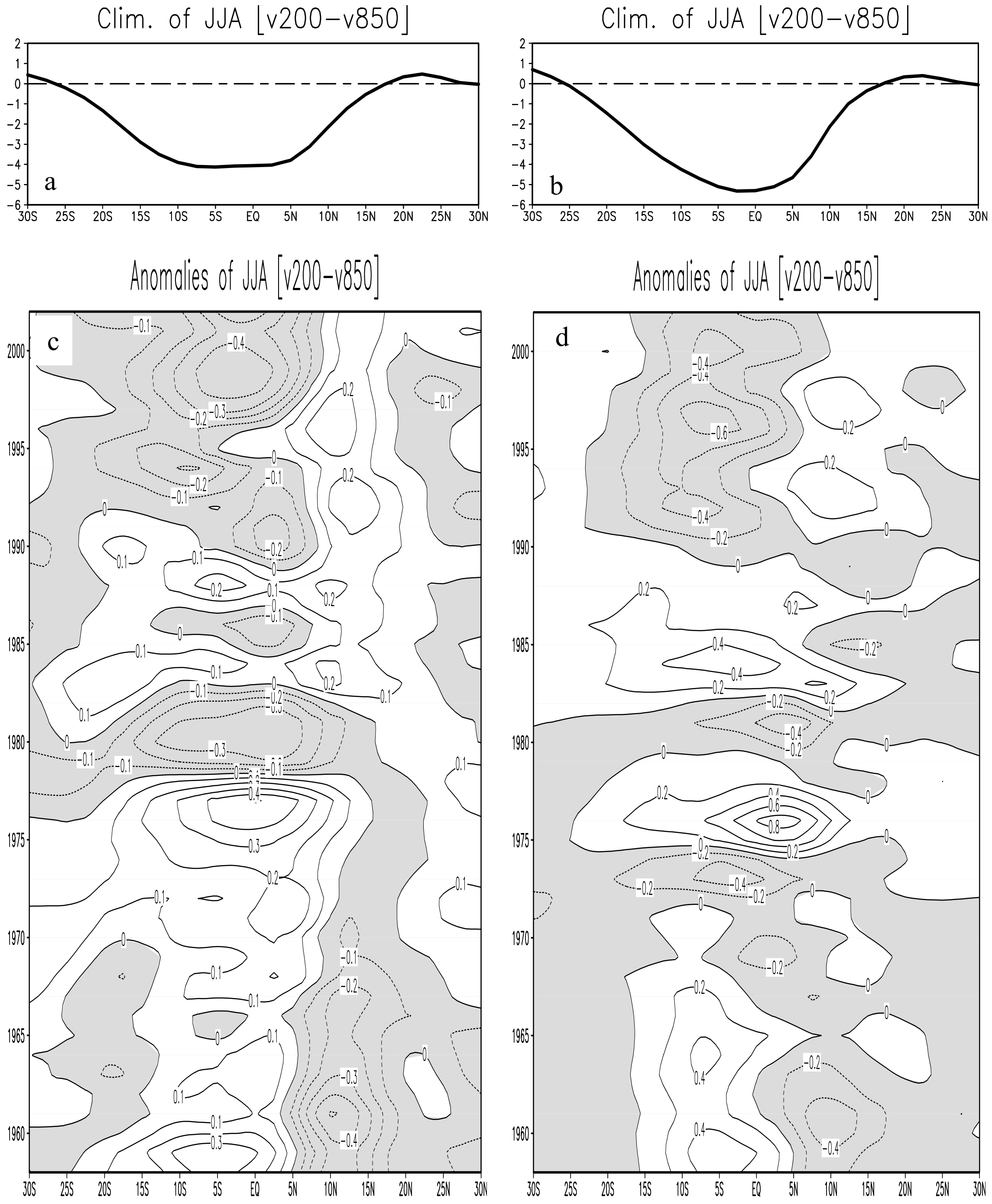

Figure 4.10: Climatology of JJA zonal mean meridional vertical shear (v_{200}-v_{850}) in the NCEP/NCAR (a) and ECMWF (b) reanalyses. Anomalies of JJA zonal mean meridional vertical shear in the NCEP/NCAR (c) and ECMWF (d) reanalyses. Negative values are shaded in grey. Unit of wind shear is m/s.

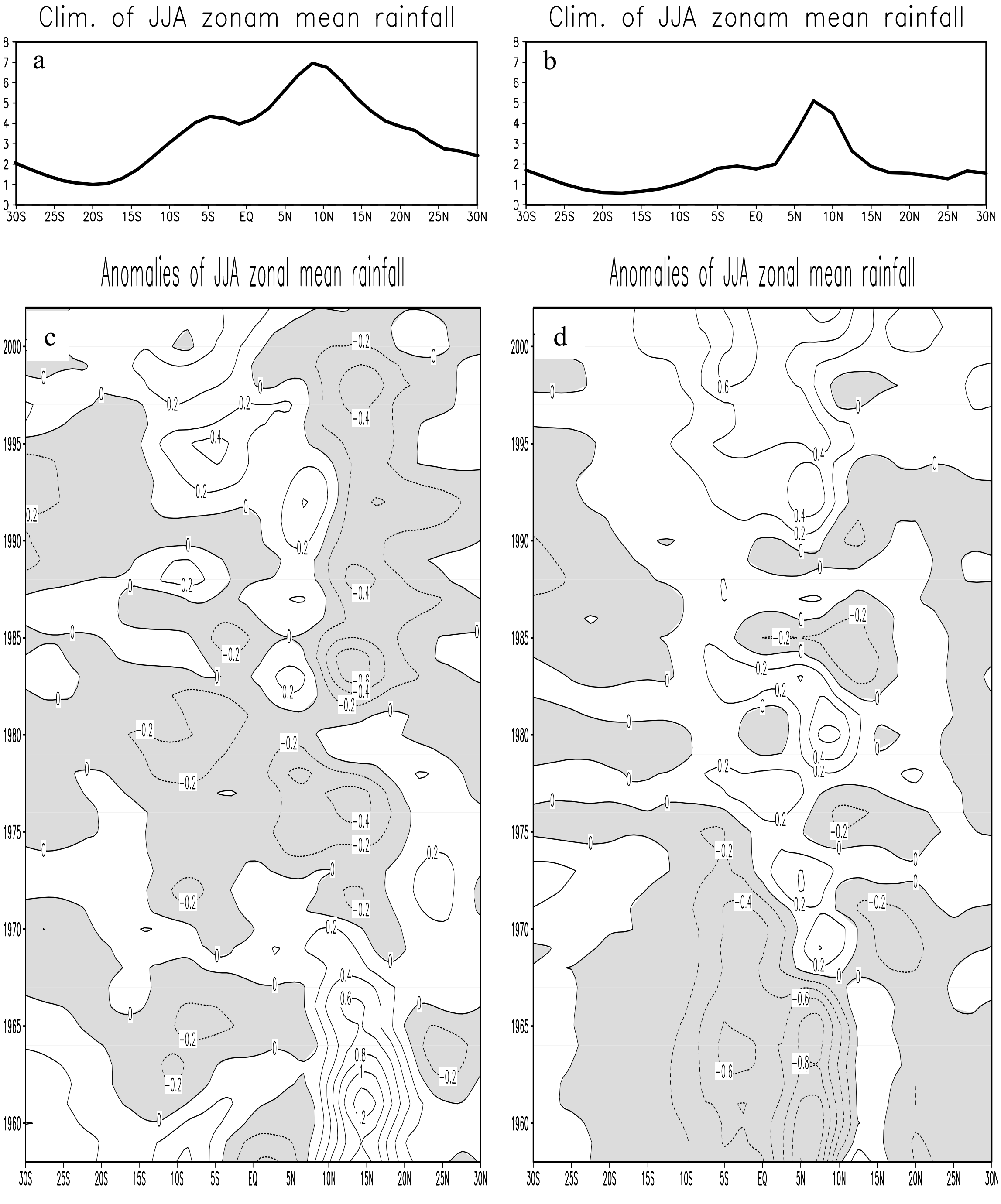

Figure 4.11: Climatology of JJA zonal mean precipitation in the NCEP/NCAR (a) and ECMWF (b) reanalyses. Anomalies of JJA zonal mean precipitation in the NCEP/NCAR (c) and ECMWF (d) reanalyses. Negative values are shaded in grey. Unit of precipitation is mm/day.

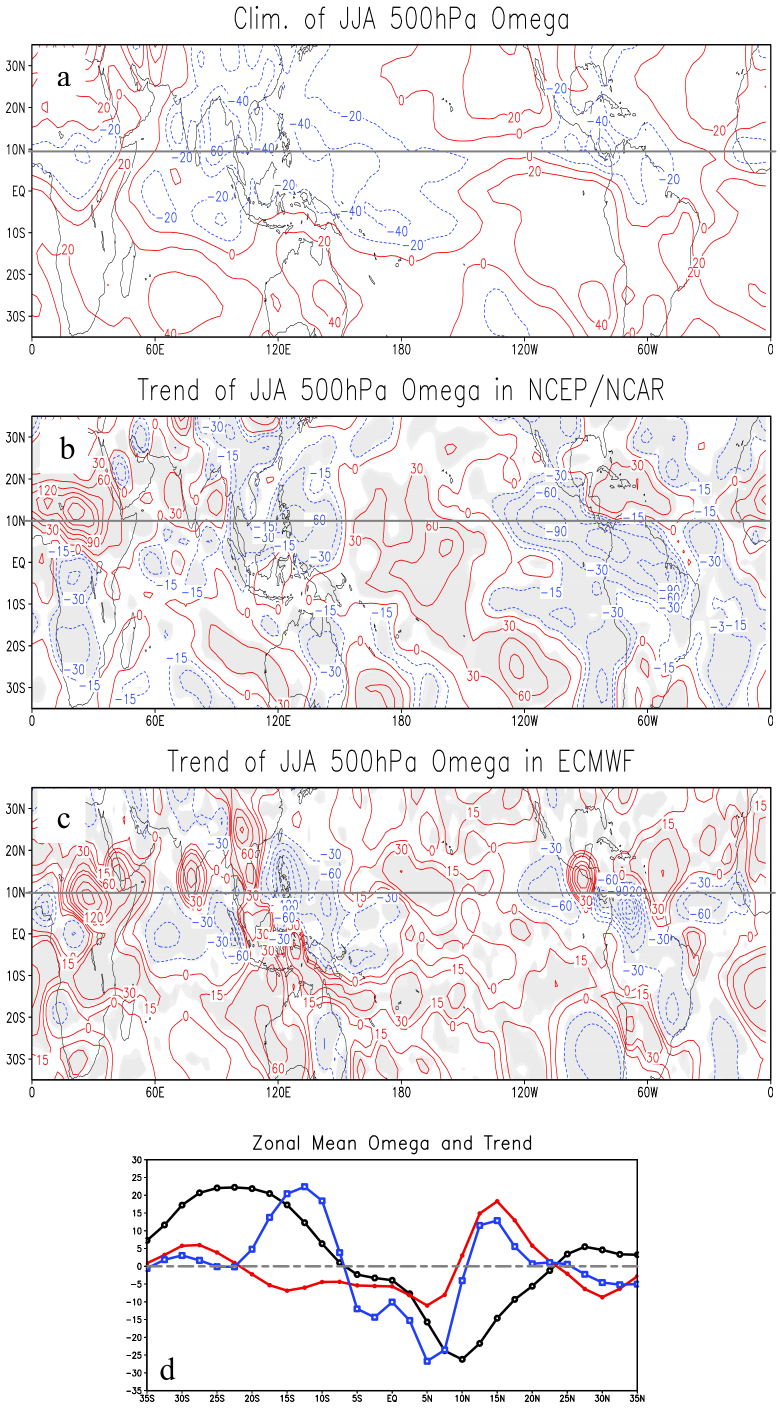

Figure 4.12: (a) is climatology of JJA 500-hPa vertical pressure velocity (omega) in the NCEP/NCAR reanalysis. (b) is linear trend of omega in the NCEP/NCAR reanalysis from 1958 to 2002. (c) is same as (b) but in the ECMWF reanalysis. (d) is zonal mean omega climatology (black), omega trends in the NCEP/NCAR reanalysis (red) and in the ECMWF reanalysis (blue). Units of omega and trend are hPa/day and hPa/day/100years respectively. Areas where trends are statistically significant at a 95% confidence level are shaded in light grey.

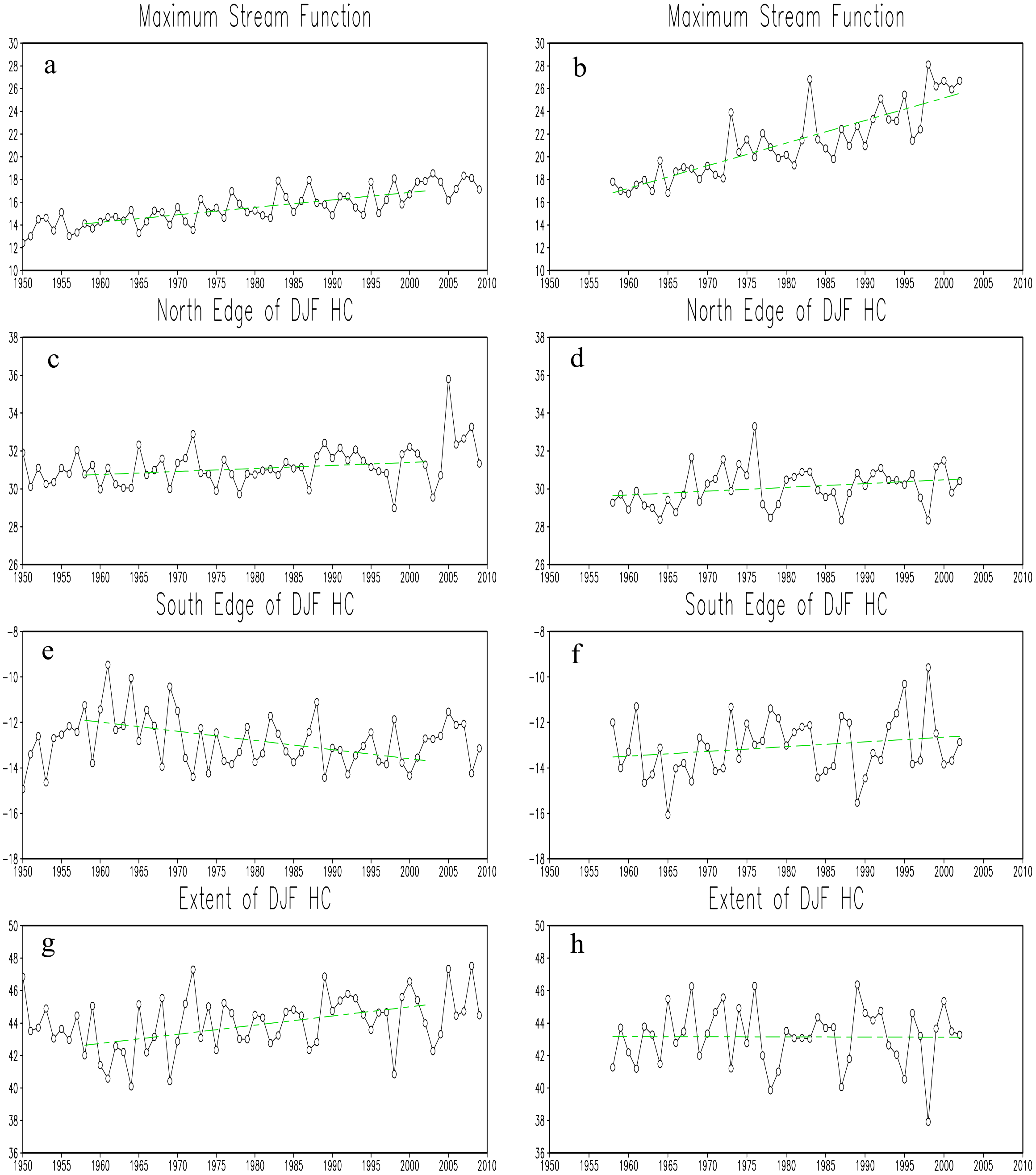

Figure 4.13: Maximum value of stream function for NH Hadley cell in NCEP/NCAR (a) and ECMWF (b) reanalyses. Time series of north-edge latitudes of NH Hadley cell at 500-hPa in the NCEP/NCAR (c) and ECMWF (d) reanalyses. (e) and (f) are same as in (c) and (d) but for south-edge. Extent of NH Hadley cell in NCEP/NCAR (g) and ECMWF (h) reanalyses. Green lines are linear regressions from 1958 to 2002. Trends are 6.57±2.00, 19.89±3.55, 1.59±1.69, 2.01±2.17, -4.04±2.34, 2.09±2.79, 5.63±3.42 and -0.08±3.94 in (a) to (h) respectively. Units of stream function and trend are 10^{10}kg/s and 10^{10}kg/s/100years respectively; Units of north-edge latitude, south-edge latitude, extent and their trends are degree and degree/100years. The ± values define the 95% confidence intervals for the trends.

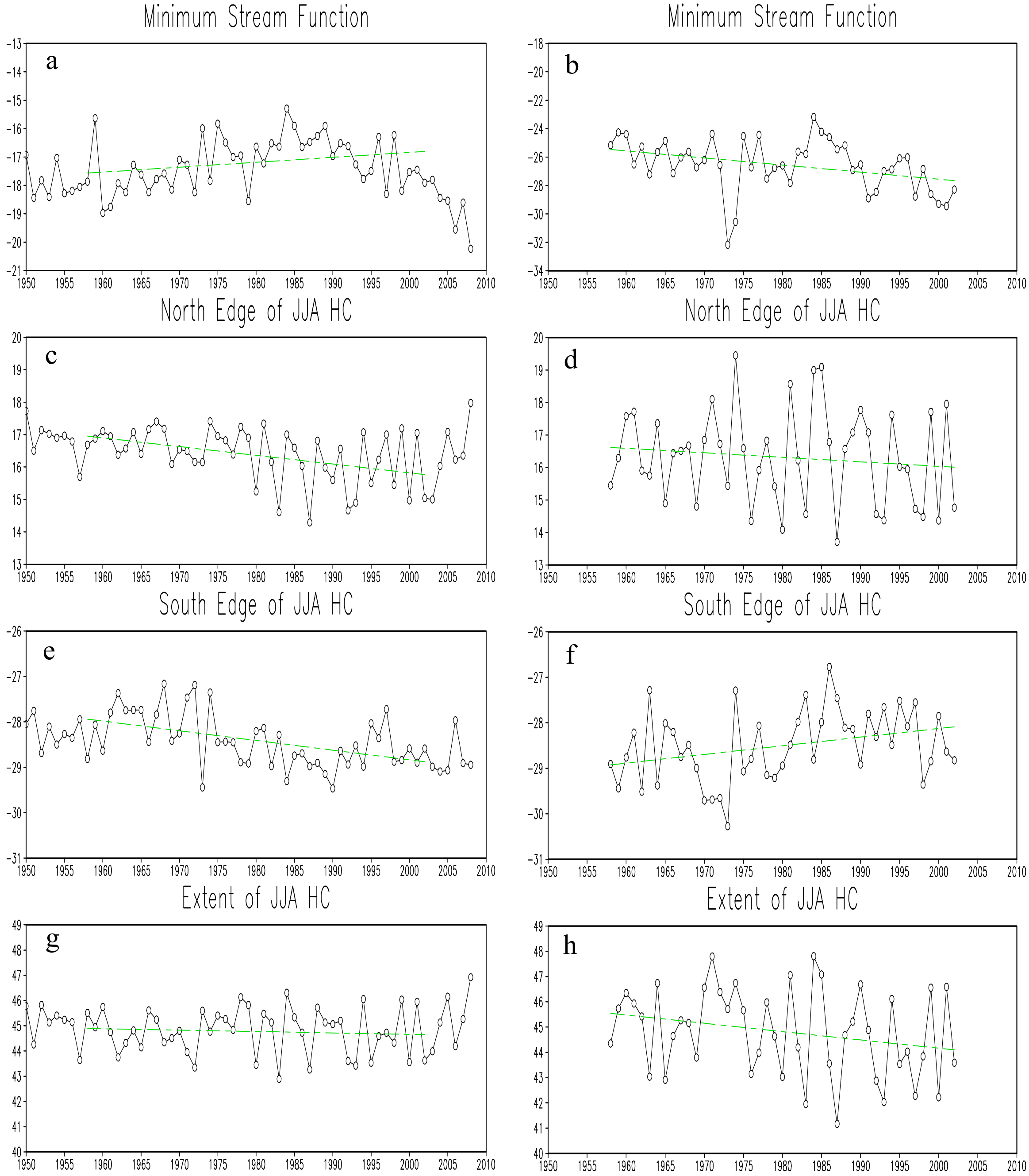

Figure 4.14: Minimum value of stream function for SH Hadley cell in NCEP/NCAR (a) and ECMWF (b) reanalyses. Time series of north-edge latitudes of SH Hadley cell at 500-hPa in the NCEP/NCAR (c) and ECMWF (d) reanalyses. (e) and (f) are same as in (c) and (d) but for south-edge. Extent of SH Hadley cell in NCEP/NCAR (g) and ECMWF (h) reanalyses. Green lines are linear regressions from 1958 to 2002. Trends are 1.74±1.90, -5.00±3.71, -2.69±1.65, -1.39±3.16, -2.14±1.15, 1.90±1.61, -0.55±1.96 and -3.29±3.60 in (a) to (h) respectively. Units of stream function and trend are 10^{10}kg/s and 10^{10}kg/s/100years respectively; Units of north-edge latitude, south-edge latitude, extent and their trends are degree and degree/100years. The ± values define the 95% confidence intervals for the trends.

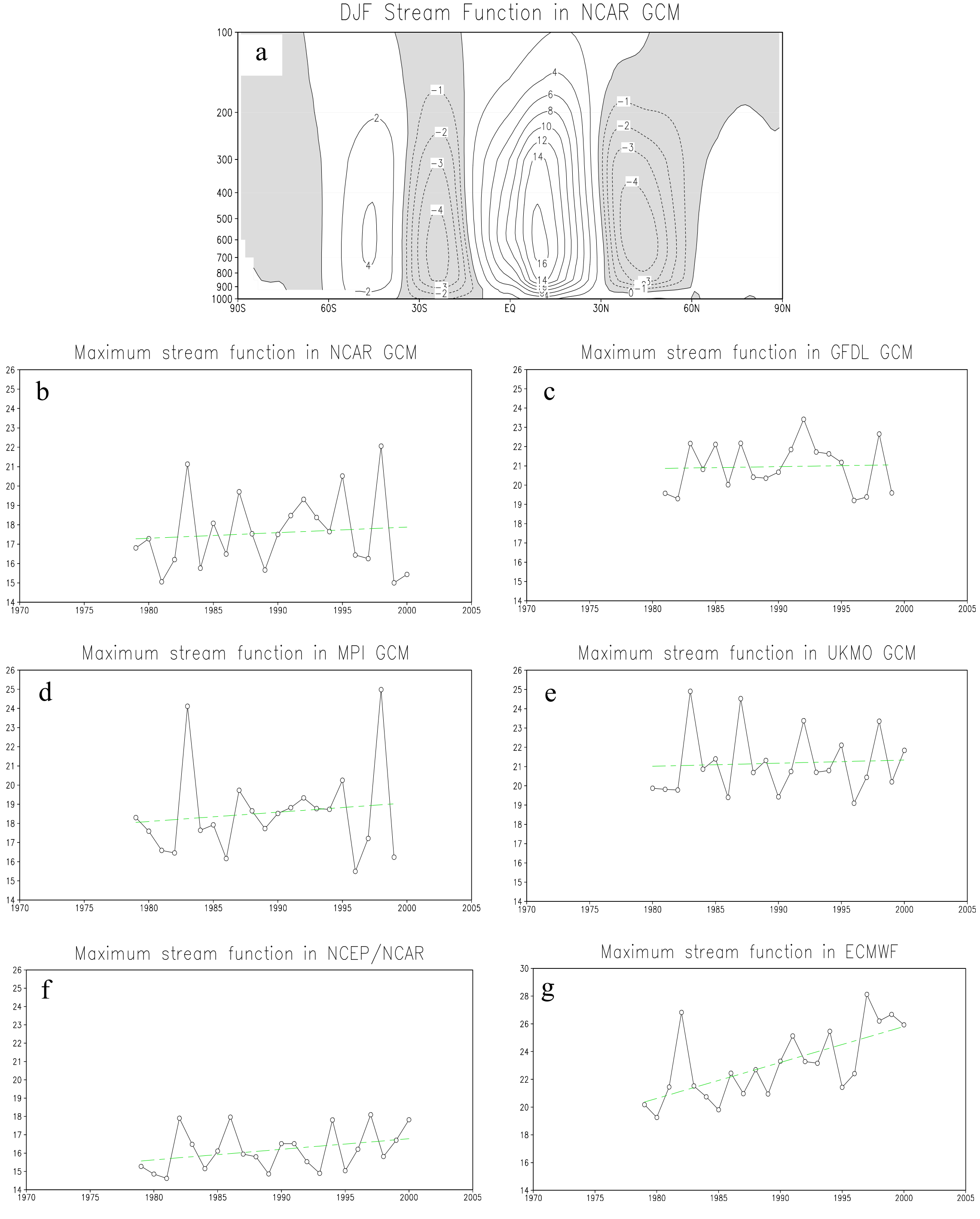

Figure 4.15: (a) is DJF stream function simulated in NCAR GCM. (b)-(g) are the time-series of maximum stream function (10ºS-30ºN) in NCAR GCM, GFDL GCM, MPI GCM, UKMO GCM, NCEP/NCAR and ECMWF reanalyses, respectively. Trends from 1979 to 2000 are 2.89 ±10.9, 1.02 ±8.73, 4.85 ±13.87, 1.60 ±9.80, 5.78 ±6.00 and 25.89 ±10.76 in NCAR, GFDL, MPI, UKMO GCMs, the NCEP/NCAR and ECMWF reanalyses, respectively. Units of stream function and trend are 10^{10}kg/s and 10^{10}kg/s/100years respectively. The ± values define the 90% confidence intervals for trends.

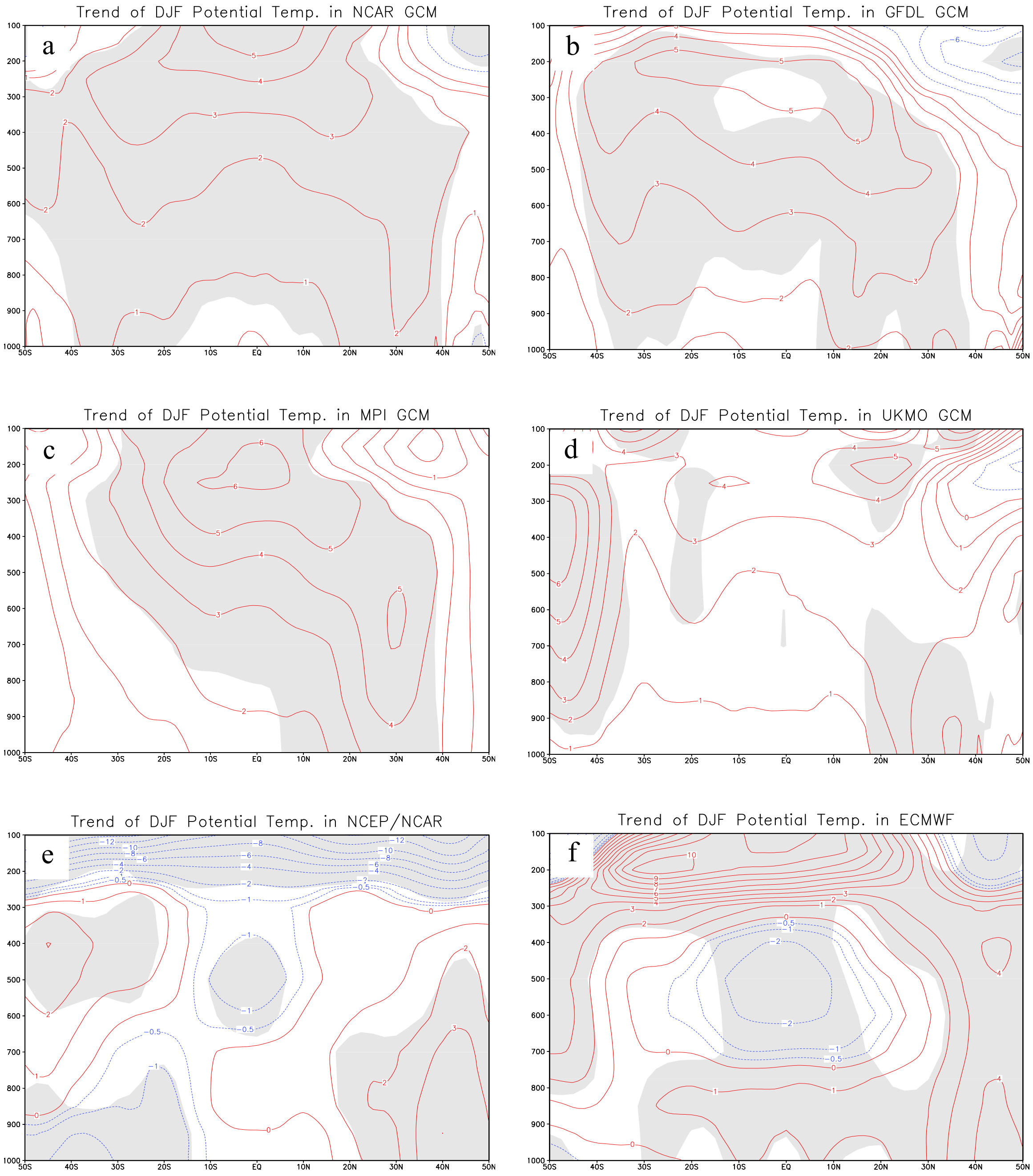
Trend of DJF Potential Temp. in NCAR GCM

Trend of DJF Potential Temp. in GFDL GCM

Trend of DJF Potential Temp. in MPI GCM

Trend of DJF Potential Temp. in UKMO GCM

Trend of DJF Potential Temp. in NCEP/NCAR

Trend of DJF Potential Temp. in ECMWF

Figure 4.16: Trend of DJF zonal mean potential temperature in the NCAR GCM (a), GFDL GCM (b), MPI GCM (c), UKMO GCM (d), NCEP/NCAR (e) and ECMWF (f) reanalyses. Trends are calculated from 1979 to 2000. Unit of trend is K/100years. Areas where trends are statistically significant at a 90% confidence level are shaded in grey.

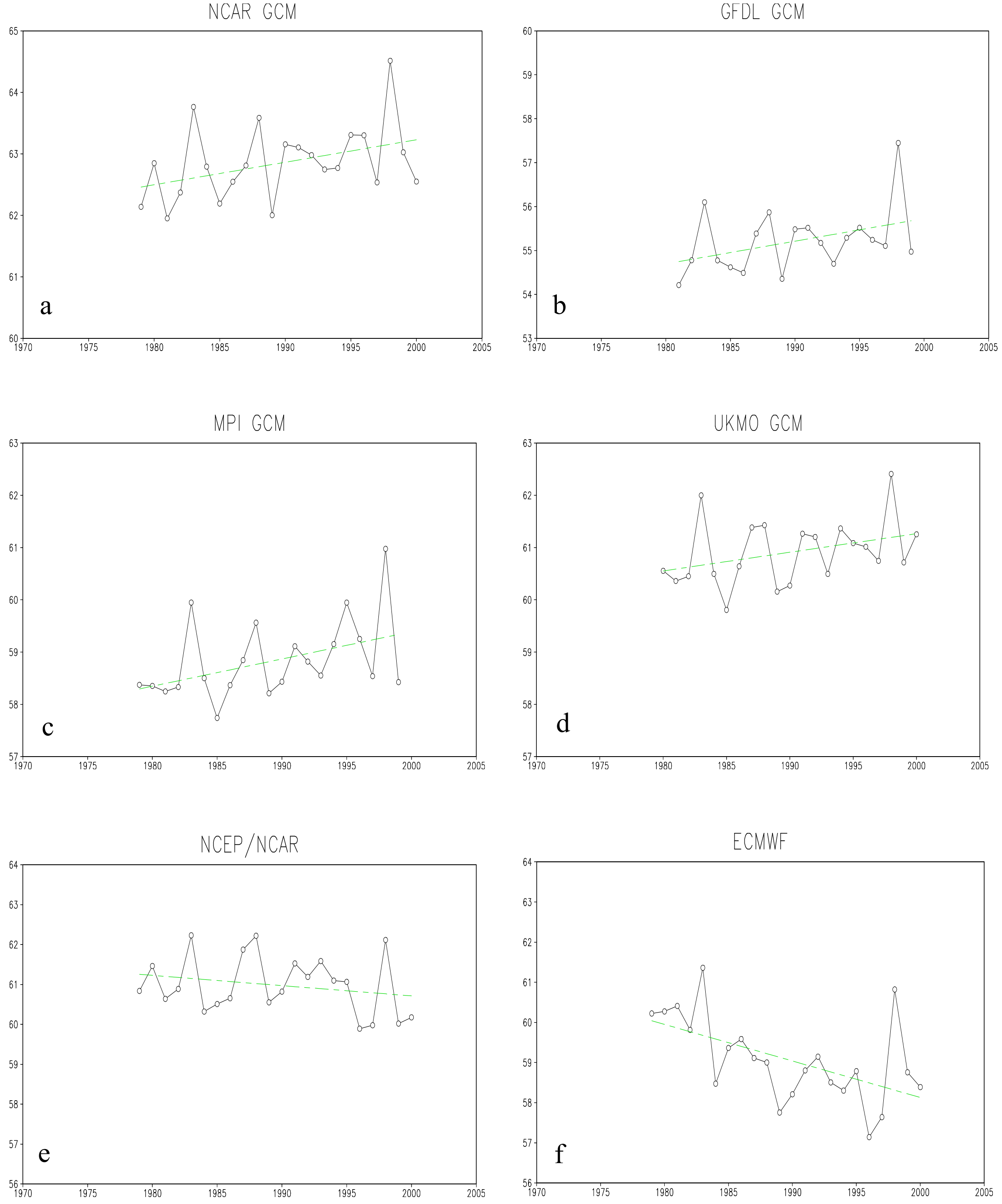

Figure 4.17: Time series of DJF static stability (-∂θ/∂p) averaged over 5ºS-15ºN, 850hPa-500hPa in the NCAR GCM (a), GFDL GCM (b), MPI GCM (c), UKMO GCM (d), NCEP/NCAR (e) and ECMWF (f) reanalyses. Trends from 1979 to 2000 are 3.66 ±3.32, 5.17 ±4.71, 5.22 ±4.39, 3.57 ±3.50, -2.57 ±3.94 and -9.12 ±4.97 in NCAR GCM, GFDL GCM, MPI GCM, UKMO GCM, NCEP/NCAR and ECMWF reanalyses, respectively. Units of static stability and trend are 10^{-3}K/hPa and 10^{-3}K/hPa/100years respectively. The ± values define the 90% confidence intervals for the trends.

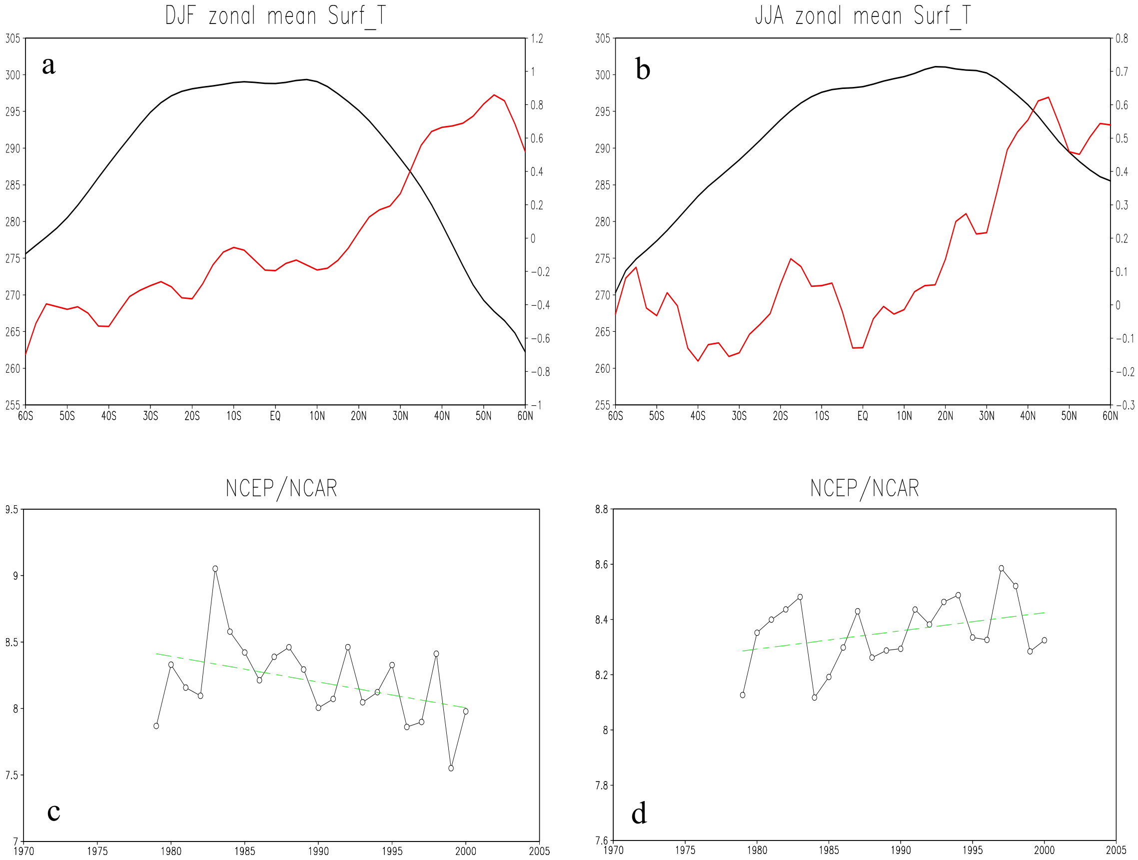

Figure 4.18: Climatology (Black, left y-axis) and linear trend (Red, right y-axis) of DJF (a) and JJA (b) zonal mean surface air temperature in the NCEP/NCAR reanalysis. Units of temperature and trend are K and K/100years respectively. Time series of DJF meridional zonal mean surface air temperature gradient ($T_{[30^{\circ}S\text{-}10^{\circ}N]}$-$T_{[15^{\circ}N\text{-}40^{\circ}N]}$) in the NCEP/NCAR reanalysis (c). Trend from 1979 to 2000 is -1.94 ±1.80. Time series of JJA meridional surface air temperature gradient ($T_{[5^{\circ}S\text{-}35^{\circ}N]}$-$T_{[40^{\circ}S\text{-}10^{\circ}S]}$) in the NCEP/NCAR reanalysis (d). Trend from 1979 to 2000 is 0.66 ±0.64. Units of temperature gradient and trend are K and K/100years respectively. The ± values define the 90% confidence intervals for the trends.

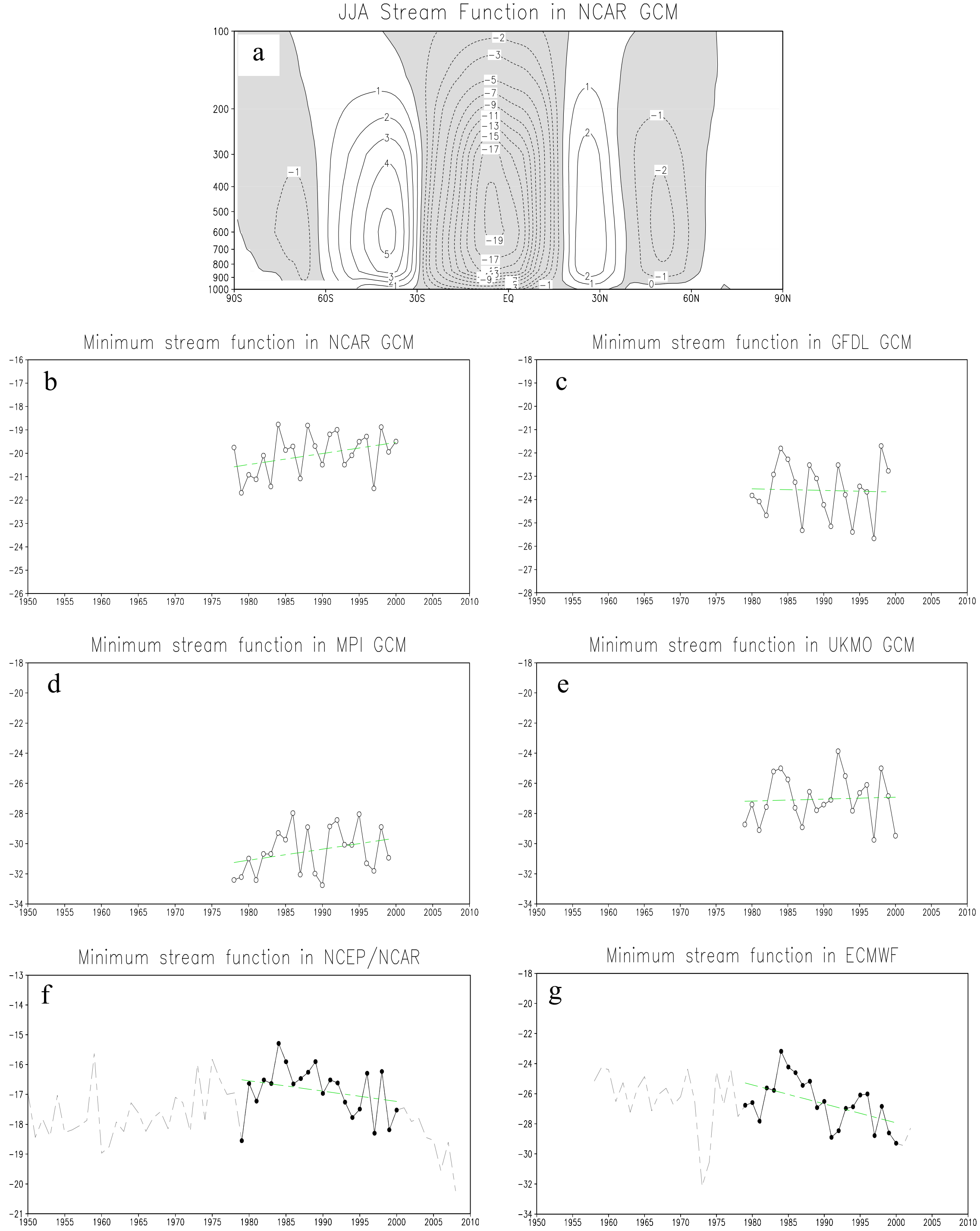

Figure 4.19: (a) is JJA stream function simulated in NCAR GCM. (b)-(g) are time-series of minimum stream function (30ºS-20ºN) in NCAR GCM, GFDL GCM, MPI GCM, UKMO GCM, NCEP/NCAR and ECMWF reanalyses, respectively. Trends from 1979 to 2000 are 4.73±4.59, -0.67±7.65, 7.35±8.12, 1.27±8.81, -3.46±4.49 and -12.62±7.43 in NCAR, GFDL, MPI, UKMO GCMs, NCEP/NCAR and ECMWF reanalyses, respectively. Units of stream function and trend are 10^{10}kg/s and 10^{10}kg/s/100years respectively. The ± values define the 90% confidence intervals for the trends.

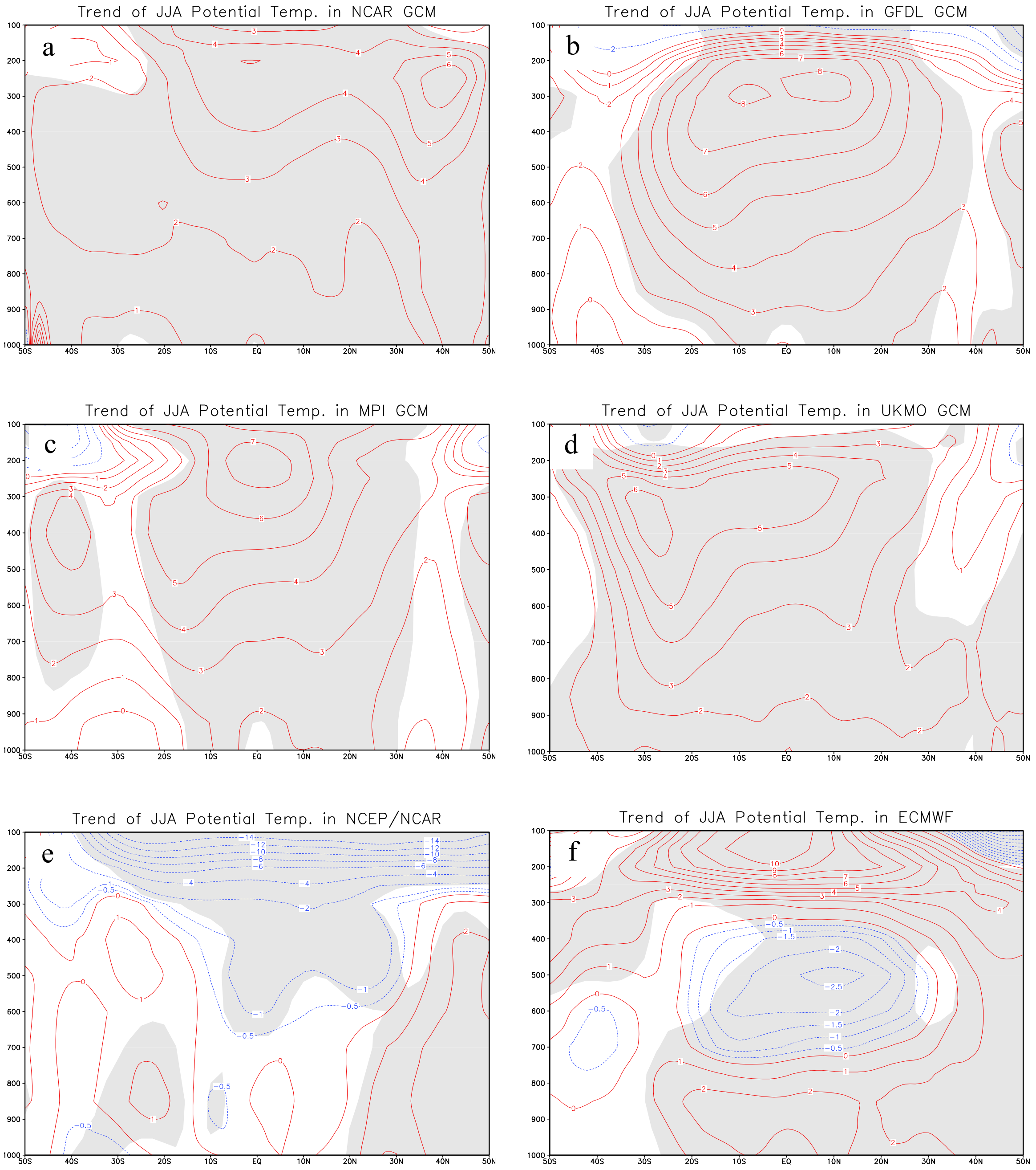

Figure 4.20: Trend of JJA zonal mean potential temperature in the NCAR GCM (a), GFDL GCM (b), MPI GCM (c), UKMO GCM (d), NCEP/NCAR (e) and ECMWF (f) reanalyses. Trends are calculated from 1979 to 2000. Unit of trend is K/100years. Areas where trends are statistically significant at a 90% confidence level are shaded in grey.

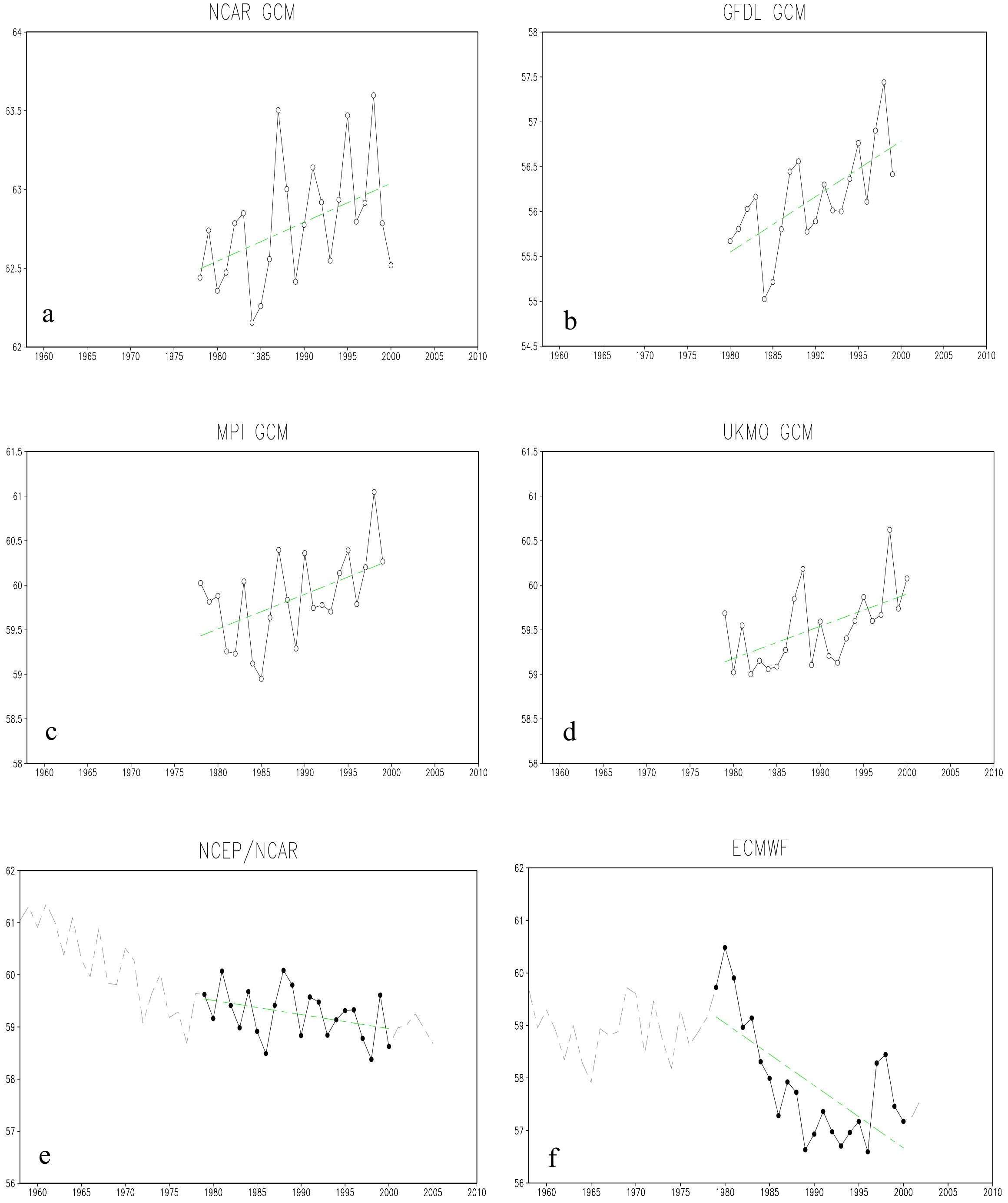

Figure 4.21: Time series of JJA static stability (-əθ/əp) averaged over 5ºS-20ºN, 850hPa-500hPa in the NCAR GCM (a), GFDL GCM (b), MPI GCM (c), UKMO GCM (d), NCEP/NCAR (e) and ECMWF (f) reanalyses. Trends from 1979 to 2000 are 2.47 ±1.94, 6.18 ±2.62, 3.89 ±2.45, 3.63 ±1.99, -2.71 ±2.49 and -11.89 ±4.58 in NCAR GCM, GFDL GCM, MPI GCM, UKMO GCM, NCEP/NCAR and ECMWF reanalyses, respectively. Units of static stability and trend are 10^{-3}K/hPa and 10^{-3}K/hPa/100years. The ± values define the 90% confidence intervals for the trends.

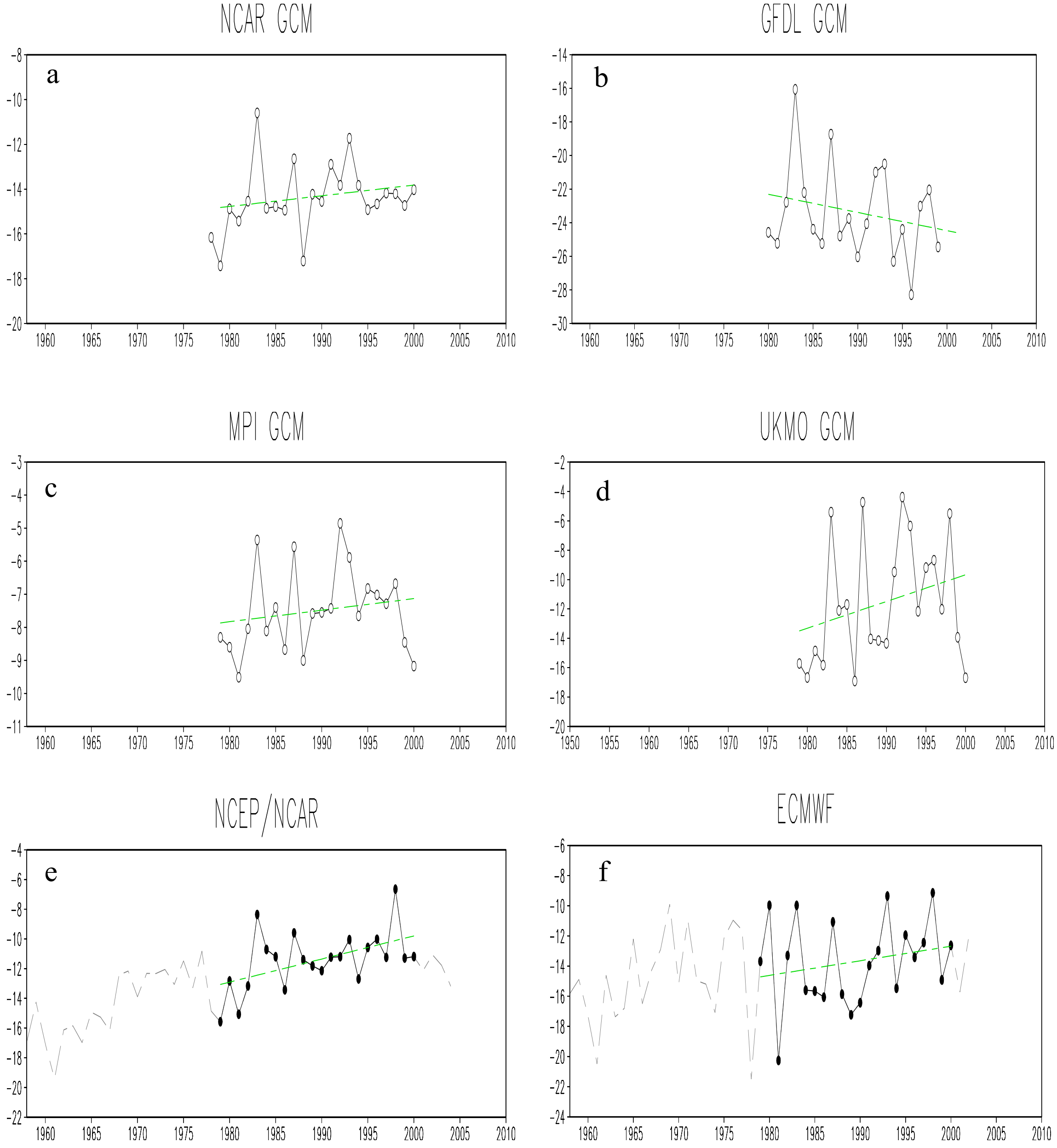

Figure 4.22: 11ºN-22ºN averaged JJA zonal mean 500-hPa vertical pressure velocity (omega) in the NCAR (a), GFDL (b), UKMO (d), NCEP/NCAR (e) and ECMWF (f) reanalyses. (c) is same as (a) but for 850-hPa divergence in MPI GCM. Units of omega and divergence are hPa/day and 10^{-7}/s, respectively. Trends from 1979 to 2000 are 4.78 ± 4.70 in NCAR GCM, -10.84 ± 8.35 in GFDL GCM, 3.50 ± 3.98 in MPI GCM, 18.20 ± 12.98 in UKMO GCM, 15.54 ± 9.53 in the NCEP/NCAR reanalysis and 9.66 ± 15.30 in the ECMWF reanalysis. Units of omega trend and divergence trend are hPa/day/100years and 10^{-7}/s/100years, respectively. The ± values define the 90% confidence intervals for the trends.

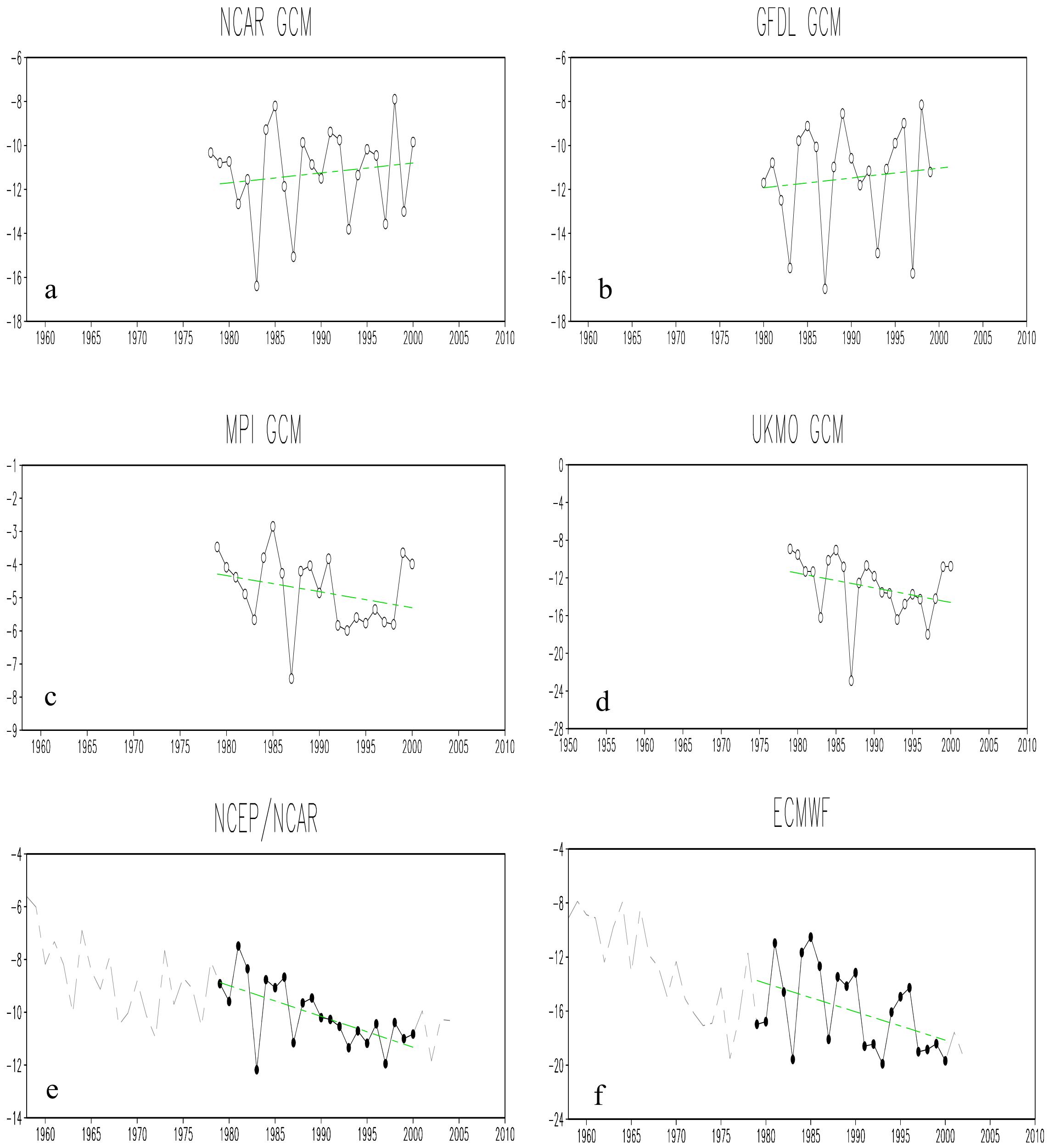

Figure 4.23: 5ºS-8ºN averaged JJA zonal mean 500-hPa vertical pressure velocity in the NCAR (a), GFDL (b), UKMO (d), NCEP/NCAR (e) and ECMWF (f) reanalyses. (c) is same as (a) but for 850-hPa divergence in MPI GCM. Units of omega and divergence are hPa/day and 10^{-7}/s, respectively. Trends from 1979 to 2000 are 4.51 ± 6.76 in NCAR GCM, 4.48 ± 7.45 in GFDL GCM, -4.83 ± 3.39 in MPI GCM, -15.53 ± 10.17 in UKMO GCM., -11.68 ± 5.25 in the NCEP/NCAR reanalysis and -20.99 ± 15.07 in the ECMWF reanalysis. Units of omega trend and divergence trend are hPa/day/100years and 10^{-7}/s/100years, respectively. The ± values define the 90% confidence intervals for the trends.

Chapter 5

Long-term Change of the Asian Summer Monsoon

As shown in the previous chapter, monsoon circulations form a large part of the seasonal Hadley circulation. This is especially true in boreal summer in which the zonally averaged meridional overturning is essentially the zonal average of the south Asian monsoon (Plumb, 2007). I will therefore focus on the long-term variation of the Asian summer monsoon. In the previous chapter, I have shown that the boreal summer precipitation belt moves southward in the two reanalyses, which is accompanied by a weakening of the rising motion in the monsoon region and strengthening near the equator from 1958 to 2002. In this chapter, I will first use observed monsoon precipitation from surface stations to evaluate the reanalyses, thereby providing further evidence of the changes in the Hadley circulation. I will then also use the NCEP/NCAR reanalysis to investigate features of the monsoon circulation changes.

5.1 Introduction

The Asian summer monsoon is not only a major component of the Hadley circulation, but also a significant atmospheric system controlling the climate and weather in a large part of the world. Therefore, there are considerable interests in the community to understand how the Asian monsoon will change in a scenario of global warming (Trenberth et al., 2007). The Asian summer monsoon refers to sharp seasonal advances of precipitation and wind fields over and around India and southeast Asia from May to September (e.g., Trenberth et al., 2000). Its variation on decadal and longer time scale provides a good test to understand and simulate regional climate changes.

Many studies have reported changes in the summer monsoon rainfall over Asia, most of them describing intraseasonal or interannual variability, and relationships with El Niño (e.g., Lau and Nath, 2006; Hoyos and Webster, 2007; Lim and Kim, 2007). Previous studies have also examined rainfall variation of Asian monsoon on decadal time scales that is directly relevant to global climate change. Among them, the more conclusive results include: (1) decrease of Asian monsoon rainfall in the last fifty years of the 20th century (e.g., Stephenson et al., 2001; Quan et al., 2003; Tanaka et al., 2004); (2) the lack of direct relationship of monsoon rainfall with global temperature (Kripalani et al., 2003; Wang and Ding, 2006); and (3) the different relationships between Asian monsoon rainfalls and El Niño events before and after 1976 (Kumar et al., 1999; Kinter et al., 2002; Chang et al., 2004; Wang et al., 2008a).

Various monsoon indices, such as the vertical wind shear index, convection index and precipitation index, have been developed to describe its long-term variability (Ding et al., 2004; Wang et al., 2008b). Since rainfall and circulation can change in opposite directions on decadal timescales – increased rainfall with decreased vertical motion – as a result of change of atmospheric moisture content (Held and Soden, 2006; Zhang and Song, 2006), it is useful to clarify how rainfall and atmospheric circulations have changed in concert in this part of the world.

5.2 Data

Two station precipitation datasets are used to describe the monsoon rainfall. One is the IITM-IRM rainfall dataset, which was derived from 306 almost uniformly distributed stations. The data span from 1871 to 2006. The other is the monthly accumulated precipitation dataset from 160 land stations in China from 1951 to 2004, which is from the IAP, CAS. Two other interpolated rain-gauge-based grid precipitation datasets are also used. One is the PREC/L dataset, the other is the CMAP dataset. The former is from January 1948 to April 2008, and the latter is from January 1979 to July 2008. Several other precipitation datasets are also available, such as those from Global Precipitation Climatology Project (GPCP) (Huffman et al., 1997), but since the data sources are largely the same and little differences exist in their description of interannual and decadal variations (Wang and Ding, 2006), they are not employed here.

To bridge the rainfall measurements with the reanalysis products, precipitation in NCEP/NCAR and ECMWF (ERA-40) reanalyses are also used. The CMAP version employed here does not include the NCEP/NCAR reanalysis precipitation forecasts. It is known that reanalysis rainfall is largely a model product with great uncertainties; using reanalysis dataset in describing the monsoon variability therefore needs to be assessed, which will be presented. Atmospheric circulations of horizontal winds, 500-hPa vertical pressure velocity, and stream function from the NCEP/NCAR reanalysis are also used. Results are presented for boreal summer (JJA) over the period 1980-2007 when significant variations of the Asian monsoon precipitation and winds exist with better quality data.

5.3 Long-term Change of the Asian Summer Monsoon Precipitation

Figure 5.1 shows the time series of the JJA precipitation anomalies over the Indian continent and southeast China from 1948 to 2007. Figures 5.1a and 5.1b are from station observation (grey dash lines), PREC/L (green solid lines) and CMAP (purple solid lines). Overall the three datasets match well, even though there are some differences after 1979 when the satellite-derived data are merged. Over India, observations show a strong decreasing trend from 1980 to 2002 but a recovery during 2003-2007. On the other side, in southeast China, observations show a strong increasing trend from 1980 to 2002 but an indication of drying after 2002. In this chapter, I will focus on the period after 1979 when satellite data become available to the reanalyses and separate the period before and after 2002.

Figures 5.1c and 5.1d compare the precipitation in the two regions in the NCEP/NCAR (blue solid lines) and ECMWF (red solid lines) reanalyses with station observations (grey dash lines). The decreasing trend of precipitation over India and the increasing trend over southeast China from 1980 to 2002 are all well captured in the NCEP/NCAR reanalysis. The ECMWF reanalysis shows a trend opposite to the station data over India, but same as the station data over southeast China.

The climatological JJA precipitation over the Asian monsoon region, averaged over the 23 years from 1980 to 2002, is shown in Figure 5.2. Precipitation was not assimilated in the two reanalysis datasets. Yet, I have found good consistency among the precipitation products of PREC/L, CMAP and the NCEP/NCAR reanalysis in the region including: the locations and the orientation of the 2 mm/day and 4 mm/day contours, the maxima along the west coasts of India and Indochina peninsula and over the Northwest Pacific near the Philippines. This consistency again, lends credence to the NCEP/NCAR reanalysis in capturing the Asian monsoon circulations in this season. The ECMWF reanalysis is less consistent.

The linear regressions of JJA precipitation against time from PREC/L, CMAP, NCEP/NCAR and ECMWF reanalyses from 1980 to 2002 are shown in Figures 5.3a to 5.3d, respectively. Twenty three years are too short for a true trend analysis, the linear regressions are therefore meant to describe decadal variability features after satellite data became available. Statistical significance tests of the linear regressions are carried out as in Wigley (2006), which takes into account temporal autocorrelations in evaluating the magnitude of the linear variations against the standard errors. Regions of linear variations with a 95% confidence interval are shaded in the figures.

The most prominent feature in the PREC/L data (Figure 5.3a) is the statistically significant decrease of precipitation over India and the increase of precipitation over southeast China. This feature is also in the CMAP analysis (Figure 5.3b). The CMAP data also indicated overall decrease of precipitation over the oceans between 10^{o}N to 15^{o}N and overall increase to the north and south. Figure 5.3c shows that all these characteristics are remarkably captured in the NCEP/NCAR reanalysis, all at statistically significant levels. The largest difference between the rainfall variations in CMAP and NCEP/NCAR are over the Tibetan Plateau where large uncertainties are expected also in the rain gauge and satellite products. The rainfall variation in the ECMWF reanalysis is dissimilar to the observations, especially over the India peninsula (Figure 5.3d).

As mentioned before, the precipitation trends in the two regions have changed sign after 2002 as shown in Figures 5.1a and 5.1b. Figures 5.1c and 5.1d show that this is also reasonably captured in the NCEP/NCAR reanalysis (blue lines). Because of the relatively short time record after 2002, I will take the difference of the 5-year means of 2003-2007 with those of 1998-2002 to investigate changes of the Asian summer monsoon rainfall and winds in the later period.

Figure 5.4 shows the difference between the 5-year mean precipitation of 2003-2007 and that of 1998-2002 in the PREC/L data, the CMAP product, and the NCEP/NCAR reanalysis. There is a strong rainfall increase in Indian continent but a significant decrease in southeast China in the PREC/L data. The CMAP dataset shows consistent features. They are well captured by the NCEP/NCAR reanalysis.

The above discussion leads me to the following conclusions: (1) the rainfall decreased over India before 2002 but increased thereafter, and the opposite changes happened over southeast China; (2) these changes are captured in the NCEP/NCAR reanalysis; and (3) the decrease of monsoon rainfall over India from 1980 to 2002 is consistent with the reduction of the upward motion in this region that was shown to be associated with the weakening of Hadley circulation from 10^{o}N to 20^{o}N shown in the previous chapter. In a warmer climate, atmospheric moisture increases, reduction of precipitation is therefore expected to be associated with reduced intensity of atmospheric circulation. This is further studied next.

5.4 Long-term Change of the Asian Summer Monsoon Circulation

The consistency of the precipitation changes between the NCEP/NCAR reanalysis and observations motivated me to use that reanalysis dataset to examine the circulation changes associated with the rainfall feature. Figures 5.5a and 5.5b show respectively the climatology of JJA 850-hPa wind and 500-hPa vertical pressure velocity. Horizontal winds in southeast Asia in the lower troposphere are dominated by three systems (Figure 5.5a): (1) westerly and southwesterly Indian monsoon extending from the Arabian Sea to Bay of Bengal and South China Sea; (2) the clockwise cross-equatorial circulation originating from the Australian winter monsoon; and (3) the anticyclonic circulation of the subtropical high in the northwest Pacific. The above-mentioned flows converge over the south Asia to give rise to the broad regions of strong upward motions depicted in Figure 5.5b.

The trend of the 850-hPa wind during the 23 years is shown in Figure 5.5c, with statistical significance indicated by shading. The following features of the wind patterns can be noted: (1) Over the Indian ocean and the equatorial western Pacific, the trends of the horizontal winds are nearly opposite to their climatologies, depicting weakened Indian summer monsoon and Australian winter monsoon; (2) Over the subtropical high in the northwest Pacific, the anticyclonic flow has strengthened; (3) Over central China, the wind trend is northerly, opposite to the southerly flow of the climatology. These wind patterns resulted in a center of cyclonic wind anomaly over south China, caused by both the strengthened flow along the subtropical high and the northerly anomaly over central China, and a center of anticyclonic wind anomaly over north India and the Bay of Bengal, caused by the weakening southwesterly monsoon flow. These changes of the lower tropospheric flows coincide well with the variation of the 500-hPa vertical pressure velocity (Figure 5.5d): increased upward motion over southeast China and decreased upward motion over the north Indian subcontinent and Bay of Bengal. These are all consistent with changes of precipitations shown in Figure 5.3c.

For the period after 2002, Figures 5.5e and 5.5f show that changes of horizontal winds and vertical motion during 2003-2007 are largely opposite to the changes during 1980-2002, which are also consistent with changes of precipitation shown in Figure 5.4c.

The climatology of the 850-hPa stream function and derived rotational winds in the NCEP/NCAR reanalysis is shown in Figure 5.6a. The Indian monsoon winds can be characterized by two systems, one is the anticyclone over Indian ocean, the other is the cyclone over the Asian continents, while the east China monsoon winds can be characterized by the anticyclonic system over the northern Pacific ocean and cyclonic system over the Asian continent. The corresponding linear trends during 1980 to 2002 are shown in Figure 5.6b. From 1980 to 2002, the cyclonic system over Asian continent has weakened, while the two anticyclonic systems are strengthened, and moved northward over the Northern Indian ocean and westward over the northern Pacific, leading to an anticyclonic anomaly in Indian region and cyclonic anomaly in southeast China. These are accompanied with the weaker lower-level convergence in India and stronger lower-level convergence in southeast China (not shown). The circulation changes after 2002, shown in Figure 5.6c as the 5-year difference between 2003-2007 and 1998-2002, are opposite to those from 1980 to 2002.

Previous studies have found it fruitful to distinguish the east Asian monsoon from the Indian monsoon (e.g., Ding et al., 2004; Wang et al., 2008b) based primarily on their different interannual variations. Our results suggest that such a distinction is also instructive for decadal time scale variations since the precipitation features shown in Figure 5.3 are clearly caused by different circulation systems. Our results also indicate that changes of the east Asian monsoon may be further related to three separate wind systems: the anticyclonic circulation of the subtropical high over the northwest Pacific, the southwestly monsoon flow over the northern Indian ocean, and the southerly flow over central China. Whether such a distinction is warranted depends on how independent these systems vary (Yu et al., 2004; Zhou et al., 2009).

5. 5 Summary and Discussion

I have shown that the variation of precipitation from 1980 to 2007 in the NCEP/NCAR reanalysis over the south Asian monsoon region is consistent with rain gauge and satellite measurements: rainfall has decreased over India but increased over southeast China from 1980 to 2002 while the patterns change signs after 2002. This consistency is exploited to reveal the following changes of the lower tropospheric atmospheric circulations associated with the rainfall features: an overall reduction of southwesterly monsoon flow over the Indian Ocean, an increase of anticyclonic flow over the northwest subtropical high, and a decrease of southerly flow over central China. The combination of these flow patterns resulted in a cyclonic anomaly center over southeast China and anticyclonic anomaly center over north India, and thus variations in vertical motion and rainfall from 1980 to 2002. The opposite circulation change has occurred after 2002.

Our results provide an observational basis to carry out mechanistic modeling studies for unraveling the effects of multiple causes on the monsoon rainfall variations. They can be also used to test the ability of climate models to simulate observed changes of monsoon rainfall and the associated atmospheric circulations.

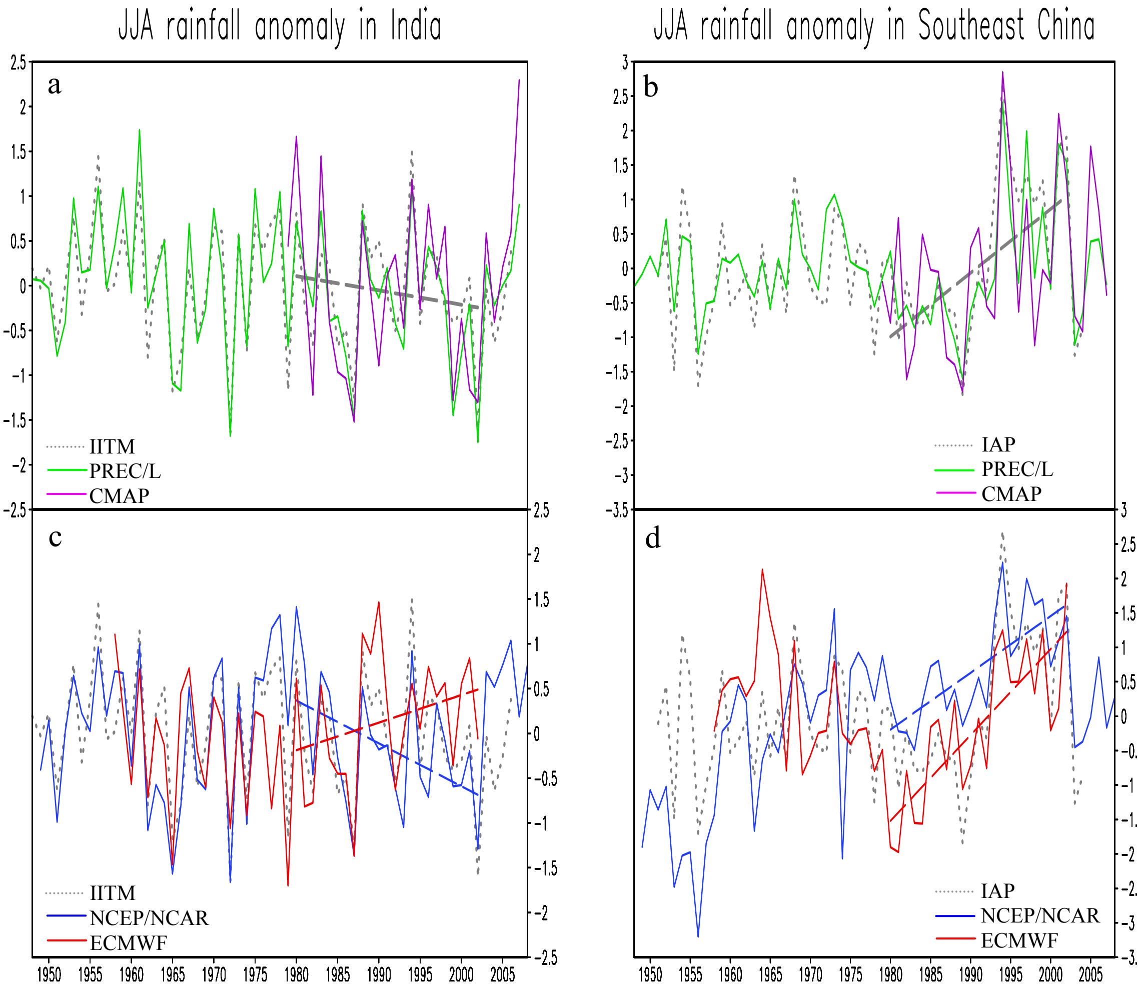

Figure 5.1: (a) is area mean JJA precipitation anomaly in India (65ºE-85ºE, 5ºN-30ºN) from station observation (grey dot line), PREC/L (green solid line) and CMAP (purple solid line), (b) is same as (a) but in southeast China (105ºE-120ºE, 15ºN-30ºN). (c) is same as (a) but from station observation (grey solid line), NCEP/NCAR (blue solid line) and ECMWF (red solid line) reanalyses. (d) is same as (c) but in southeast China. Grey dash lines are linear trends of precipitation from observation, blue and red dash lines are linear trends of precipitation from NCEP/NCAR and ECMWF reanalyses, respectively. Station observations are from IITM in India and from IAP in China. Unit of precipitation anomaly is mm/day. Trends of the Indian rainfall are -2.7 ± 4.2 mm/day/100years, -3.5 ± 2.0 mm/day/100years, and 3.1 ± 4.0 mm/day/100years in observation, NCEP/NCAR and ECMWF reanalyses, respectively. Trends of southeast China rainfall are 9.3 ± 5.5 mm/day/100years, 8.2 ± 3.4 mm/day/100years, and 12.4 ± 4.3 mm/day/100years in observations, NCEP/NCAR and ECMWF reanalyses, respectively. The ± values define the 95% confidence intervals for the trends.

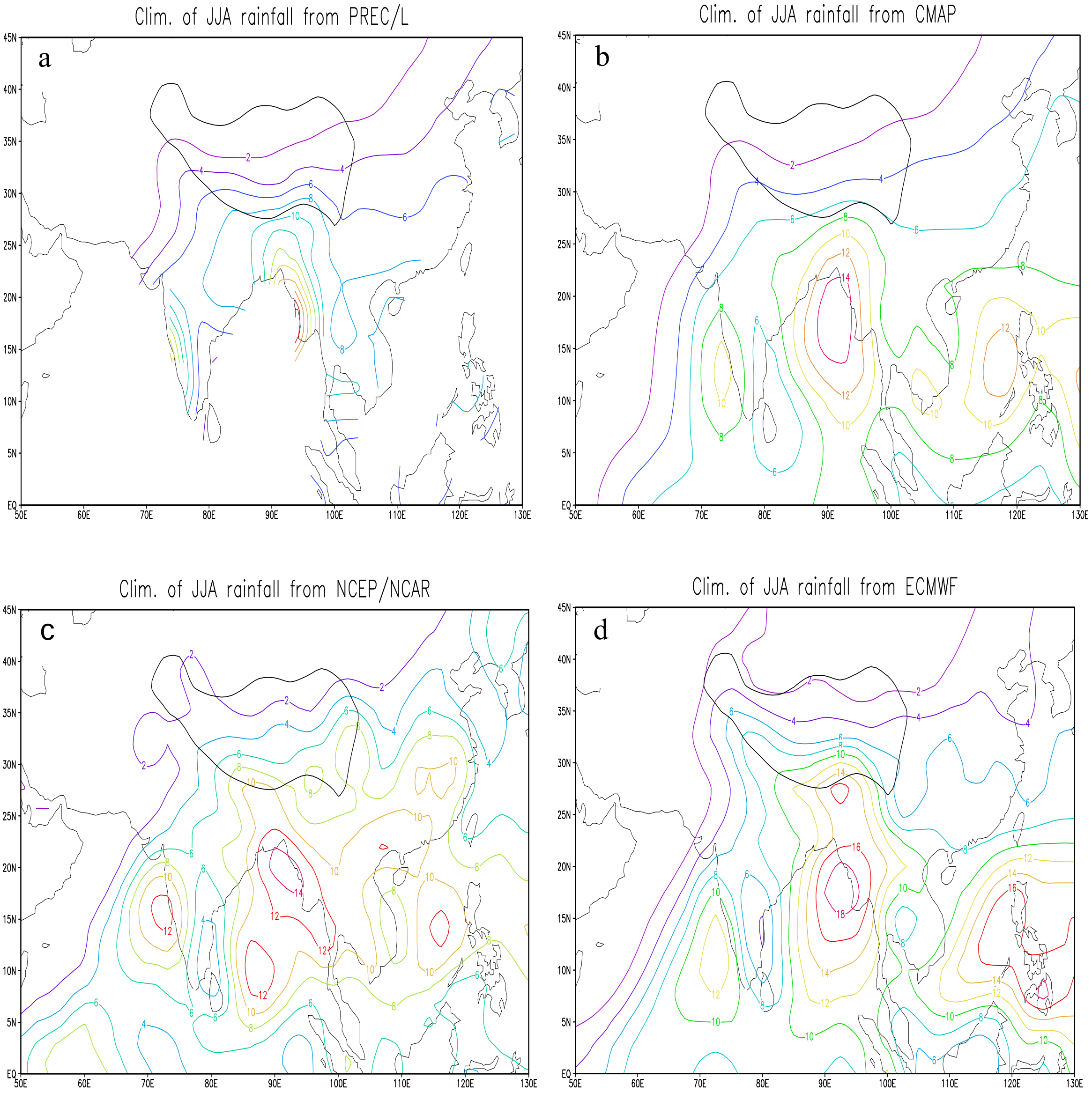

Figure 5.2: Climatology of JJA precipitation from the PREC/L (a), CMAP (b), NCEP/NCAR reanalysis (c), and ECMWF reanalysis (d). Unit of precipitation is mm/day. Black line represents 3-km-height level to outline the Tibetan Plateau.

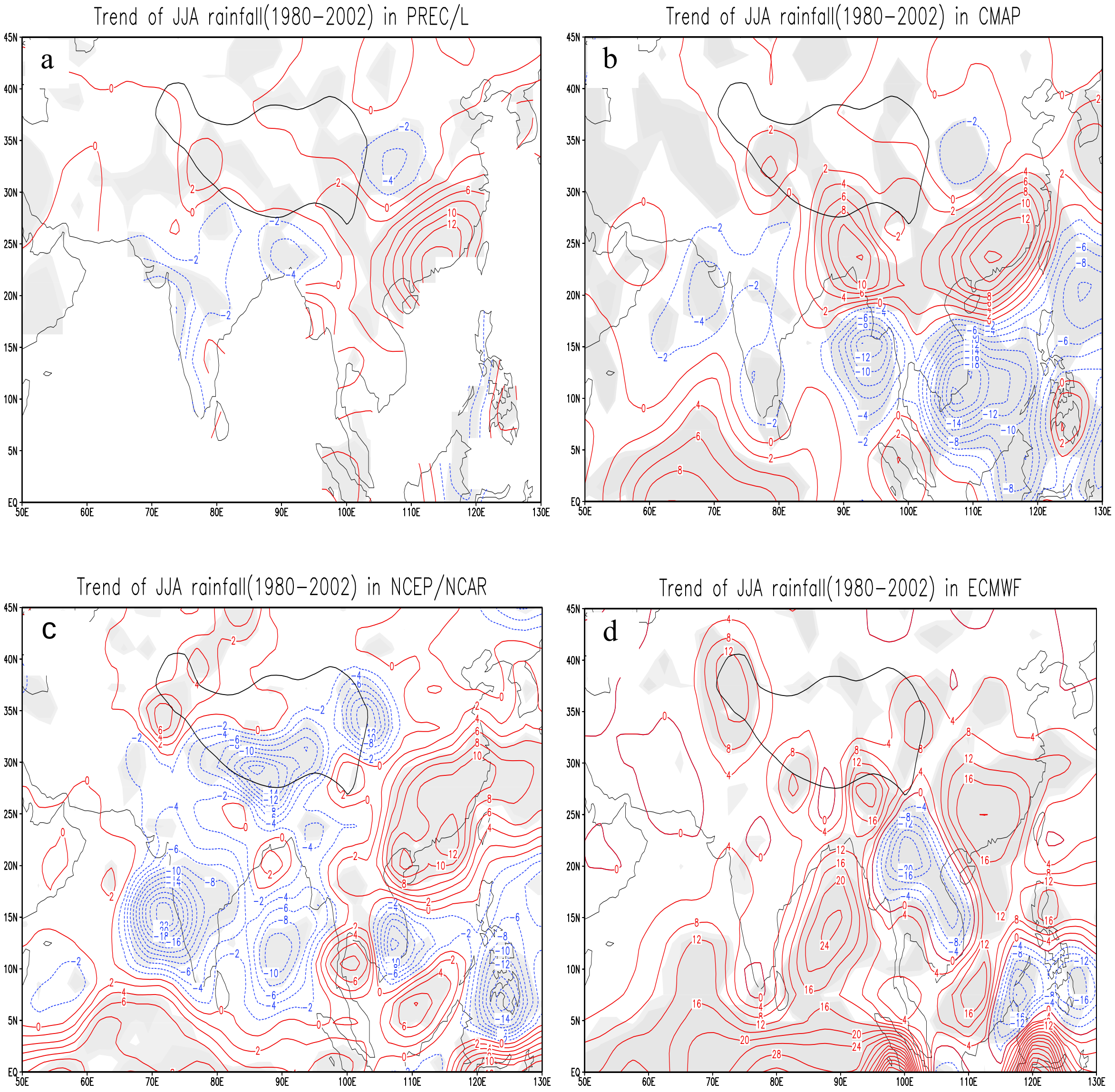
Trend of JJA rainfall(1980–2002) in PREC/L

Trend of JJA rainfall(1980–2002) in CMAP

Trend of JJA rainfall(1980–2002) in NCEP/NCAR

Trend of JJA rainfall(1980–2002) in ECMWF

Figure 5.3: Linear trend of JJA precipitation from PREC/L (a), CMAP (b), NCEP/NCAR reanalysis (c), and ECMWF reanalysis (d) from 1980 to 2002. Unit of the trend is mm/day/100years. Areas where trends are statistically significant at a 95% confidence level are shaded in grey. Black line represents 3-km-height level to outline the Tibetan Plateau.

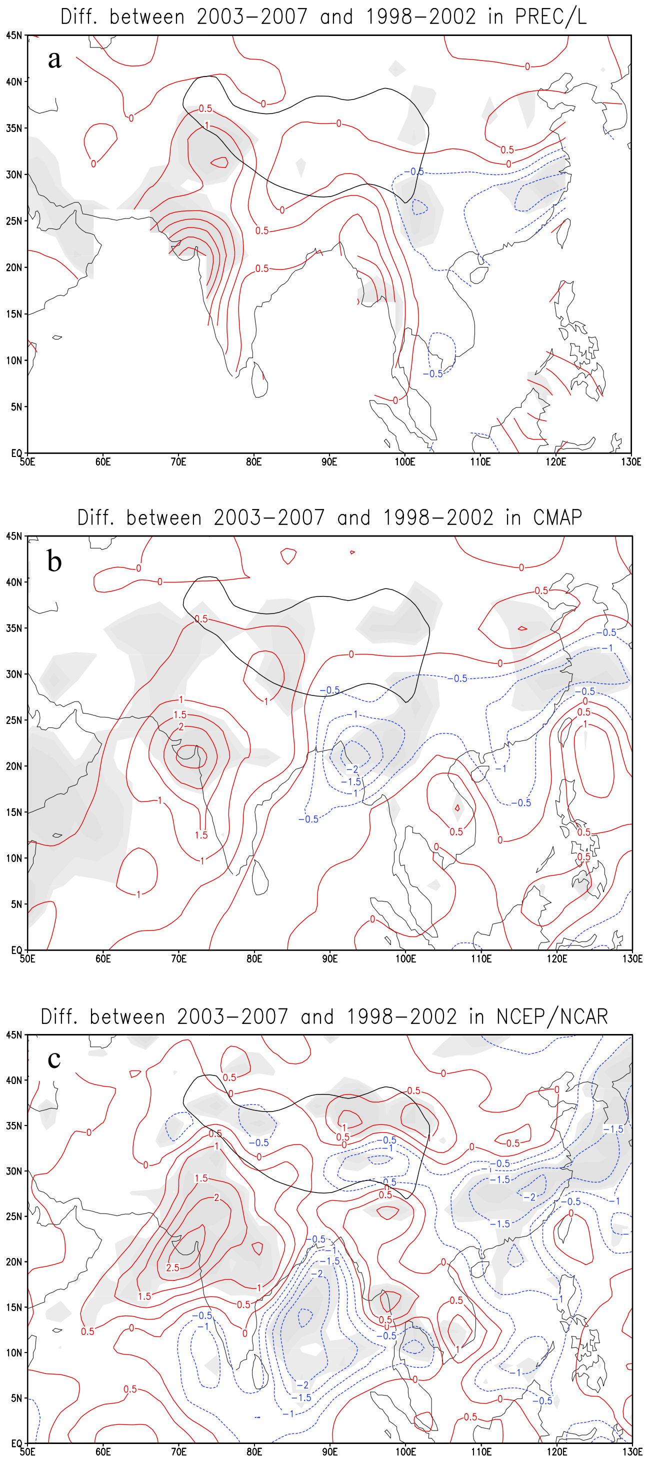

Figure 5.4: JJA precipitation difference between 2003-2007 and 1998-2002 in PREC/L (a), CMAP (b) and NCEP/NCAR reanalysis (c). Areas where differences are statistically significant at a 95% confidence level are shaded in grey. Unit of precipitation is mm/day.

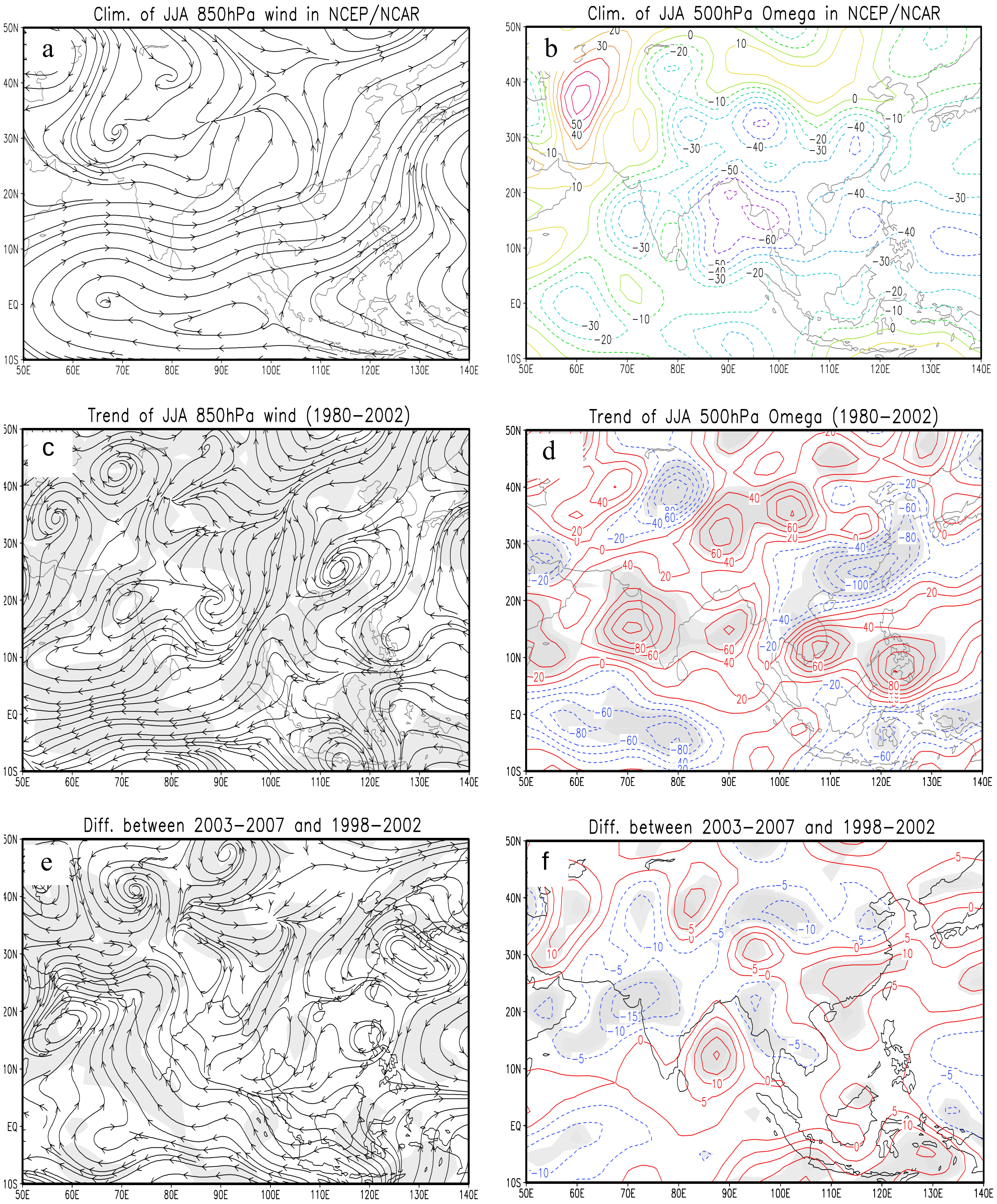

Figure 5.5: (a) is climatology of 850-hPa wind, (b) is climatology of 500-hPa vertical pressure velocity (omega), (c) is linear trend of 850-hPa wind from 1980 to 2002, (d) is same as (c) but for 500-hPa omega, (e) is difference of 850-hPa wind between 2003-2007 and 1998-2002. (f) is same as in(e) but for 500-hPa omega. The data are from the NCEP/NCAR reanalysis. Units of omega and its trend are hPa/day and hPa/day/100years, respectively. Areas where trends or differences are statistically significant at a 90% confidence level are shaded in grey.

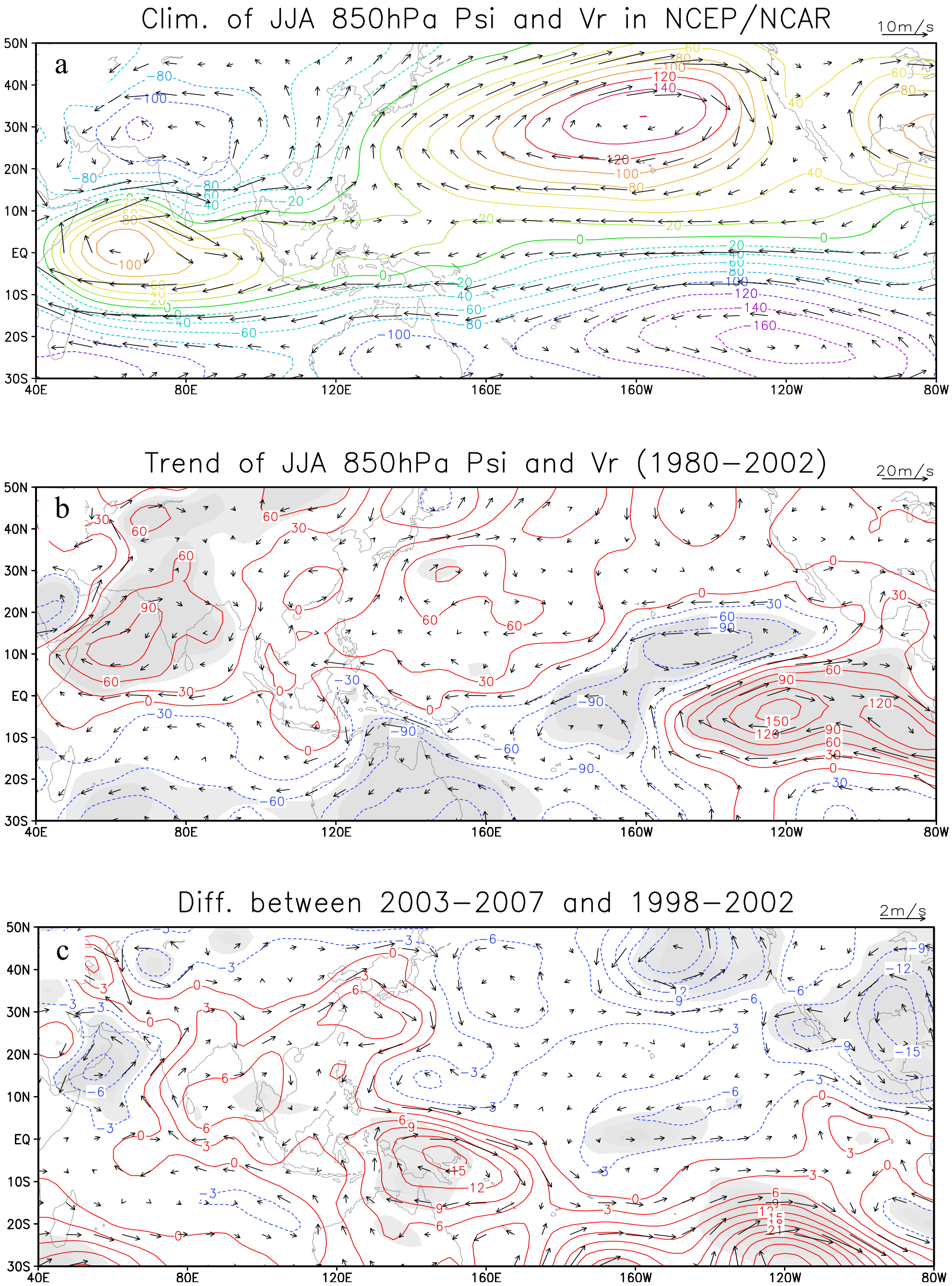

Figure 5.6: 850-hPa stream function and rotational wind vectors in the NCEP/NCAR reanalysis: (a) climatology, (b) linear trend from 1980 to 2002, (c) difference between 2003-2007 and 1998-2002. Areas where trends or differences are statistically significant at a 90% confidence level are shaded in grey. Units of stream function, wind, trend of stream function and trend of wind are $10^5 m^2/s$, m/s, $10^5 m^2/s/100years$ and m/s/100years, respectively.

Chapter 6

Model Simulations

In Chapter 5, I have shown that Asian summer monsoon precipitation decreased over India but increased over southeast China from 1980 to 2002 while the patterns become opposite after 2002. Variations of the observed SSTs (Figure 6.1) also show significantly different patterns before and after 2002 especially in the tropics: Before (after) 2002, SSTs become warmer (colder) in equatorial Indian ocean, western Pacific and tropical southeastern Atlantic, and colder (warmer) in the northern Indian ocean, tropical eastern Pacific and tropical northern Atlantic. Recent studies based on both observations and numerical experiments suggest that the oceanic forcing plays a key role in the monsoon rainfall variation (e.g., Chung and Ramanathan, 2006; Zhou et al., 2008a). In this chapter, I will carry out model simulations to investigate the causes of the observed changes of Asian monsoon precipitation and the associated circulations by addressing the following questions: Can the observed significant changes of the Asian summer monsoon precipitation be explained by the atmosphere's response to the observed SST variations? Which features of SST variations have been the most relevant to the changes of the Asian summer monsoon rainfall? What is the possible physical mechanism?

6.1 Model Description and Design of Experiments

A series of numerical experiments were conducted with the National Center for Atmospheric Research (NCAR) Community Atmospheric Model, version 3 (CAM3) (Collins et al., 2006a). CAM3 serves as the atmospheric component of the Community Climate System Model, version 3 (CCSM3) (Collins et al., 2006b), and is coupled to the Community Land Surface Model, version 3 (CLM3) (Dickinson et al., 2006). The model used here is a global spectral model with a horizontal T42 spectral resolution, which prescribes a roughly uniform 2.8°lat × 2.8°lon Gaussian grid on the Earth's surface. Vertically, the resolution is 26 levels using the hybrid sigma and pressure coordinate, and the top height is 2.917-hPa. The integration time step is 20 minutes for all dynamical and physical process except radiation. The radiation is calculated once an hour and held fixed during the hour. In my simulations, I adopted the Eulerian dynamic core with prescribed seasonally varying SST. The SST data used is a blended version of the HadISST and Reynolds SST datasets (Hurrell et al., 2008).

Control simulation (Hereafter referred as CONT) is conducted with climatological SSTs. Experiment simulations are run by superposing the observed SST changes on the climatological SSTs. Table 6.1 lists the specifications of the experiments conducted for this study. Each experiment includes full seasonal cycle and is integrated for 25 model years. The first five years of output are discarded to exclude any possible transient spinup effects; results reported below are averaged over the last 20 years. Statistical significance is assessed by use of a Student's t-test (95% level) applied to the difference between each pair of experiments where the standard deviations and degrees of freedom were based on the averages of the 20 individual years.

6.2 Results

6.2.1 Asian Summer Monsoon's Response to Global SST Forcing

As a reference, Figure 6.2a shows the observed 1980-2002 trend of JJA rainfall in units of millimeters per day over the 23 years. There are statistically significant negative rainfall trends over India and positive rainfall trends over southeast China. Figure 6.2b shows the observed difference of precipitation between the two periods of 2003-2007 and 1998-2002. After 2002, there is rainfall recovery in India but drying in southeastern China. The simulated precipitation changes forced by the two sets of observed global SST changes in Figure 6.1 are shown in Figures 6.2c and 6.2d. It is seen that in both cases, the observed rainfall change in India can be clearly deduced from atmosphere's response to the observed SST variations. The simulated rainfall change pattern in southeast China roughly resembles that of the observation except for the first period.

The left panels of Figure 6.3 show the climatology, changes of 850-hPa zonal winds for the first period (1980 to 2002) and for the second period (2003-2007 minus 1998-2002) in the NCEP/NCAR reanalysis. There is reduction of zonal wind from 10^oN to 20^oN over the Indian ocean, but increase of the zonal wind in the second period. Over southeast China, the zonal wind has increased in the first period but weakened in the second period.

The corresponding simulations are shown in the three panels of Figure 6.3 in the right column. The model has captured the broad features of the circulation changes revealed by the NCEP/NCAR reanalysis. Specifically, the simulated 850-hPa zonal winds have significantly weakened over India and strengthened over southeast China from 1980 to 2002, but they show opposite patterns after 2002.

The left panels of Figure 6.4 show the climatological distribution of the 850-hPa meridional wind and its changes in the two periods in the NCEP/NCAR reanalysis. The right panels show the corresponding simulations. For the climatologies shown in Figures 6.4a and 6.4b, while there are differences in the magnitudes of the simulated winds, the locations of the maximum and minimum over south Asia depicting the trough and ridge are reasonably simulated. For the changes, Figures 6.4c and 6.4e show that the 850-hPa variation of the meridional wind is out of phase with the climatology in south Asia from 1980 to 2002 but in phase with the climatology in south Asia after 2002 in the NCEP/NCAR reanalysis. These are also captured in the simulations shown in Figures 6.4d and 6.4f. In southeast China, the trend distribution of meridional wind revealed by the reanalysis is not well reproduced by the model in the first period. In the reanalysis, the meridional wind is strengthened along the coastlines of the southeast China but it is weakened over the inland of China. I will revisit this difference later. Zhou et al. (2008b) pointed out that specifying SST to an AGCM generally shows poor performance in reproducing the SLP response over the North Pacific. The simulated change of meridional winds in the second period is more consistent with that in the reanalysis.

Figure 6.5 shows the corresponding figure for the 500-hPa vertical pressure velocity. Weakened southwestly wind in the Arabian Sea leads to less low level convergence and weakened vertical rising motion (Figures 6.5c and 6.5d) in India from 1980 to 2002. The pattern is opposite after 2002 (Figures 6.5e and 6.5f). For southeast China, consistent with the comparison of the meridional wind variations, the model does not capture strengthening of the rising motion in the first period (Figures 6.5c and 6.5d), but it simulated the weakened rising motion in the second period (Figures 6.5e and 6.5f). These changes in the vertical velocity are consistent with the simulated precipitation variations in Figure 6.2.

To examine the vertical structure of the changes of monsoon circulation in India, I show in Figure 6.6 a cross section of JJA meridional wind (contour) and vertical pressure velocity (image) averaged over 65°E-95°E, along with the changes from the GO1 and GO2 runs, forced with SST anomalies for the two periods in Figures 6.1a and 6.1b respectively. It is seen that with the SST forcing in the first period from 1980 to 2002 (Figure 6.6b), the rising motion has weakened, and this is accompanied by a meridional circulation anomaly with northerly near the surface and southerly aloft that is opposite to the mean circulation. With the SST forcing in the second period however, Figure 6.6c shows an overall increase of the meridional circulation north of the equator. The rising motion is increased to the north of 15^{o}N and weakened to the south, but the overall strength has increased as seen in Figure 6.5f.

The climatologies of JJA vertically integrated moisture transport in the NCEP/NCAR reanalysis and in the CONT run are shown in Figures 6.7a and 6.7b. In the summer season, the main moisture fluxes originate from the southern hemisphere, flow cross the equator along the Somali coast and down to the Arabian Sea, Indian subcontinent and Bay of Bengal. The moisture transport then extends northeastward from the South China Sea to eastern China and northwestern Pacific. Figures 6.7c to 6.7f show that in India, the moisture transport toward the northeast is weakened from 1980 to 2002, but it is strengthened after 2002 in both the reanalysis and model simulations. Over southeast China, the change of the moisture transport revealed by the reanalysis is not well reproduced by the model in the first period. In the reanalysis, there is a low level moisture transport convergence in southeast China from 1980 to 2002 but the model showed an opposite change. These are again consistent with the precipitation comparison.

In summary, the NCAR CAM3 forced by the observed different global SST variations before and after 2002 can largely reproduce the observed changes of the Asian summer monsoon rainfall. In the Indian region, the overturning circulation and moisture transport are weakened which is accompanied with decreased precipitation from 1980 to 2002, while after 2002, the overturning circulation and moisture transport are strengthened which is accompanied with enhanced precipitation. Over southeast China, the model failed to simulate the precipitation increase from 1980 to 2002 and the associated change in horizontal and vertical winds. As will be further discussed later, this is likely due to the overestimated response of reduced monsoon rainfall in India in the simulation. The model however reproduced the variation of precipitation and associated circulation changes over southeast China in the reanalysis for the second period after 2002.

6.2.2 Asian Summer Monsoon's Response to Regional SST Forcing

6.2.2a Simulation Forced by Regional SST Variation from 1980 to 2002

To answer which features of the SST variations are the most relevant to the long-term trend of the Asian summer monsoon rainfall, we have performed several sensitivity experiments forced by different regional SST variations. Figure 6.8a shows the changes of JJA precipitation forced by the observed SST variations in the Indian ocean (30ºE-

105ºE, 60ºS-30ºN) for the first period from 1980 to 2002. It is seen that the SST anomalies in the Indian ocean can significantly reduce precipitation in India and enhances precipitation in southeast China. The magnitudes of the change of the precipitation near the Indian subcontinent are comparable to those in the simulated precipitation anomaly forced by the global SST perturbations shown in Figure 6.2c (GO1-CONT).

Figure 6.8b shows the response of simulated precipitation to the observed SST variations in the Pacific (110ºE-80ºW, 60ºS-60ºN). It is seen that the SST variation in Pacific leads to increased precipitation in India and decreased precipitation in southeast China. The changes in precipitation over India and southeast China are however smaller than those forced by the Indian ocean SST. The SST anomalies in the Pacific however forced a large precipitation response in the southern part of the Bay of Bengal and the equatorial western Pacific.

I have also carried out a similar experiment by using the SST anomaly in the Atlantic ocean as the forcing. The response of rainfall in the study domain is much smaller and therefore not presented.

Previous studies (e.g., Deser et al., 2004; Li et al., 2008) have suggested that the recent warming over the tropical ocean has played a major role in the weakening of east Asian summer monsoon circulation. To investigate the role of the tropical SST, I further looked at the simulated changes of JJA precipitation forced by the observed SST in the tropical Indian ocean and tropical Pacific ocean from 30^{o}N to 30^{o}S, respectively.

Figure 6.9a shows the response of precipitation to SST forcing in the tropical Indian ocean from 1980 to 2002. It is seen that both the spatial pattern and the magnitudes of the precipitation change are very similar to those in Figure 6.8a. Figure

6.9b shows the corresponding precipitation responses to the SST forcing in the tropical Pacific, which is again very similar to those in Figure 6.8b. Therefore, the SST anomalies in the tropics have played a dominant role in the precipitation response during the period from 1980 to 2002.

I have conducted another experiment in which SST anomalies in Figure 6.1a from the whole tropics are used to force the model. Figure 6.10a shows the precipitation response. This is now compared with the sum of the two responses from the tropical Indian ocean and Pacific separately in Figure 6.10b. It is seen the SST anomalies from 1980 to 2002 in the tropical Indian ocean and tropical Pacific can largely explain the spatial pattern of the precipitation change over India and southeast China. This comparison also implies that the precipitation response is largely linear with respect to SST forcing in different regions, even though the parameterization of precipitation in the model is a highly nonlinear process.

The associated circulation changes at 850-hPa induced by the tropical Indian ocean SST variation and tropical Pacific ocean SST variation are shown in Figures 6.11b and 6.11c respectively, which are to be compared with the mean winds in Figure 6.11a. The tropical Indian ocean SST variation induces a low-level anticyclonic anomaly along the coastlines of the south Asia, and weakened monsoon winds from 10^{o}N to 20^{o}N over the Indian ocean (Figure 6.11b). Figure 6.12a shows the change of the vertical velocity zonally averaged from 65^{o}E to 95^{o}E overlaid by the contours of the climatological vertical pressure velocity. It is seen that the Indian SST variation suppressed the overturning circulation.

In contrast to the Indian ocean SST forcing, the tropical Pacific SST variation produces a low-level cyclonic anomaly over India (Figure 6.11c), and strengthened monsoon winds as well as enhanced overturning circulation (Figure 6.12b).

In east Asia, the tropical Indian ocean SST forcing induced intensified rising motions when averaged over 105°E to 120°E in southeast China and weakened rising motions in Indochina and south China sea (Figure 6.13a), while the tropical Pacific ocean SST forcing induces weakened rising motions in southeast China and intensified rising motions in Indochina and south China sea (Figure 6.13b). The latitudes of the maximum changes are between 25°N to 30°N. These variation patterns of vertical pressure velocity are consistent with the simulated precipitation changes as shown in Figures 6.9a and 6.9b except that they are further to the north of the observed maximum precipitation change in southeast China as shown in Figure 6.2, which has led to the failure of the model in simulating the precipitation change in this region from 1998 to 2002.

6.2.2b Simulation Forced by Regional SST Variation between 2003-2007 and 1998-2002

Figure 6.14 shows the simulated precipitation changes after 2002 forced by SST changes of the entire tropical oceans, the tropical Indian ocean and tropical Pacific ocean between the two periods of 2003-2007 and 1998-2002. It is seen that SST forcing from the tropics can account for most of the observed rainfall changes of the Asian summer monsoon after 2002 as shown in Figure 6.2d.

Figures 6.14b and 6.14c show that the changes of SST in both the tropical Indian ocean and the tropical Pacific lead to the increased precipitation in India and the decreased precipitation in southeast China after 2002.

The associated circulation changes induced by the SST changes in the tropics, tropical Indian ocean, and tropical Pacific ocean are shown in Figure 6.15. The tropical SST changes after 2002 lead to the increased 850-hPa geopotential heights to the south of 20ºN and the decreased 850-hPa geopotential heights to the north of 20ºN, producing increased low-level northward pressure gradient forces and enhanced westerly winds as well, therefore the monsoon flow. The wind response to the forcing from the SST anomalies in the tropical Indian ocean and tropical Pacific are similar in the Indian ocean except that the center of the anticyclonic circulation anomaly moved further to the east in the response to the tropical Pacific forcing.

6.3 Summary and Discussion

In this chapter, I have shown the following:

(1) The NCAR CAM3 simulated the decrease of monsoon rainfall over India before 2002 and increase of rainfall after 2002 when it is forced with prescribed SST anomalies. These are consistent with observations. The model also simulated the decrease of monsoon rainfall after 2002 in southeast China, but failed to simulate the increase of monsoon rainfall before 2002.

(2) SST forcing from the tropical Indian ocean and from the tropical Pacific can largely explain the simulated changes of Asian monsoon both before and after 2002. SST anomalies in the tropical Indian ocean dominate the those in the tropical Pacific for their impact on Indian monsoon rainfall.

(3) Reduction of Indian monsoon rainfall before 2002 is associated with reduced westerly monsoon flow in the Indian ocean and upward motion from 15^{o}N to 20^{o}N over

the Indian subcontinent in the model simulation. This is the opposite after 2002. These are all consistent with results in the reanalysis.

For the plausible mechanisms of the simulated changes in monsoon rainfall and circulation, my speculation based on Gill (1980) is: the anomalous SST near the equator south of 10^oN in the central Indian ocean before and after 2002 can produce a direct response in the diabatic heating, which can then force a Rossby-gravity wave response that weakens the westerly monsoon from 15^oN to 20^oN before 2002 and intensifies it after 2002. For the response to the tropical Pacific ocean, the SST anomaly maximum at 25^oN before 2002 draws a westerly response over the Indian ocean and this increased precipitation over India. After 2002, the relative minimum of SST anomaly in the western central Pacific forces a westward wind anomaly near the equator and thus westerly from 15^oN to 20^oN. This also increased the precipitation over India. A more definitive answer requires further numerical experiments that I will pursue in the future.

In my study, only the observed SST variation was prescribed as the cause of the observed Asian monsoon changes. Wang et al. (2005) pointed out that coupled ocean-atmosphere processes are crucial in monsoon regions where atmospheric feedback on SST is critical. Using AGCMs, instead of the coupled atmosphere-ocean models, may not adequately represent the air-sea interactions, which could contribute to the deficiencies in precipitation simulation over east China. This may explain the overestimated response of Indian monsoon rainfall to the SST anomalies in the Indian ocean. But the present study suggests to the first order, the atmospheric response to SST forcing can explain the main features of the observed changes of the monsoon circulation.

In the real climate system, both natural and anthropogenic forcings contribute to the summer monsoon rainfall change. Previous studies show that the greenhouse gases forcing induces a uniform warming of the tropical Indian ocean, which leads to intensified evaporation from the Indian ocean, enhanced moisture and increased monsoon rainfall in India (Meehl et al., 1993; Ramanathan et al., 2005). On the other side, recent studies show that sulfate and black carbon aerosols have played a role in forcing the recent changes of the monsoon rainfall by cooling the surface or reducing the latitudinal SST gradient (Lau et al., 2006; Meehl et al., 2008). It is unclear how aerosol-induced inhomogeneous cooling may counteract relatively uniform warming caused by greenhouse gases as the Earth's climate system responds to them. There is a need to better understand how these forcings impact the SST and whether they can induce separate changes in the monsoon circulations.

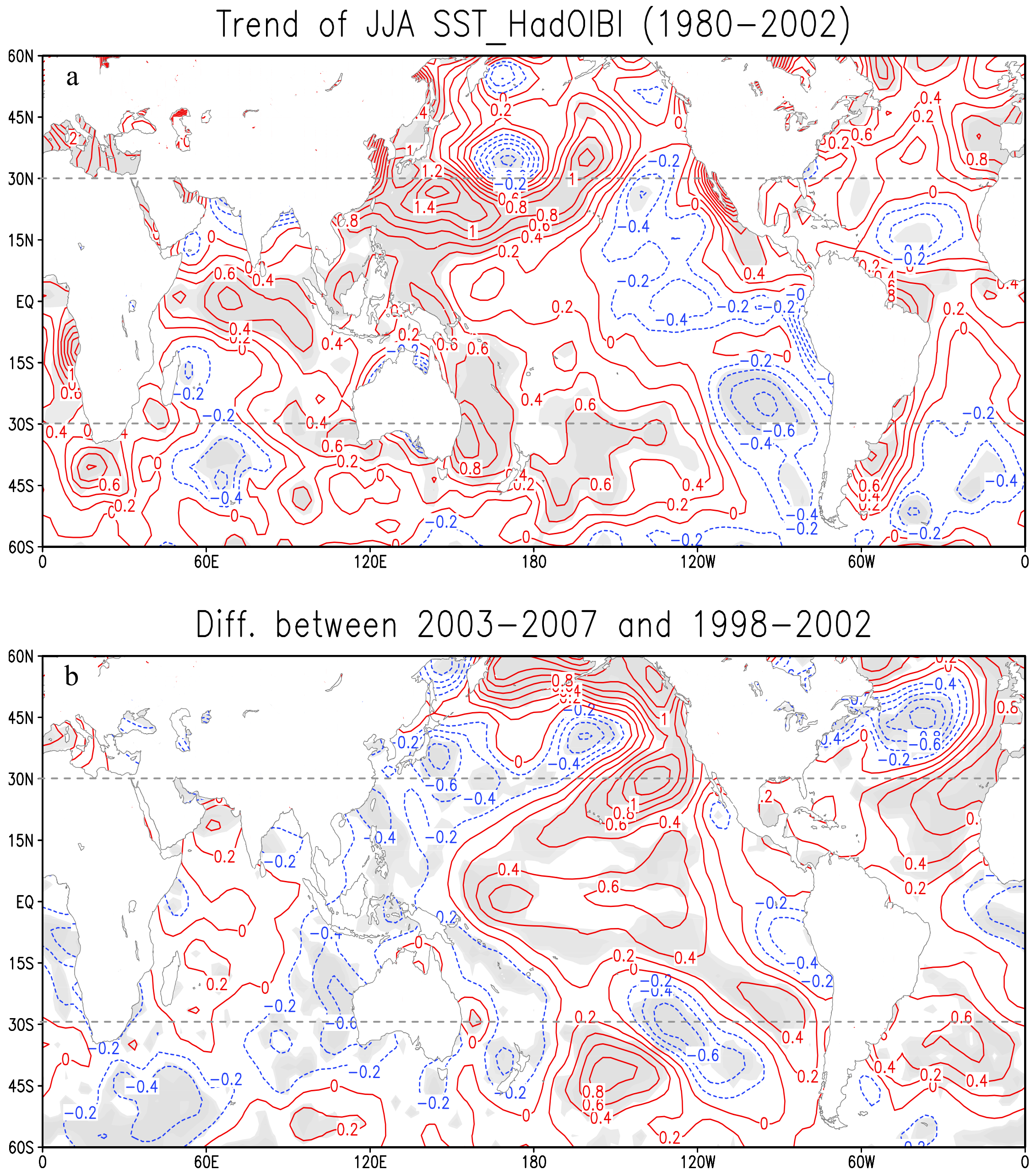

Figure 6.1: (a) is the linear trend of JJA SST from 1980 to 2002. (b) is difference of JJA SST between years 2003-2007 and years 1998-2002. Units of the linear trend and SST difference are K/23years and K, respectively. Areas where trends and differences are statistically significant at a 95% confidence level are shaded in grey.

Table 6.1: List of all the numerical experiments in this study. All experiments are performed using the NCAR CAM3 with yearly repeating SSTs.

Acronym	Prescribed SSTs
CONT	Climatology
GO1	1980-2002 trend imposed globally
GO2	Difference of SSTs(2003-2007) and SSTs(1998-2002) imposed globally
IO	1980-2002 trend imposed in Indian ocean (30ºE-105ºE, 60ºS-30ºN)
PO	1980-2002 trend imposed in Pacific ocean (110ºE-80ºW, 60ºS-60ºN)
TO1	1980-2002 trend imposed in the tropical ocean (180ºW-180ºE, 30ºS-30ºN)
TIO1	1980-2002 trend imposed in tropical Indian ocean (30ºE-105ºE, 30ºS-30ºN)
TPO1	1980-2002 trend imposed in tropical Pacific ocean (110ºE-80ºW, 30ºS-30ºN)
TO2	Diff. of SSTs(03-07) and SSTs (1998-2002) imposed in tropical ocean
TIO2	Diff. of SSTs(03-07) and SSTs (1998-2002) imposed in tropical Indian ocean
TPO2	Diff. of SSTs(03-07) and SSTs (1998-2002) imposed in tropical Pacific

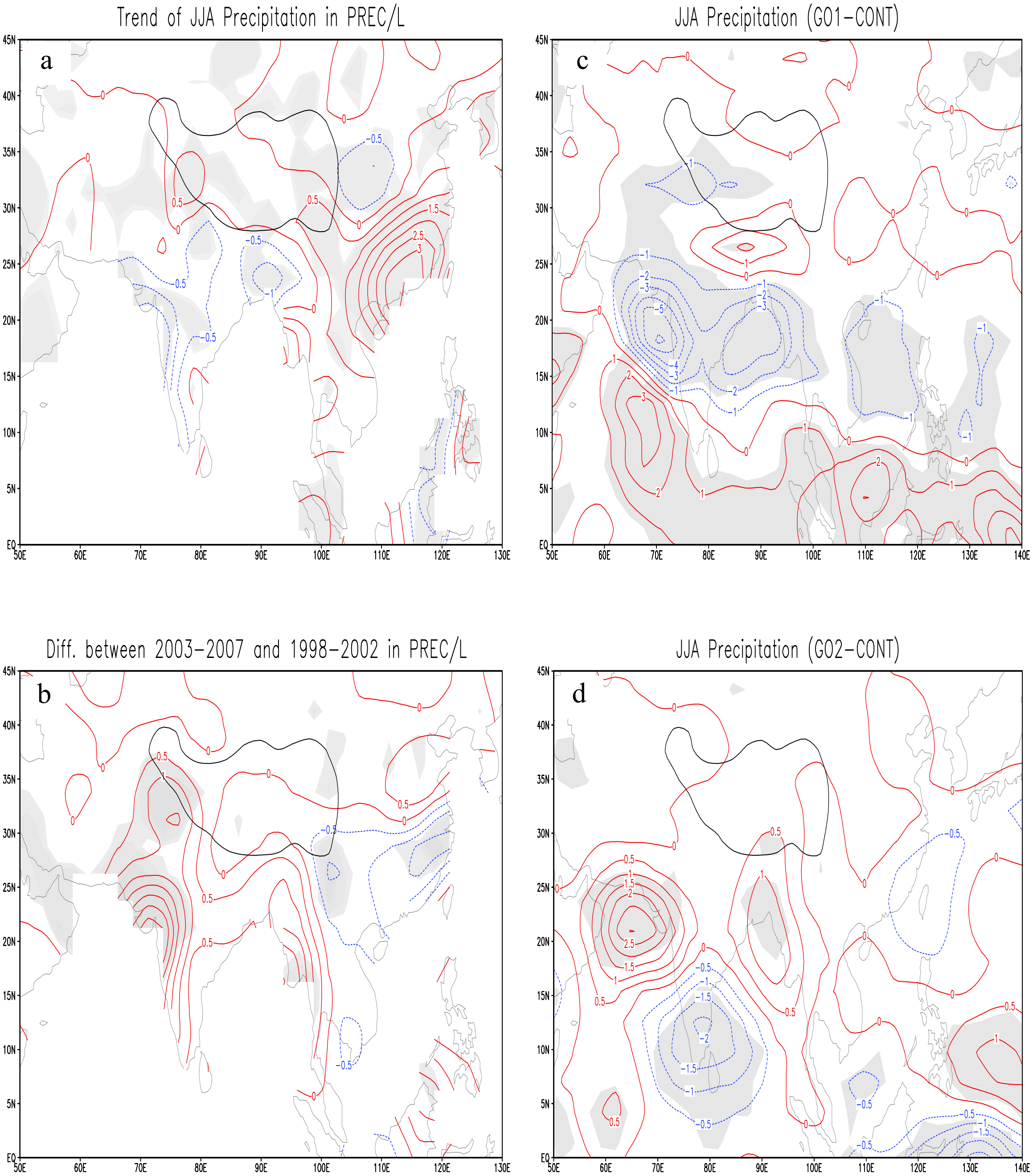

Figure 6.2: (a) is the linear trend of JJA precipitation in PREC/L. (b) is the difference of JJA precipitation between years 2003-2007 and 1998-2002 in PREC/L. (c) is the difference of JJA precipitation between GO1 and CONT runs (GO1 minus CONT). (d) is same as in (c) but between GO2 and CONT runs (GO2 minus CONT). Areas where differences are statistically significant at a 95% confidence level are shaded in grey. Units of precipitation and trend are mm/day and mm/day/23years, respectively. Black line represents 3-km-height level to outline the Tibetan Plateau.

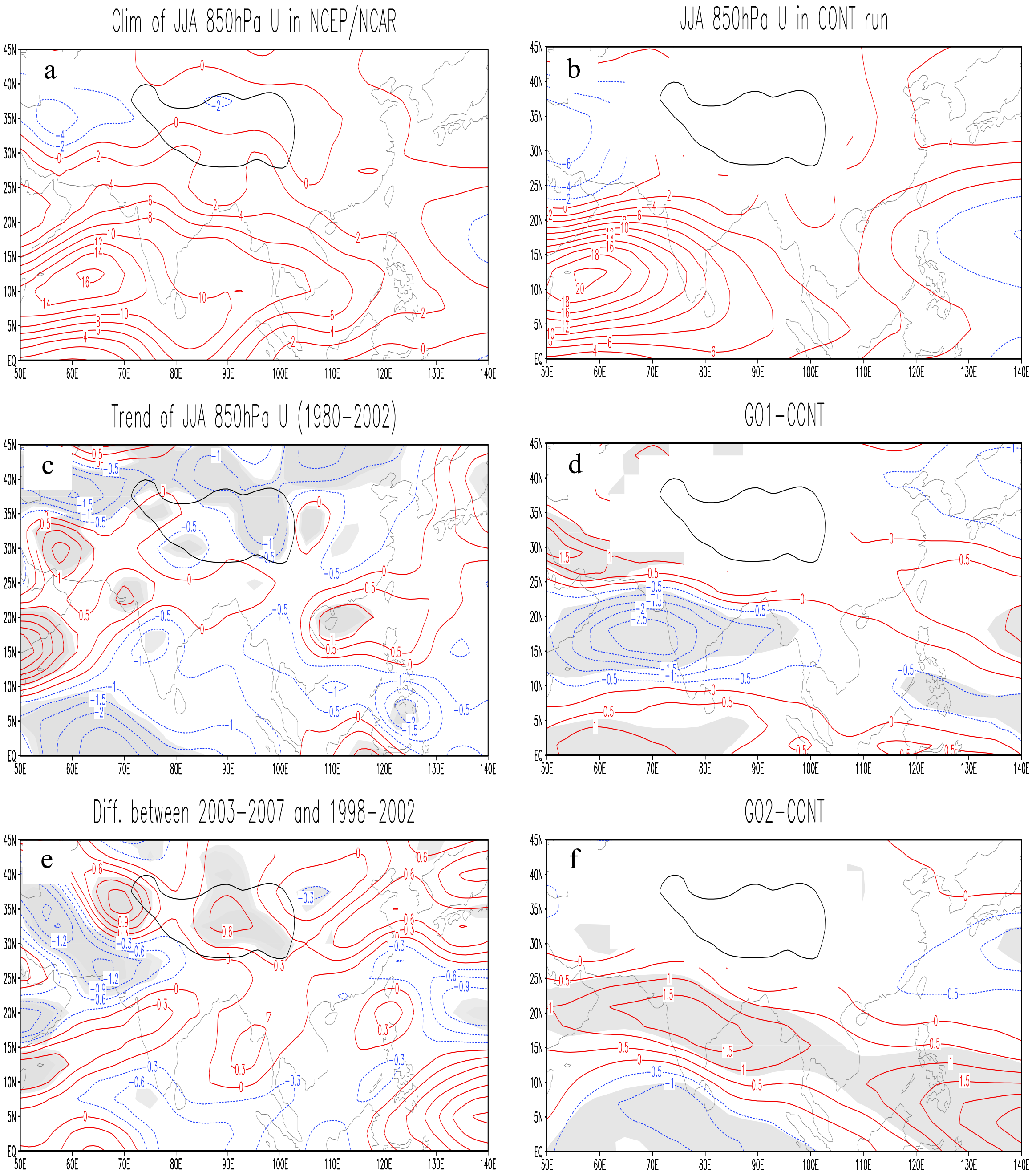

Figure 6.3: Climatology of JJA 850-hPa zonal wind in the NCEP/NCAR reanalysis (a) and in the CONT run (b). Linear trend of JJA 850hPa zonal wind in the NCEP/NCAR reanalysis from 1980-2002 (c). Difference of JJA 850-hPa zonal wind between GO1 and CONT runs (d). Same as in (d) but between years 2003-2007 and 1998-2002 in the NCEP/NCAR reanalysis (e). Same as in (d) but between GO2 and CONT runs (f). Areas where trends or differences are statistically significant at a 95% confidence level are shaded in grey. Units of zonal wind and trend are m/s and m/s/23years, respectively.

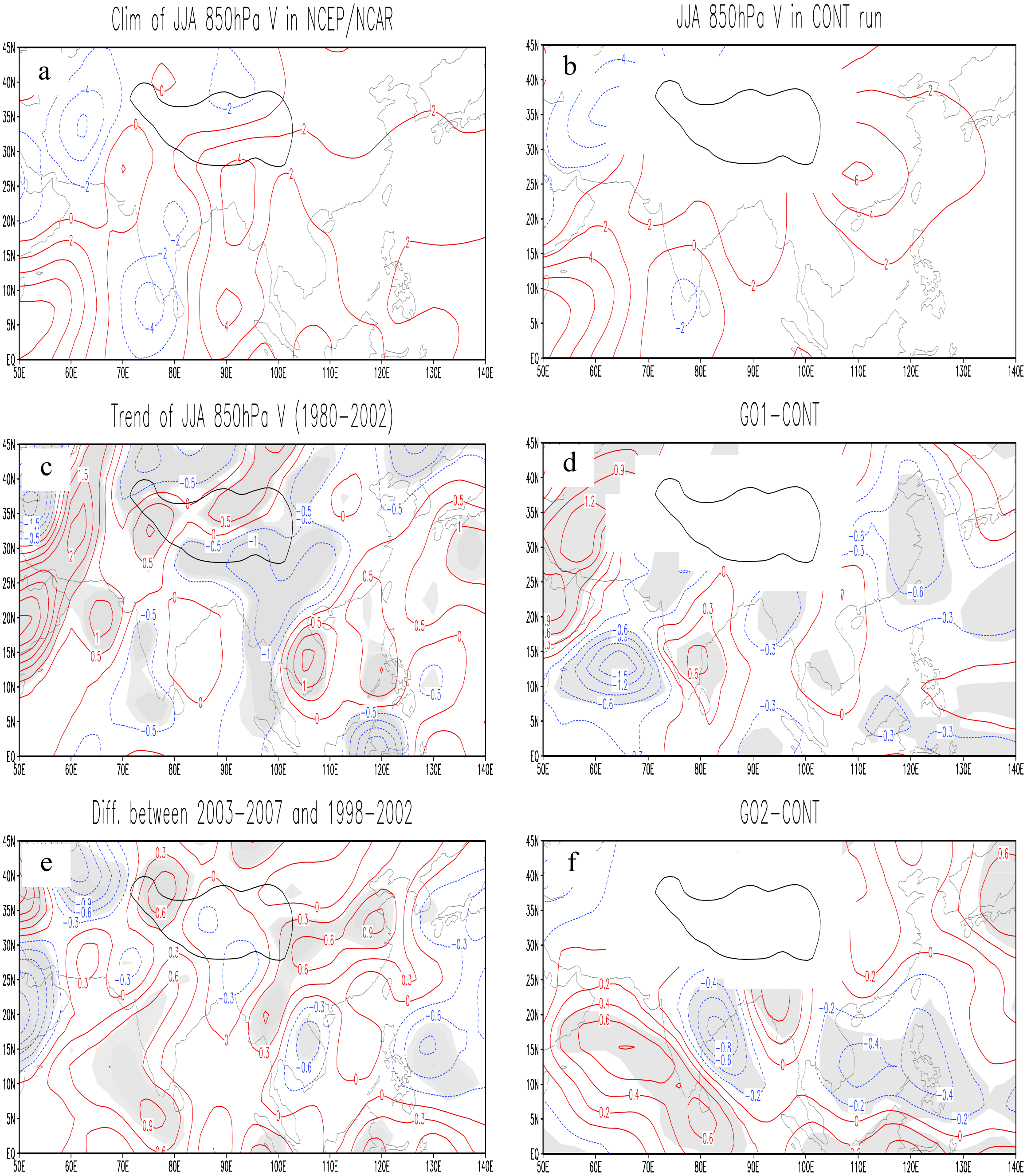

Figure 6.4: Climatology of JJA 850-hPa meridional wind in NCEP/NCAR reanalysis (a) and in CONT run (b). Linear trend of JJA 850-hPa meridional wind in the NCEP/NCAR reanalysis from 1980-2002 (c). Difference of JJA 850hPa meridional wind between GO1 and CONT runs (d). Same as in (d) but between years 2003-2007 and 1998-2002 in NCEP/NCAR reanalysis (e). Same as in (d) but between GO2 and CONT runs (f). Areas where trends or differences are statistically significant at a 95% confidence level are shaded in grey. Units of wind and trend are m/s and m/s/23years, respectively.

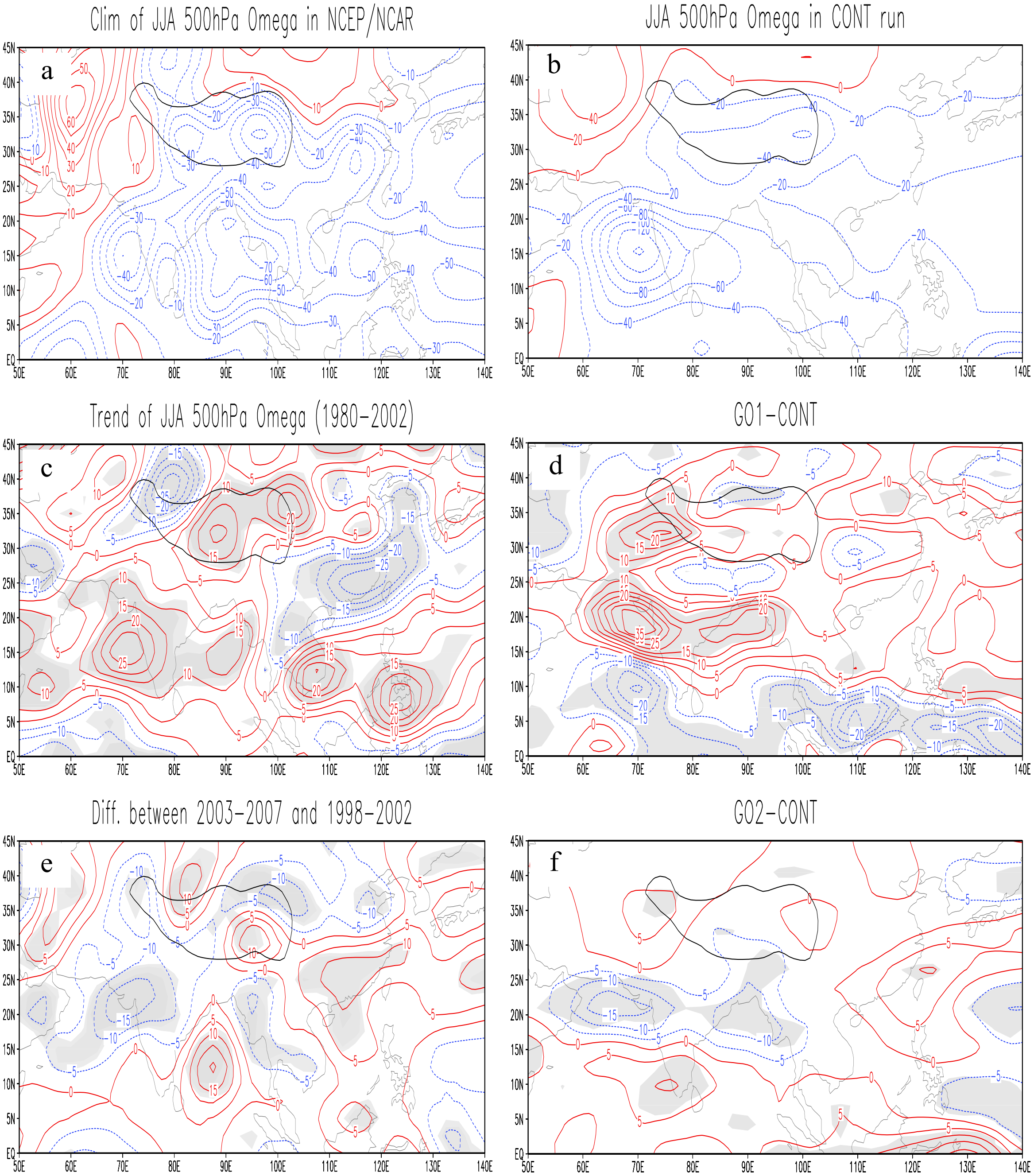

Figure 6.5: Climatology of JJA 500-hPa vertical pressure velocity (omega) in the NCEP/NCAR reanalysis (a) and in the CONT run (b). Linear trend of JJA 500hPa omega in the NCEP/NCAR reanalysis from 1980-2002 (c). Difference of JJA 500hPa omega between GO1 and CONT runs (d). Same as in (d) but between years 2003-2007 and 1998-2002 in the NCEP/NCAR reanalysis (e). Same as in (d) but between GO2 and CONT runs (f). Areas where trends or differences are statistically significant at a 95% confidence level are shaded in grey. Units of omega and trend are hPa/day and hPa/day/23years, respectively.

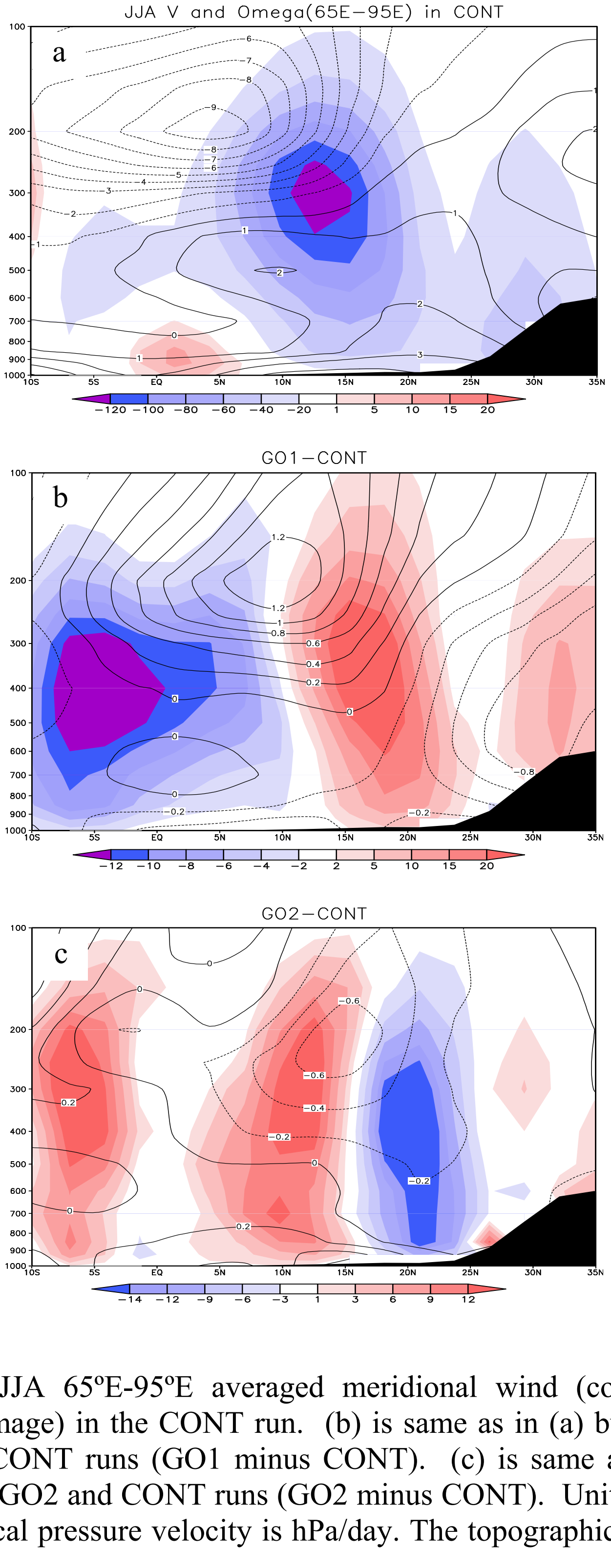

JJA V and Omega(65E−95E) in CONT

GO1−CONT

GO2−CONT

Figure 6.6: (a) is JJA 65ºE-95ºE averaged meridional wind (contour) and vertical pressure velocity (image) in the CONT run. (b) is same as in (a) but for the difference between GO1 and CONT runs (GO1 minus CONT). (c) is same as in (a) but for the difference between GO2 and CONT runs (GO2 minus CONT). Unit of meridional wind is m/s. Unit of vertical pressure velocity is hPa/day. The topographic elevation is shaded in black.

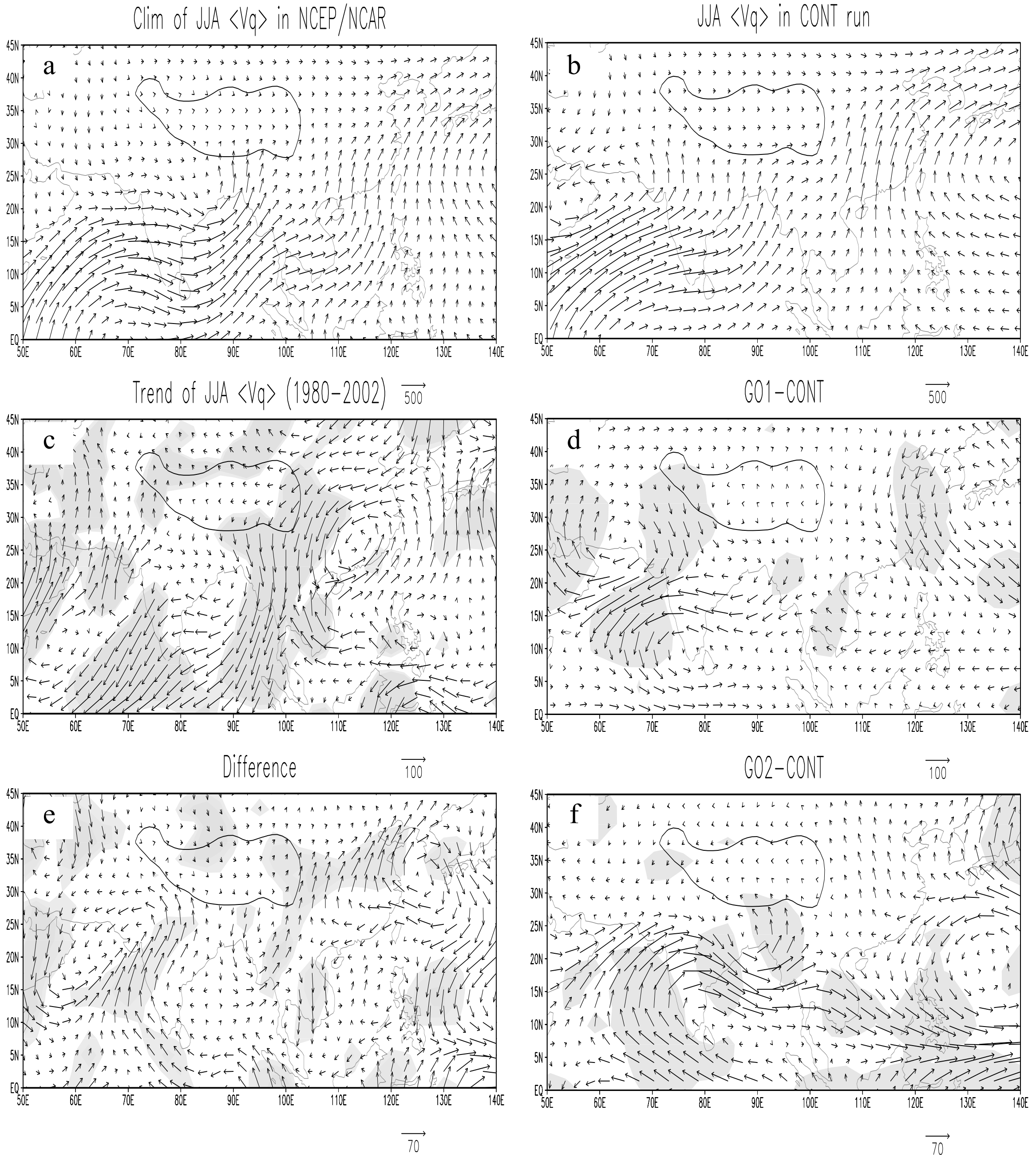

Figure 6.7: Climatology of JJA vertically integrated moisture transport in the NCEP/NCAR reanalysis (a) and in CONT run (b). Linear trend of vertically integrated moisture transport in the NCEP/NCAR reanalysis from 1980-2002 (c). Difference of vertically integrated moisture transport between GO1 and CONT runs (d). Same as in (d) but between years 2003-2007 and 1998-2002 in the NCEP/NCAR reanalysis (e). Same as in (d) but between GO2 and CONT runs (f). Areas where trends or differences are statistically significant at a 95% confidence level are shaded in grey. Units of vertically integrated moisture transport and trend are kg/m/s and kg/m/s/23years, respectively.

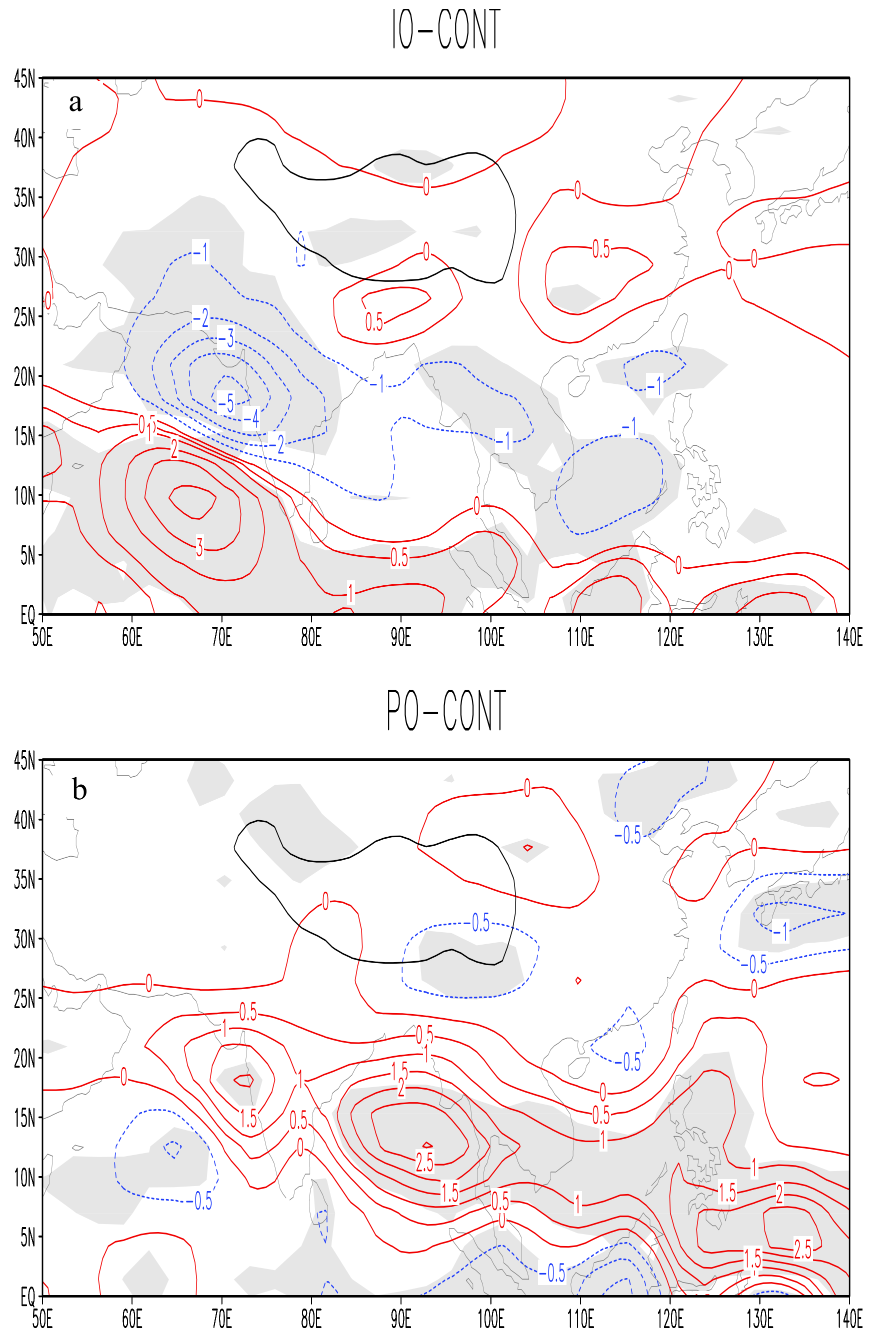

Figure 6.8: (a) is the difference of JJA precipitation between IO and CONT runs (IO minus CONT). (b) is the difference of JJA precipitation between PO and CONT runs (PO minus CONT). Areas where differences are statistically significant at a 95% confidence level are shaded in grey. Unit of precipitation is mm/day.

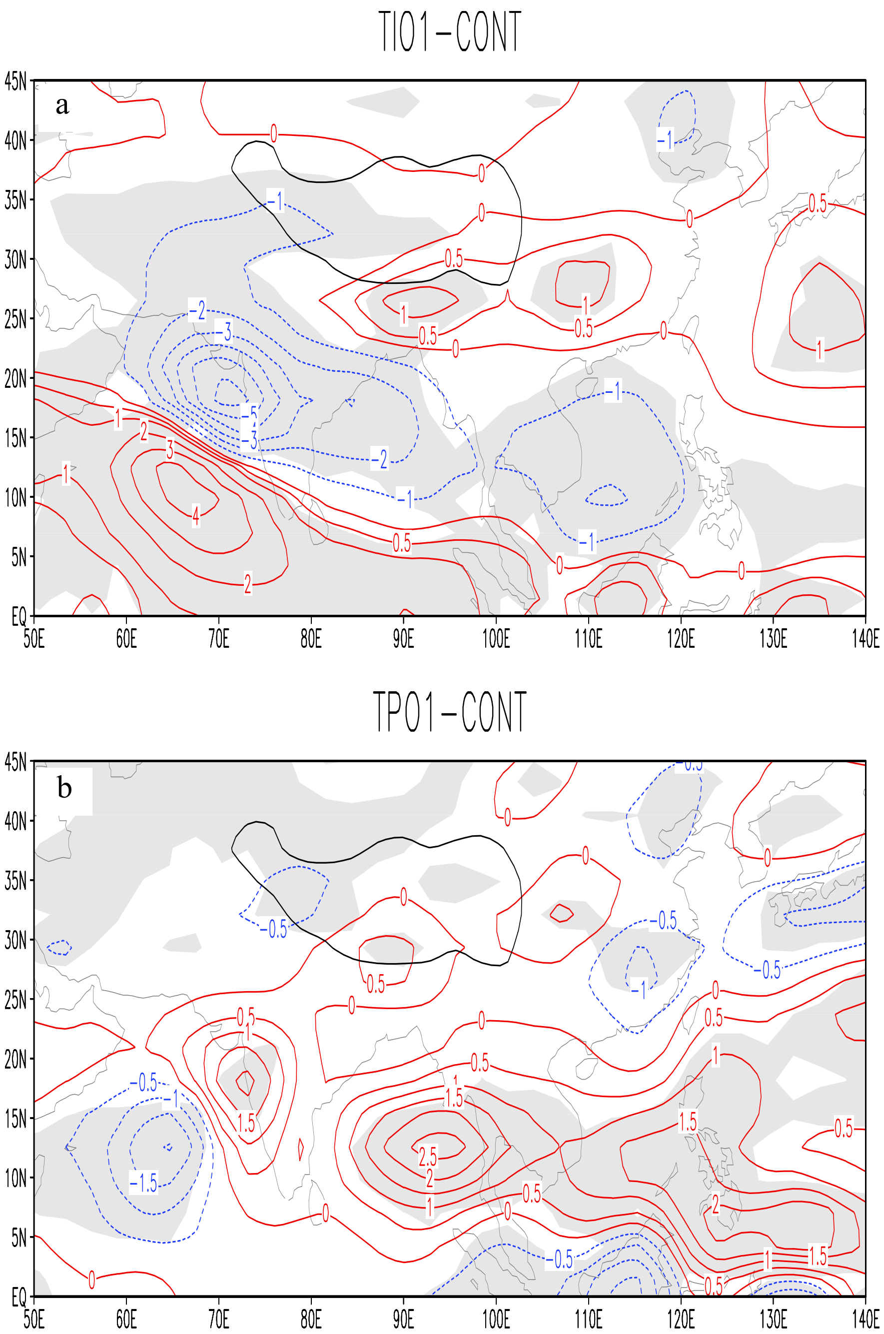

Figure 6.9: (a) is the difference of JJA precipitation between TIO1 and CONT runs (TIO1 minus CONT). (b) is the difference of JJA precipitation between TPO1 and CONT runs (TPO1 minus CONT). Areas where differences are statistically significant at a 95% confidence level are shaded in grey. Unit of precipitation is mm/day.

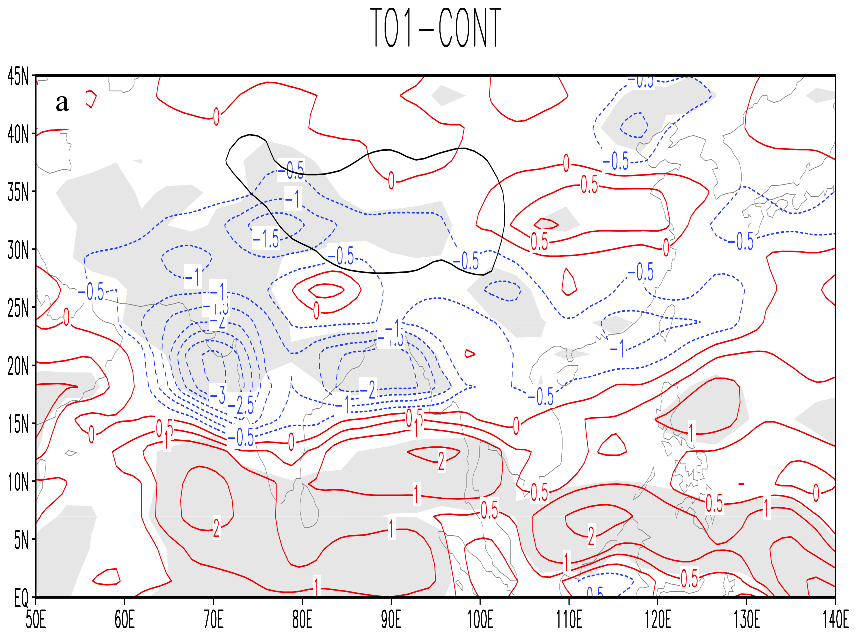
TO1-CONT

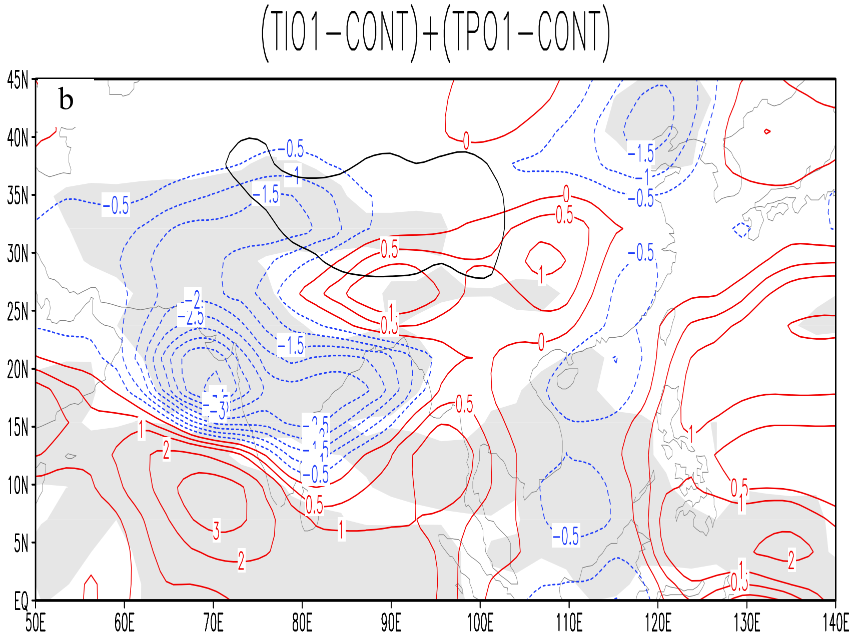
(TIO1-CONT)+(TPO1-CONT)

Figure 6.10: (a) is the difference of JJA precipitation between TO1 and CONT runs (TO1 minus CONT). (b) is the sum of JJA precipitation difference between TIO1 and CONT runs and that between TPO1 and CONT runs ([TIO1-CONT]+[TPO1-CONT]). Areas where differences are statistically significant at a 95% confidence level are shaded in grey. Unit of precipitation is mm/day.

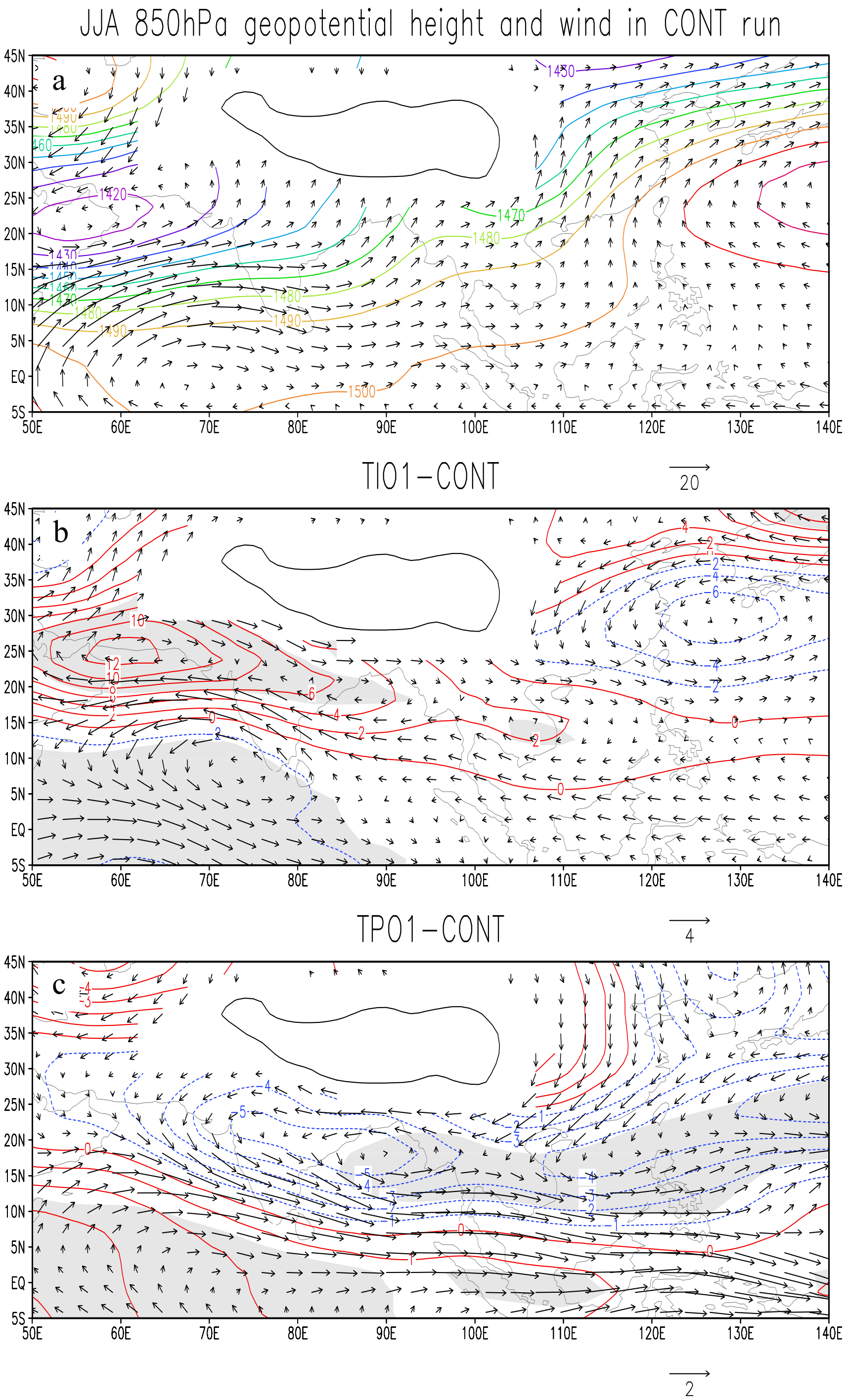

Figure 6.11: (a) is JJA 850-hPa geopotential height (contour) and horizontal wind (vector) in the CONT run. (b) is same as in (a) but for the difference between TIO1 and CONT runs (TIO1 minus CONT). (c) is same as in (a) but for the difference between TPO1 and CONT runs (TPO1 minus CONT). Areas where differences are statistically significant at a 95% confidence level are shaded in grey. Units of geopotential height and wind are m and m/s, respectively.

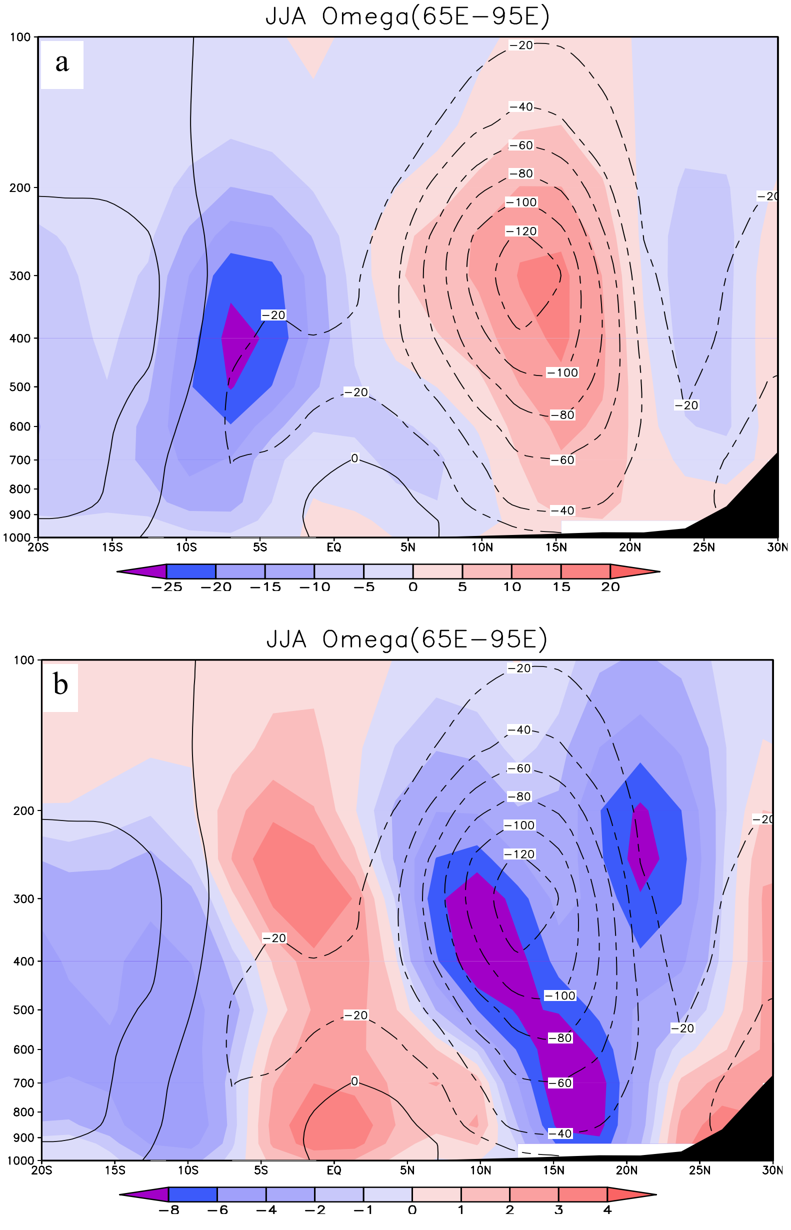

Figure 6.12: 65ºE-95ºE averaged JJA vertical pressure velocity. Contours are the vertical pressure velocity in CONT run. Images are the difference in vertical pressure velocity between TIO1 and CONT runs (a), and between TPO1 and CONT runs (b), respectively. Unit of vertical pressure velocity is hPa/day. The topographic elevation is shaded in black.

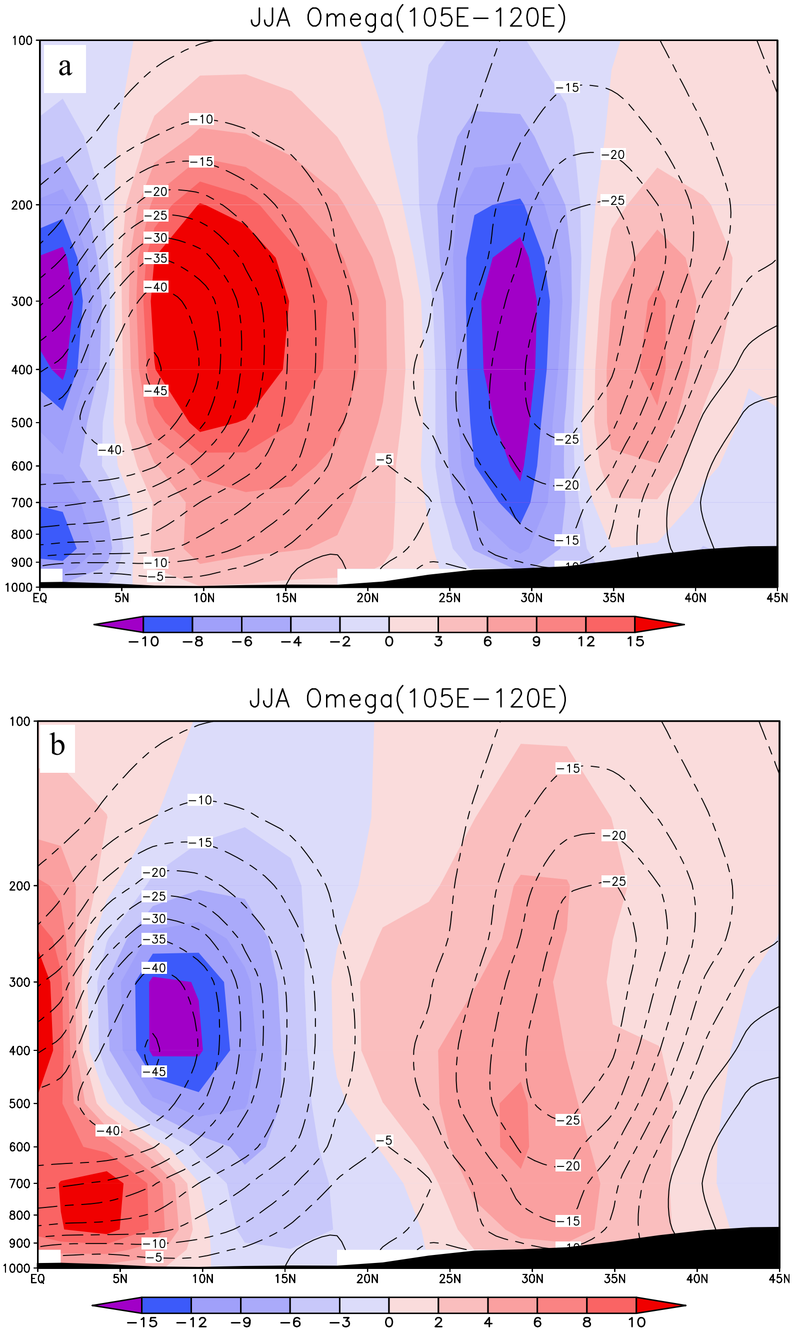

Figure 6.13: 105°E-120°E averaged JJA vertical pressure velocity. Contours are the vertical pressure velocity in CONT run. Images are the difference in vertical pressure velocity between TIO1 and CONT runs (a), and between TPO1 and CONT runs (b), respectively. Unit of vertical pressure velocity is hPa/day. The topographic elevation is shaded in black.

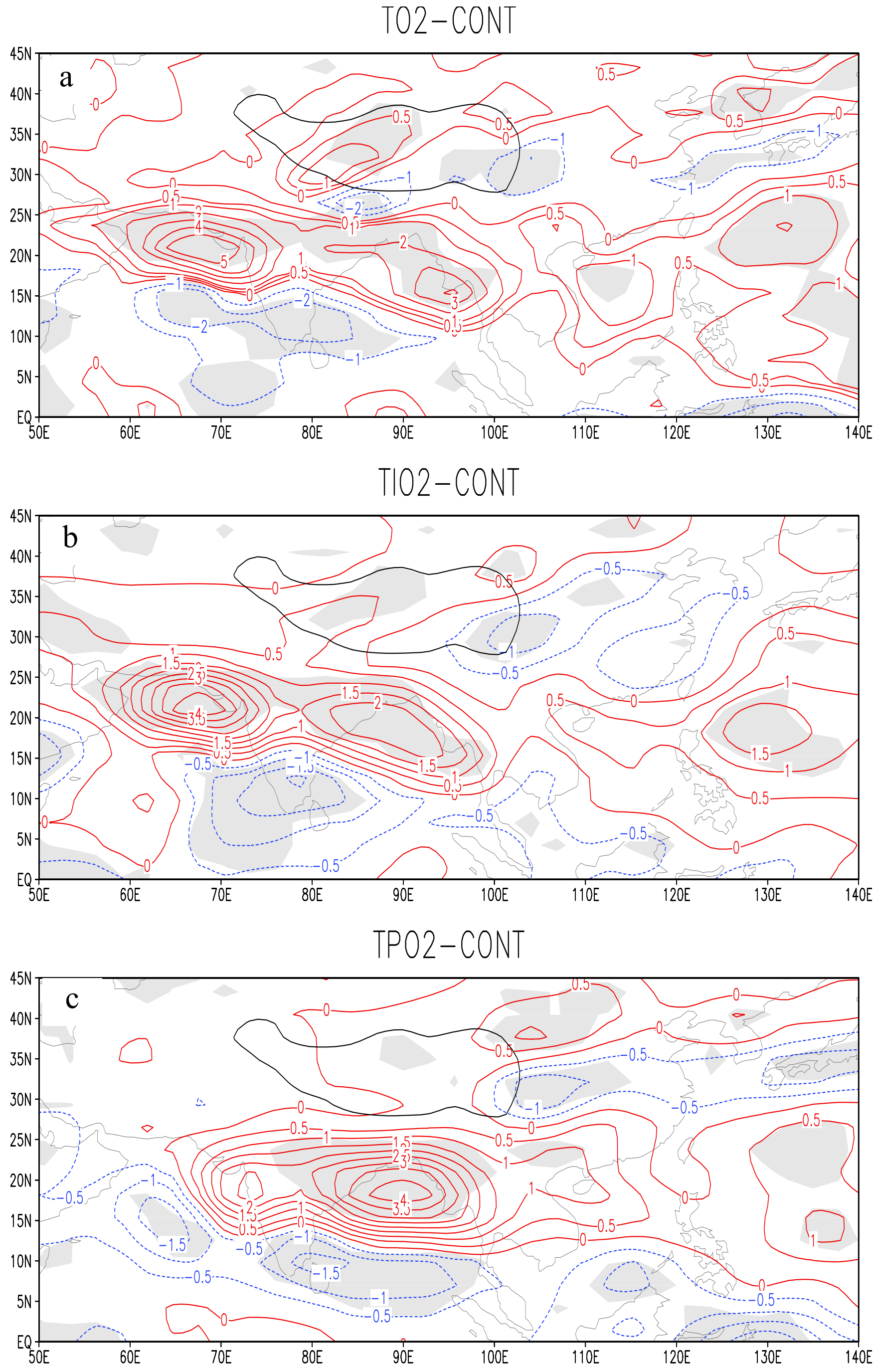

Figure 6.14: (a) is the difference of JJA precipitation between TO2 and CONT runs (TO2 minus CONT). (b) is the difference of JJA precipitation between TIO2 and CONT runs (TIO2 minus CONT). (c) is the difference of JJA precipitation between TPO2 and CONT runs (TPO2 minus CONT). Areas where differences are statistically significant at a 95% confidence level are shaded in grey. Unit of precipitation is mm/day.

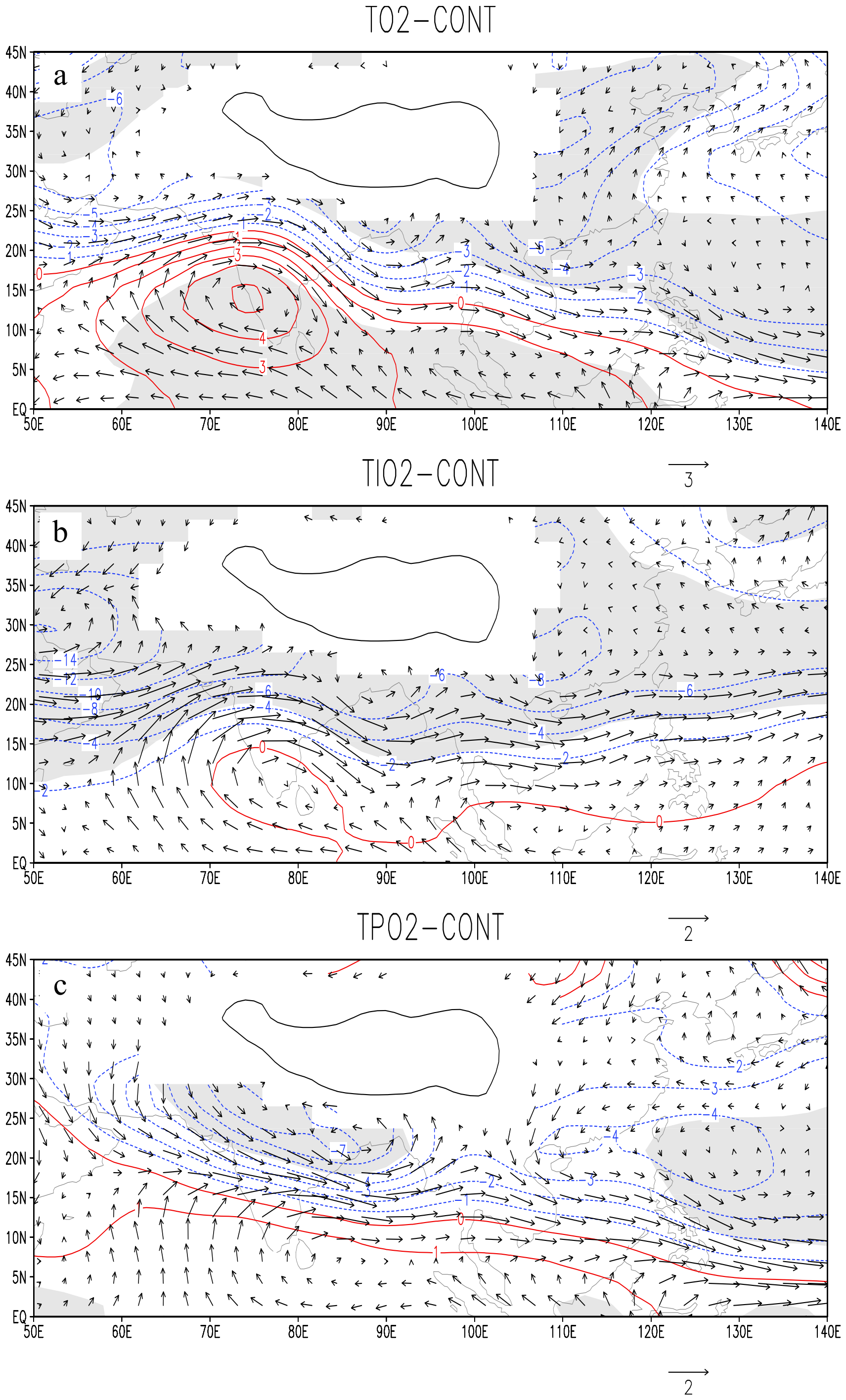

Figure 6.15: (a) is the difference of JJA 850hPa geopotential height (contour) and horizontal wind (vector) between TO2 and CONT runs. (b) is same as in (a) but for the difference TIO2 and CONT runs. (c) is same as in (a) but for the difference between TPO2 and CONT runs. Areas where differences are statistically significant at a 95% confidence level are shaded in grey. Units of geopotential height and wind are m and m/s, respectively.

Chapter 7

Conclusions and Future Work

7.1 Conclusions

In this dissertation study, I have investigated the long-term changes of the tropical atmospheric circulations by using a variety of data and numerical models. The following is a summary of my work in the thesis.

(1) Long-term change of the Walker circulation has been investigated. Analyses of ship-based measurements of sea level pressure reveal a systematic weakening of the horizontal pressure gradient across the Pacific in the latter half of the 20th century. This reduction is also present in the NCAR/NCEP and ECMWF reanalysis sea level pressure products. This weakening is consistent with simulations from AGCMs when SSTs are uniformly raised. It is also consistent with reductions of the large-scale subsidence in the NCEP/NCAR reanalysis and models. Since the reduction of vertical circulation in the models can be explained through fundamental thermodynamic constraints on the atmospheric circulation, I conclude that the weakening of the sea level pressure gradient and the Walker circulation is an intrinsic characteristic of the tropical atmosphere in a warmer climate (Zhang and Song, 2006).

(2) Long-term change of the Hadley circulation has been investigated. Previous studies have reported that both the NCEP/NCAR and the ECMWF reanalyses show strengthening of the Hadley circulation in boreal winter in the last fifty years of the twentieth century, and the intensification is much stronger in the ECMWF than in the NCEP/NCAR reanalysis. These are confirmed in my analysis, but I have also shown that trends in the Hadley circulation in the two reanalyses differ mainly over the tropical western Pacific. Furthermore, this difference is found to be consistent with respective trends of the atmospheric transport of moist static energy, longwave cloud radiative forcing, and upper-level clouds in the two reanalyses. Using two independent datasets of upper-level cloud cover and sea level pressure from ship-based measurements have shown that the large strengthening of the Hadley circulation in the ECMWF reanalysis is not realistic (Song and Zhang, 2007). The strengthening of the boreal winter Hadley circulation in the two reanalyses is also inconsistent with the change of the meridional surface temperature gradient and with simulations in atmospheric general circulation models. The intensification of the Hadley circulation in the boreal winter in the reanalyses is either an artifact or small. During the boreal summer, the rising branch of the Hadley circulation consists of upward motions over a broad range of latitudes because of the monsoon systems. I have found the weakening of the rising motion in the northern portion of the boreal summer Hadley circulation is largely ascribed to changes of the summer monsoons in the two reanalyses, which is further supported by my subsequent study on the Asian monsoon. The rising motion of the Hadley circulation in the boreal summer increased near the equator in the two reanalyses, but it is still unclear whether this strengthening is real or not.

(3) Long-term change of the Asian summer monsoon circulation has been investigated. Using surface rain gauge and satellite measurements, I have found that Asian summer monsoon precipitation decreased over India but increased over southeast China from 1980 to 2002 while the patterns become opposite after 2002; and these features are realistically captured in the NCEP/NCAR reanalysis. Wind fields from the reanalysis are then used to reveal the following association of rainfall variations with wind patterns in the lower troposphere: from the period of 1980-2002, the decrease of precipitation over India is with a systematic reduction of the southwesterly monsoon over the north Indian ocean; the increase of precipitation over southeast China is with a strengthening of the anticyclonic flow over northwest Pacific subtropical high, which is further reinforced by a weakening southerly monsoon flow over central China (Song and Zhang, 2009a).

(4) I have carried out model simulations to study the causes of the variations of the Asian summer monsoon by using the NCAR CAM3. My results show that the observed significant changes of Asian summer monsoon precipitation can be accounted for by the atmosphere's response to the observed SST variations. The tropical SST, especially the tropical Indian ocean SST, plays a dominant role in the observed Indian monsoon suppression (Song and Zhang, 2009b). The positive heating anomaly near equatorial Indian ocean before 2002 induces cyclonic circulation anomaly over the northern Indian ocean, leading to the weakening of southwestly monsoon wind along the south Asia and suppressed precipitation in India, Bay of Bengal, Indochina peninsular and South China Sea. On the other side, the positive heating anomaly around tropical western Pacific induces an intensified westerly winds along the south Asia, which leads

to enhanced precipitation in India, Bay of Bengal, Indochina peninsular and South China Sea. The impact of the Indian ocean SST dominates that of the Pacific SST for rainfall over India. After 2002, SST anomalies in both the tropical Indian ocean and the Pacific ocean contributed to the precipitation increase in India. There is the increase of westerly monsoon flow.

The single most important result of my research is weakening of the large-scale tropical atmospheric circulation in a warmer climate. I have used the atmospheric thermodynamic constraint to explain the weakening of the Walker circulation. The same mechanism should presumably operate for the Hadley circulation. However, because of additional controlling factors such as the meridional surface temperature gradient and change of energy transport to middle latitudes, the change of the Hadley circulation is much less clear. My study helps to rule out the large intensification as described in the ECMWF reanalysis. Furthermore, it pointed out the weakening of the boreal summer rising motions of the Hadley circulation in the monsoon regions. The physical mechanism of the monsoon change is drawn from the linear response of atmospheric circulation to diabatic heating in the equatorial region. This may not be independent of the mechanism of the thermodynamic constraint of the tropical atmosphere, since in a warmer climate, for the same intensity of vertical motion, large latent heating is expected near the equator.

7.2 Future Work

Several lines of research will be pursued to solidify the results presented above. These are described as follow.

First, there is still a general lack of direct observations to describe the long-term changes of the tropical atmospheric circulations primarily because of the known biases of temperature records in the historical radiosonde data. Paleoclimate data may be used to investigate evidences of the weakening and strengthening of the trade winds the warm and cold episodes in the past. The satellite data records may soon be long enough to infer changes in atmospheric winds. In this study, I have used the calendar years to study the trend during the time period when SST continuously increased. In the future, it could be more insightful to use physical variables such as the global or tropical SST to study the relationships between global SST and tropical circulations.

Second, the mechanism of the response of Asian monsoon to the SST forcing will be further studied. It is preferable to use a linear model, with prescribed diabatic heating calculated from SST forcing near and off the equator, as in Gill (1980) but with mean winds, to study whether the responses of vertical motion similar to those in the GCM can be obtained, and to separate the atmospheric response from the forcing. If the linear response is truly the responsible mechanism, it should also operate in other models. A preliminary analysis has indeed shown that monsoon winds over the Indian ocean has weakened with the prescribed SST changes before 2002 in several models that I have examined.

Third, in this dissertation, only long-term change of Asian summer monsoon circulation has been studied. As shown in Figure 7.1, the decreasing (increasing) Indian monsoon precipitation before (after) 2002 is accompanied with fewer (more) strong synoptic systems. How the regional monsoon circulation changes on short time scales to display the long-term change should be studied. Synoptic systems affecting the Asian summer monsoon precipitation will be investigated through using the high resolution nested regional climate model study (e.g., Ashfaq et al., 2009; Stowasser et al., 2009).

Finally, the roles of aerosols on the tropical atmospheric circulations should be explored. In the last several decades, Asian region has experienced rapid increases in aerosols. Model simulations reveal a marked sensitivity of the surface temperature and precipitation changes in Asia to the evolution of sulfate and carbonaceous aerosol concentrations (e.g., Held et al., 2005; Lau et al., 2006). My future research will be focusing on the effects of aerosols (both direct and indirect) on the tropical atmospheric circulation changes and the possible physical mechanisms of these effects. This will be carried out through sensitivity experiments with the GFDL and the NCAR models, comparison of model results with observations, and analysis of the roles of aerosols in controlling the variability of surface properties, vertical stability of air temperature, cloud optical and microphysical properties, and surface heat fluxes.

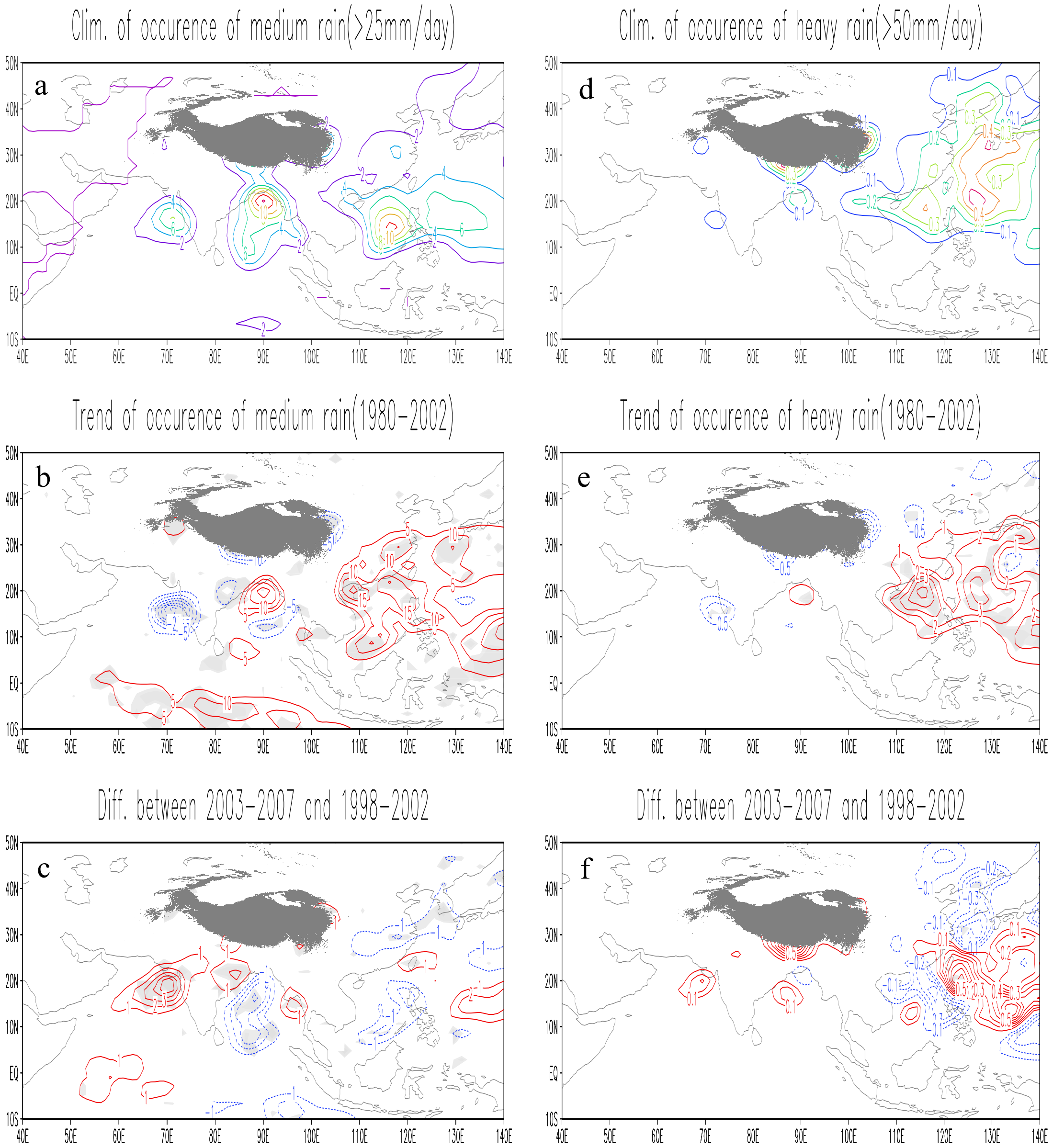

Figure 7.1: Occurrence of medium rain (>25mm/day) in south Asia: (a) Climatology, (b) linear trend from 1980 to 2002 (multiplied by 100), (c) difference between 2003-2007 and 1998-2002. Occurrence of heavy rain (>50mm/day) in south Asia: (d) Climatology, (e) linear trend from 1980 to 2002(multiplied by 100), (f) difference between 2003-2007 and 1998-2002. Estimates are from daily precipitation data of the NCEP/NCAR reanalysis. The units are numbers per 2.5º square box per 3-month (JJA, 92days) period. Areas where trends or differences are statistically significant at a 95% confidence level are shaded in light grey.

References

Abe, M., A. Kitoh and T. Yasunari, 2003: An evolution of the Asian summer monsoon due to mountain uplift - Simulation with the MRI atmosphere-ocean coupled GCM. *J. Meteor. Soc*. Japan, 81, 909-933.

An, S., and B. Wang, 2000: Interdecadal change of the structure of the ENSO mode and its impact on the ENSO frequency, *J. Climate*, 13(12), 2044–2055.

Arken, G., 1985: *Mathematical Methods for Physicists*, 3rd ed. San Diego, California: Academic Press, 1029 pp.

Ashfaq, M., and Coauthors, 2009: Suppression of south Asian summer monsoon precipitation in the 21st century, *Geophys. Res. Lett.,* 36, L01704, doi:10.1029/2008GL036500.

Bengtsson, L., S. Hagemann, and K. I. Hodges, 2004: Can climate trends be calculated from reanalysis data?, *J. Geophys. Res.*, *109*,D11111, doi:10.1029/2004JD004536.

Betts, A., and W. Ridgeway, 1989: Climatic equilibrium of the atmospheric convective boundary layer over a tropical ocean, *J. Atmos. Sci.*, 46, No 17, pp. 2621–2641.

Bony, S., and Coauthors, 2005: On dynamic and thermodynamic components of cloud changes, *Climate Dyn*., 22, 71-86.

Bretherton, C. S., R. Ferrari, and S. Legg, 2004: Climate process teams: A new approach to improving climate models, *U. S. CLIVAR Variations*, 2(1), 1-6.

Cess, R. D., and Coauthors, 1996: Cloud feedback in atmospheric general circulation models: an update, *J. Geophys. Res*., 101, 12791.

Chang C.-P., Z. Wang, J. Ju, and T. Li, 2004: On the relationship between western maritime continent monsoon rainfall and ENSO during northern winter. *J. Climate*, 17, 665–672.

Chen, M., P. Xie, J. E. Janowiak, and P. A. Arkin, 2002: Global land precipitation: A 50-yr monthly analysis based on gauge observations. *J. Hydrometeor*., 3, 249–266.

Chen, J. Y., B. E. Carlson, and A. D. Del Genio, 2002: Evidence for strengthening of the tropical general circulation in the 1990s, *Science*, 295(5556), 838–841.

Chung, C. E., and V. Ramanathan, 2006: Weakening of north Indian SST gradients and the monsoon rainfall in India and the Sahel, *J. Climate*, 19, 2036-2045.

Collins, W. D., and Coauthors, 2006a: The formulation and atmospheric simulation of the Community Atmosphere Model version 3 (CAM3). *J Climate*, 19, 2144–2161.

——, and Coauthors, 2006b: The Community Climate System Model version 3 (CCSM3). *J. Climate*, 19, 2122–2143.

Deser, C., A. S. Phillips, and J. W. Hurrell, 2004: Pacific interdecadal climate variability: Linkages between the tropics and the north Pacific during boreal winter since 1900, *J. Climate*, 17, 3109–3124.

Dickinson, R. E., and Coauthors, 2006: The Community Land Model and its climate statistics as a component of the Community Climate System Model, *J. Clim.*, 19, 2302-2324.

Ding, Y. H, C. Y. Li, and Y. J. Liu, 2004: Overview of the south China seas monsoon experiment. *Adv. Atmos. Sci.*, 21, 343–360.

Durre, I., R. S. Vose and D. B. Wuertz, 2006: Overview of the integrated global radiosonde archive. *J. Climate*, 19(1), 53-68.

Gibson, J. K., and Coauthors, 1999: ECMWF reanalysis project report series 1, ECMWF Tech. Rep., Shinfield Park, Reading, United Kingdom, 84 pp.

Gill, A. E., 1980: Some simple solutions for heat-induced tropical circulation, *Quart. J. Roy. Meteor. Soc.*, 106, 447-462.

The GFDL Global Atmospheric Model Development Team, 2004: The new GFDL global atmosphere and land model AM2-LM2: evaluation with prescribed SST simulations, *J. Climate,* 17, 4641-4673.

Hahn, C. J., and S. G. Warren, 1999: Extended edited synoptic cloud reports from ships and land stations over the globe, 1952-1996. *NDP026C, Carbon Dioxide Information Analysis Center, Oak Ridge National Laboratory, Oak, Ridge, TN.*

Held, I. M., and Coauthors, 2005: Simulation of Sahel drought in the 20th and 21st centuries, *PNAS*, 102(50): 17891-17896.

——, and B. J. Soden, 2006: Robust responses of the hydrological cycle to global warming, *J. Climate*, 19(21), 5686-5699.

Hoyos, C. D., and P. J. Webster, 2007: The role of intraseasonal variability in the nature of Asian monsoon precipitation. *J. Climate*, 20, 4402–4424.

Huffman, G. J., and Coauthors, 1997: The global precipitation climatology project (GPCP) combined precipitation dataset, *Bull. Am. Meteorol. Soc.,* 78, 5–20.

Hurrell, J. W., and Coauthors, 2008: A new sea surface temperature and sea ice boundary data set for the Community Atmosphere Model. *J. Climate*, 21(19):5145–5153

——, and K. E. Trenberth, 1999: Global sea surface temperature analyses: Multiple problems and their implications for climate analysis, modeling, and reanalysis. *Bull. Amer. Meteor. Soc.,* 80, 2661-2678.

Kalnay, E., and Coauthors, 1996: The NCEP/NCAR 40-year reanalysis project, *Bull. Am. Meteorol. Soc*., 77(3), 437–471.

Kinter III, J. L., and Coauthors, 2004: An evaluation of the apparent interdecadal shift in the tropical divergent circulation in the NCEP–NCAR Reanalysis, *J. Climate,* 17, 349–361.

——, K. Miyakoda, and S. Yang, 2002: Recent change in the connection from the Asian monsoon to ENSO. *J. Climate*, 15, 1203–1215.

Knutson, T. R., and S. Manabe, 1995: Time-mean response over the tropical Pacific to increase CO2 in a coupled ocean-atmosphere model, *J. Climate*, 8, 2181-2199.

Kripalani, R. H., and Coauthors, 2003: Indian monsoon variability in a global warming scenario, *Nat. Hazards*, 29, 189–206.

Kumar, K. K., B. Rajagopalan, and M. A. Cane, 1999: On the weakening relationship between the Indian monsoon and ENSO. *Science*, 284, 2156–2159.

Lau, K. M., and K. M. Kim, 2006: Observational relationships between aerosol and Asian monsoon rainfall, and circulations. *Geophys. Res. Lett.,* 33, doi: 10.1029/2006GL027546.

Lau, N. C., and M. J. Nath, 2006: ENSO Modulation of the interannual and intraseasonal variability of the east Asian monsoon—A model study. *J. Climate*, 19, 4508–4530.

Li, H., and Coauthors, 2008: Responses of east Asian summer monsoon to historical SST and atmospheric forcing during 1950-2000, *Climate Dyn*., DOI 10.1007/s00382-008-0482-7.

Lim, Y. K., and K. Y. Kim, 2007: ENSO Impact on the space–time evolution of the regional Asian summer monsoons. *J. Climate*, 20, 2397–2415.

Meehl, G. A., and Coauthors, 2000: Response of the NCAR climate system model to increased CO2 and the role of physical processes, *J. Climate*, 13, 1879-1898.

——, and J.M. Arblaster, 2003: Mechanisms for projected future changes in south Asian monsoon precipitation. *Climate Dyn.*, 21, 659-675.

——, J.M. Arblaster, and W.D. Collins, 2008: Effects of black carbon aerosols on the Indian monsoon. *J. Climate*, 21, 2869-2882.

Mitas, C. M., and A. Clement, 2005: Has the Hadley cell been strengthening in recent decades?, *Geophys. Res. Lett.*, 32, L03809, doi:10.1029/2004GL021765.

——, and ——, 2006: Recent behavior of the Hadley cell and tropical thermodynamics in climate models and reanalyses, *Geophys. Res. Lett.*, 33, L01810, doi:10.1029/2005GL024406.

Norris, J. R., 2005: Trends in upper-level cloud cover and surface divergence over the tropical Indo-Pacific ocean between 1952 and 1997. *J. Geophys. Res.*, 110, D21110, doi:10.1029/2005JD006183.

Oort, A. H., and J. J. Yienger, 1996: Observed interannual variability in the Hadley circulation and its connection to ENSO, *J. Climate*, 9, 2751-2767.

Plumb, R. A., 2007: Dynamical constraints on monsoon circulations. *The global circulation of the atmosphere*, edited by T. Schneider and A. H. Sobel, Princetion University Press, 252-266.

Quan, X.W., H. F. Diaz, and C. B. Fu, 2003: Interdecadal change in the Asia-Africa summer monsoon and its associated changes in global atmospheric circulation. *Global and Planetary Change*, 37, 171-188.

——, ——, and M. P. Hoerling, 2004: Change of the Hadley circulation since 1950. *The Hadley Circulation: Past, Present, and Future*, edited by H. F. Diaz and R. S. Bradley, Kluwer Academic Publishers, 85-120.

Ramanathan, V., and Coauthors, 2006: Atmospheric brown clouds: Impacts on south Asian climate and hydrological cycle. *PNAS*, 102(15), 5326-5333.

Rind, D., 1998: Latitudinal temperature gradients and climate change. *J. Geophys. Res.*, 103, 5943-5971.

Santer, B. D., and Coauthors, 2005: Amplification of surface temperature trends and variability in the tropical atmosphere, *Science*, *309*(5740), 1551–1556.

Sherwood, S., J. Lanzante, and C. Meyer, 2005: Radiosonde daytime biases and late 20th century warming, *Science*, 309, 1556-1559.

Smith, T. M., and R. W. Reynolds, 2004a: Reconstruction of monthly mean oceanic sea level pressure based on COADS and station data (1854-1997), *J. Oceanic Atmos. Tech.,* 21, 1272-1282.

——, and ——, 2004b: Improved extended reconstruction of SST (1854-1997), *J. Climate*, 17, 2466-2477.

Soden, B. J., A. J. Broccoli, and R. S. Hemler, 2004: On the use of cloud forcing to estimate cloud feedback. *J. Climate*, 17, 3661–3665.

Song, H., and M. Zhang, 2009a: Robust change of wind pattern associated with rainfall variation of the Asian summer monsoon from 1980 to 2007, submitted to *Geophys. Res. Lett.*

——, and ——, 2009b: Impacts of tropical SSTs, aerosols and greenhouse gases on the Asian summer monsoon. In preparation.

——, and ——, 2007: Changes of the boreal winter Hadley circulation in the NCEP/NCAR and ECMWF reanalyses: A comparative study. *J. Climate*, 20, 5191-5200

Stephenson, D. B., H. Douville, and K. Rupa Kumar, 2001: Searching for a fingerprint of global warming in the Asian summer monsoon. *Mausam*, 52, 213-220.

Stowasser M, H. Annamalai, and J. Hafner, 2009: Response of the south Asian summer monsoon to global warming: Mean and synoptic systems. *J. Climate*, 22(4): 1014-1036.

Tanaka, H. L., N. Ishizaki, and A. Kitoh, 2004: Trend and interannual variability of Walker, monsoon and Hadley circulations defined by velocity potential in the upper troposphere, *Tellus, Ser. A,* 56(3), 250–269.

Trenberth, K. E., and J. W. Hurrell, 1994: Decadal atmosphere–ocean variations in the Pacific, *Climate Dyn.*, 9, 303–319.

——, 1997: Using atmospheric budgets as a constraint on surface fluxes, *J. Climate*, 10, 2796-2809.

——, and C. J. Guillemot, 1998: Evaluation of the atmospheric moisture and hydrologic cycle in the NCEP/NCAR reanalyses. *Climate Dyn.,* 14, 213-231.

——, D. P. Stepaniak, and J. M. Caron, 2000: The global monsoon as seen through the divergent atmospheric circulation. *J. Climate*, 13, 3969-3993.

——, D. P. Stepaniak and J. W. Hurrell, 2001: Quality of reanalyses in the tropics. *J. Climate*, 14, 1499-1510.

——, 2002: Changes in tropical clouds and radiation: Are they real?, *Science*, 296, 2095a

——, and Coauthors, 2007: Observations: surface and atmospheric climate change. In, Climate Change 2007: The Physical Science Basis: Contribution of Working Group I to the Fourth Assessment Report of the Intergovernmental Panel on Climate Change, edited by S. Solomon et al., pp. 235-336, Cambridge Univ. Press, Cambridge, UK.

Uppala, S. M., and Coauthors, 2005: The ERA-40 reanalysis. *Quart. J. Roy. Meteor. Soc.*, 131, 2961-3012.

Wang, B., and Coauthors, 2005: Fundamental challenges in simulation and prediction of summer monsoon rainfall, *Geophys. Res. Lett.*, 32, L15711, doi: 10.1029/2005GL022734.

——, and Q. Ding, 2006: Changes in global monsoon precipitation over the past 56 years, *Geophys. Res. Lett.,* 33, L06711, doi:10.1029/2005GL025347.

——, and Coauthors, 2008a:, How to measure the strength of the east Asian summer monsoon. *J. Climate*, 21, 4449–4463.

——, J. Yang, T. Zhou, and B. Wang, 2008b: Interdecadal changes in the major modes of Asian–Australian monsoon variability: Strengthening relationship with ENSO since the late 1970s. *J. Climate*, 21, 1771–1789.

Webster, P. J., 1987: The elementary monsoon. *Monsoons*, edited by Fein, J. S. and P. L. Stephens, John Wiley, New York, 3–32.

Woodruff, S. D, R. J. Slutz, R. L. Jenne, and P. M. Steurer, 1987: A comprehensive ocean-atmosphere data set, *Bull. Am. Meteorol. Soc.*, 68 (10), 1239–1250.

Wyant, M. C., and Coauthors, 2006: A comparison of tropical cloud properties and responses in GCMs using mid-tropospheric vertical velocity, *Climate Dyn.*, 27(2-3), 261-279, doi:10.1007/s00382-006-0138-4.

Xie, P., and P. A. Arkin, 1997: Global Precipitation: A 17-Year monthly analysis based on gauge observations, satellite estimates, and numerical model outputs. *Bull. Amer. Meteor. Soc.*, 78, 2539-2558.

Yu, R., B. Wang, and T. Zhou, 2004: Tropospheric cooling and summer monsoon weakening trend over east Asia, *Geophys. Res. Lett.*, 31, L22212, doi:10.1029/2004GL021270.

Zhang, M.H., 1997: Impact of the convection-wind-evaporation feedback on surface climate simulation in general circulation models, *Climate Dyn.*, 12, 5, 299-315.

——, and Coauthors, 1994: Diagnostic study of climate feedback processes in atmospheric general circulation models. *J. Geophy. Res.*, 99, 5525-5537.

——, and H. Song, 2006: Evidence of deceleration of atmospheric vertical circulation over the tropical Pacific, *Geophys. Res. Lett.*, 33, L12701, doi: 10.1029/2006GL025942.

Zhou, T., and Coauthors, 2009: Why the western Pacific subtropical high has extended westward since the late 1970s. *J. Climate,* 22, 2199-2215.

——, and Coauthors, 2008a: Ocean forcing to changes in global monsoon precipitation over the recent half-century. *J. Climate,* 21, 3833–3852.

——, and Coauthors, 2008b: The CLIVAR C20C Project: Which components of the Asian-Australian monsoon circulation variations are forced and reproducible?, *Climate Dyn.*, DOI 10.1007/s00382-008-0501-8.